Università degli Studi della Basilicata

International PhD Program in

Applied Biology and Environmental Safeguard

Nanotransporters for the release of bioactive molecules

SSD

Chim-09

Coordinator

Prof. Patrizia Falabella

PhD student

Dr. Maria De Luca

Tutor

Prof. Antonio Vassallo

XXXV Cycle

“Do what you can, with what you have, where you are.”

CONTENTS

Abstract

In this project, the nanoformulation of plant extracts in phospholipid vesicles was performed to improve phytochemicals' applicability in potential skin products. In recent years, the scientific community and pharmaceutical and cosmetic industries gave much attention to plant-derived products with active ingredients. The antioxidant, antibacterial, wound healing, anti-ageing, sun protection, and anti-inflammatory activities are some of their properties highlighted for topical application. Despite this, plant compounds present some drawbacks related to their poor solubility, instability, reduced skin permeation, and low skin retention time, which strongly restrict their topical application. Nanotechnology emerges as an innovative strategy to tackle these limitations: by manipulating materials and reducing their size at the nanometer scale, new structures able to incorporate different active molecules are produced. Nanocarrier-based delivery preserves biomolecules from degradation and increases their bioavailability, at the same time.

In this project, the plant material was obtained through alcoholic extractions of different parts of some common plants. Their incorporation in phospholipid vesicles was carried out by a simple sonication of extracts and phospholipids in dispersant solutions. To verify that the nanoformulations had optimal features for skin delivery, a deep characterization was performed, in terms of size, surface charge, sample homogeneity, shape, degree of lamellarity, and entrapment efficiency of the main compounds characteristic of each extract. Their biocompatibility was assayed with different skin cell lines as well as their antioxidant potential. Our results suggest that phospholipid vesicles incorporating plant extracts could be good candidates for topical delivery.

Riassunto

In questo progetto, è stata eseguita la formulazione di alcuni estratti vegetali in vescicole fosfolipidiche per migliorarne l'applicabilità per potenziali applicazioni sulla pelle. Negli ultimi anni la comunità scientifica e le industrie farmaceutiche e cosmetiche hanno prestato molta attenzione ai prodotti di origine vegetale contenenti molecole bioattive. Le attività antiossidanti, antibatteriche, cicatrizzanti, anti-età, di protezione solare e antinfiammatorie sono solo alcune delle loro proprietà evidenziate per l'applicazione topica. Nonostante ciò, i composti vegetali presentano alcuni inconvenienti legati alla loro scarsa solubilità, instabilità, ridotta permeazione cutanea e basso tempo di ritenzione cutanea, che ne limitano fortemente l'applicazione topica. Le nanotecnologie emergono come una strategia innovativa per affrontare questi limiti: manipolando i materiali e riducendone le dimensioni su scala nanometrica, vengono sviluppate nuove strutture in grado di incorporare molecole attive con diverse caratteristiche chimico-fisiche. Il delivery mediato da nanocarrier preserva le biomolecole dalla degradazione e allo stesso tempo aumenta la loro biodisponibilità.

In questo progetto, il materiale vegetale è stato ottenuto attraverso estrazioni alcoliche effettuate da diverse parti di alcune piante comuni. L'incorporazione in vescicole fosfolipidiche è stata effettuata con la semplice sonicazione di estratti e fosfolipidi in soluzioni disperdenti acquose. Per verificare che le formulazioni avessero caratteristiche ottimali per il rilascio cutaneo, è stata eseguita un'approfondita caratterizzazione, in termini di dimensione, carica superficiale, omogeneità del campione, forma, grado di lamellarità ed efficienza di incorporazione dei principali composti caratteristici di ciascun estratto. La loro biocompatibilità è stata analizzata in diverse linee cellulari, così come il loro potenziale antiossidante. I nostri risultati suggeriscono che le vescicole fosfolipidiche che incorporano estratti vegetali potrebbero essere buoni candidati per la somministrazione topica.

1.Nanocarriers

Nanotechnology is the science focused on the manipulation and reduction of materials to the nanometer scale conferring them improved or new properties, which enable the regulation of varied aspects. It is an active research area with applications in different fields. Particularly, the health sector benefited from the innovative approach to drug delivery: the manipulation of the nanoscale materials allows optimal targeting and delivery as well as the controllable release of drugs. Taking advantage of the nano-sized structures, nanocarriers help poorly soluble molecules to become more bioavailable and protect them from degradation. The modifiable surfaces of nanocarriers extend their usability in different biomedical applications, especially in targeted therapy: their modification not only stabilizes but also functionalizes them to be responsive to different stimuli [1].

A variety of nanocarriers was developed to improve the molecules' delivery and to satisfy different clinical needs. One of the main classes of nanocarriers, the liposomes, is described below. Discovered in 1965 by Bangham et al. [2], liposomes have been extensively studied over time. In 1995, the approval by the Food and Drug Administrations of Doxil as the first liposomal drug paved the way for the clinical translation of nanocarriers that now have found an application in the treatment of patients suffering from cardiovascular and neurodegenerative disease, diabetes, cancer, and many inflammation disorders [3–10].

Liposomes have attractive biological properties, including biocompatibility, biodegradability, low toxicity, small size, and different cargo transportability, that increase their application area from drug and gene delivery to the diagnostic sector, and cosmetics, food, and chemical industries [11–13].

1.1. Liposomes

Liposomes are spherical-shaped vesicles consisting of phospholipid bilayers enclosing an aqueous space, able to entrap both lipophilic and hydrophilic compounds, in the lipid membrane and aqueous core, respectively (Fig. 1). Generally, liposome composition includes natural and/or synthetic phospholipids such as phosphatidylethanolamine, phosphatidylglycerol, phosphatidylcholine, phosphatidylserine, and phosphatidylinositol, which are also physiological lipids of cell membranes, so they are relatively biocompatible, biodegradable, and non-immunogenic material [11].

In an aqueous environment, phospholipids have a strong ability to form stable bilayers due to their amphipathic character and their three-dimensional cylinder-like shape [14]. The spontaneous phospholipid reorganization in bilayers is mainly driven by the hydrophobic effect, which organizes these amphiphilic molecules so as to minimize entropically unfavourable interactions between hydrophobic acyl chains and surrounding aqueous medium. Beyond hydrophilic interactions between polar head groups, various intermolecular forces such as van der Waals forces between hydrocarbon chains, as well as hydrogen bonding with water molecules, and other electrostatic interactions, further settle this effect [11,15].

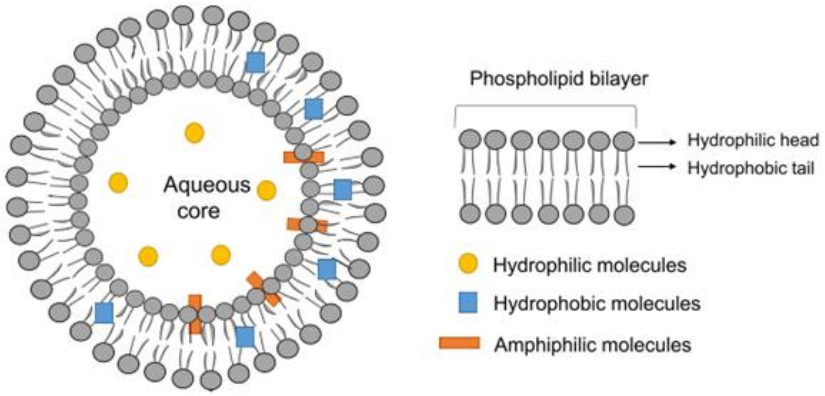

Figure 1. Representation of the general structure of liposomes. Adapted from Guimaraes et al. 2021 [15].

In an aqueous medium, phospholipids can be arranged in single or multiple concentric lipid bilayers (lamellae) to form enclosed vesicles. Based on their lamellarity, liposomes can be classified as unilamellar vesicles (ULVs, all size range), multilamellar vesicles (MLVs, >500 nm), and multivesicular vesicles (MVVs, >1000 nm); the ULVs can also be classified according to their size as small unilamellar vesicles (SUVs, 20-100 nm), large unilamellar vesicles (LUVs, >100 nm), and giant unilamellar vesicles (GUVs, >1000 nm) (Fig. 2) [15].

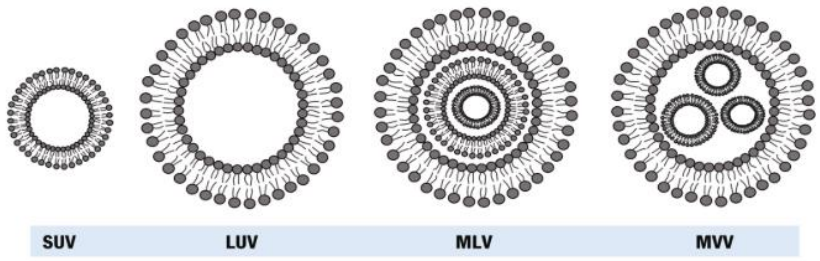

Figure 2. Liposomal classification based on lamellarity and size. SUV (Small Unilamellar Vesicles), LUV (Large Unilamellar Vesicles), MLV (Multilamellar Vesicles), and MVV (Multi Vesicular Vesicles). Adapted from Guimaraes et al. 2021 [15].

Generally, according to composition, three different generations of liposomes were described. The *first generation* includes liposomes made only of phospholipids, and possibly cholesterol to stabilize the structure. To improve some drawbacks that sometimes occur, like low loading efficiency, leakage of cargo, and rapid clearance of liposomes by the mononuclear phagocyte system or reticuloendothelial system, liposomal surface modification led to the formation of *second-generation* liposomes. The structural engineering is performed by coating the liposome surface with natural biological materials such as oligosaccharides, glycoproteins, polysaccharides, and/or synthetic polymers: these engineered liposomes can evade the body's immune system and their uptake by the reticuloendothelial system is minimized; the adding of polyethylene glycol (PEG) to liposomes surface (PEGylation) is an ordinary surface modification [1]. Binding specific molecules or functional materials like antibodies and low-molecular probes to the liposomes led to the development of *third-generation* liposomes. These can also be coupled to trigger systems that can be functionalized with physicochemical alterations in the microenvironment like heat, ultrasound, light, enzymes, or pH [13].

1.1.1. Liposomes preparation

Several methods are available for the preparation of liposomes, each with its advantages and disadvantages. Almost all the techniques for liposome preparation involve the dissolution of phospholipids in an organic solvent that is later removed [16,17]. The classical ways of liposome manufacturing are described below.

The *thin film hydration* technique or Bangham method was the first used for liposome production. Phospholipids are dissolved in an organic solvent (such as chloroform, and/or methanol) and dried down under a vacuum to form a thin lipid film.

When hydrated with an aqueous solution, liposomes are formed with different structural organizations (mainly MLVs and GUVs) that depend on hydration conditions. It is an easy method, but the main drawbacks are the production of larger and heterogeneous liposomes, low entrapment efficiency (EE), difficulty in completely removing the organic solvent, and scale-up.

In the *reverse-phase evaporation* method, a lipid film is prepared by evaporating the organic solvent under reduced pressure. The lipids are re-dissolved in a second organic phase, which usually is diethyl ether and/or isopropyl ether. The addition of an aqueous phase results in the formation of an oil-in-water emulsion. Sonication of the mixture produces inverted micelles forming a homogeneous emulsion. The final evaporation of the organic solvent under reduced pressure forms a viscous gel that results subsequently into a liposomal suspension. This method has high EE but it uses organic solvents and is time-consuming.

The *solvent injection* method involves the dissolution of the lipid into an organic phase (ethanol or ether), followed by the injection of the lipid solution into aqueous media, forming liposomes. The advantages are simplicity, reproducibility, fast implementation, easy scale-up, no lipid degradation or oxidative alterations, and the use of an acceptable solvent for *in vivo* applications (at low concentrations). Despite all the benefits, poor solubility of some lipids in ethanol, heterogeneity of liposomes produced, very low EE of hydrophilic compounds, and incomplete removal of ethanol from the liposomes, are the major concerns about this method.

Another classical method is *detergent removal*. Liposomes are formed by solubilizing lipids with detergent at critical micelle concentrations, yielding defined mixed micelles. As the detergent is removed by controlled dialysis, phospholipids form homogeneous unilamellar vesicles with a usefully large encapsulating volume. The drawbacks can be the presence of impurities in the final liposomal formulation, possible interactions between the detergent and the encapsulated compounds, and the long time needed.

However, these classical techniques require large amounts of organic solvents, which are harmful both to the environment and to human health, requiring complete removal of residual organic solvents, and additional techniques to reduce their sizes, such as sonication, homogenization, or extrusion.

Sonication can be used also for the preparation of liposomes. With sonication, lipid suspensions are mixed with other compounds using acoustic energy from either a bath or a probe tip sonicator. When the ultrasound is transmitted through the medium, the acoustic cavitation, formation, growth, and rapid implosive collapse of microbubbles occur, generating high pressure and high temperature that mix compounds. Moreover, the induced pressure breaks up the larger, multilamellar vesicles in the sample to form smaller vesicles that may be either unilamellar or oligolamellar in composition. The time over which lipid dispersions are sonicated determines the size of the vesicles. This is a less time-consuming technique and does not use hazardous solvents; however, the resulting liposome batch-to-batch mean diameter and size distribution are not always as reproducible as those made by extrusion through a polycarbonate membrane with a well-defined pore size [18,19].

Novel methods are being investigated to facilitate the scale-up of industrial production.

The *heating method* is a new method for the fast production of liposomes without the use of any hazardous chemicals. This method involves the hydration of liposome components in an aqueous medium followed by the heating of these components, in the presence of glycerol (3% v/v), up to 120 ^{o}C [20]. The *spray-drying* is a very simple and industrially applicable method, the direct spray-drying of a mixture of lipids and drugs is applied for the preparation of liposomes, but organic solvents are used [21]. The *freeze-drying* is based on the formation of a homogenous dispersion of lipids in water-soluble carrier materials such as sucrose, dissolved in tert-butyl alcohol/water cosolvent systems to form an isotropic monophase solution that is sterilized by filtration and freeze-dried. In addition to water, the lyophilized product spontaneously forms homogenous liposomes [22,23]. S*upercritical reverse phase evaporation* is a one-step new method that uses supercritical carbon dioxide. An aqueous dispersion of liposomes is obtained through emulsion formation by introducing a given amount of water into a homogeneous mixture of supercritical carbon dioxide/L-R-dipalmitoylphosphatidylcholine/ethanol under sufficient stirring and subsequent pressure reduction [24,25].

Novel approaches based on the principle of the ethanol injection technique such as the *microfluidic channel* method [26,27], the *cross flow-injection* technique [28,29], and the *membrane contactor* method [30] were recently reported for liposome production.

1.1.2. Liposomes characterization

After production, liposomes need to be extensively characterized for evaluation of their physical and chemical properties to guarantee their *in vitro* and *in vivo* performance.

Size and size distribution

The average mean diameter and polydispersity index (PDI) of liposomes are the most relevant features in liposome characterization and are commonly assessed by dynamic light scattering (DLS), also known as photon correlation spectroscopy (PCS).

The principle of dynamic light scattering is that particles that are in constant random thermal motion (Brownian motion) diffuse at a speed related to their size (and temperature that is accurately controlled): smaller particles diffuse faster than larger particles. To measure the diffusion speed, the speckle pattern produced by illuminating the particles with a laser is observed. The scattering intensity at a specific angle will fluctuate with time, and this is detected using a sensitive avalanche photodiode detector (APD). The intensity changes are analysed with a digital autocorrelator, which generates a correlation function. This curve can be analysed to give the size and the size distribution.

The size is a crucial factor to determine the circulation half-life of liposomes: generally, small liposomes can circulate in the body for a long time while large liposomes are more quickly eliminated from blood circulation [31,32]. For drug delivery, the desirable size of liposomes usually ranges between 50 and 200 nm [33].

The PDI is a dimensionless value in the range of 0 - 1 which calculation is based on the particle size, the refractive index of the solvent, the measurement angle, and the variance of the distribution [34]. This value reveals in terms of size, the degree of sample heterogeneity, which can be monodisperse or polydisperse. In drug delivery, a PDI value equal to or below 0.3 indicates an acceptable and homogenous liposomal population [35].

Zeta potential

The charge acquired by a particle in a medium is its zeta (ζ) potential and arises from the surface charge (related to composition) and the concentration and types of ions in the solution [36]. Zeta potential is an extremely important parameter to predict nanoparticle stability in colloidal dispersions. Liposomes

with low ζ potential or uncharged have more probability to aggregate over time, because there will be no force to prevent the liposomes from flocculating; on the other hand, the liposomes in suspension with a large negative or positive ζ-potential charge present repulsive forces in the medium that prevents the natural tendency to aggregation [11].

The ζ-potential measurements are commonly assessed by electrophoretic light scattering (ELS) measuring nanoparticles' velocity while they are moving due to electrophoresis. Particles and molecules with a ζ-potential will migrate toward an electrode if an electric field is applied. The speed they move is proportional to the electric field strength and their ζ-potential. If this strength is known, the speed of movement is simply measured, using laser Doppler electrophoresis, and then ζ-potential is calculated by determining the electrophoretic mobility, i.e. the velocity of a particle in an electric field, and then applying specific equations (Henry equation) [11,37].

Shape and lamellarity

Microscopy is the most selected tool for the ascertainment of liposome morphological features [38]. The visualization of liposomes by microscopy techniques provides a direct observation of their shape. Electron microscopy techniques such as TEM (transmission electron microscopy) and cryo–TEM (cryogenic-transmission electron microscopy) have been widely implemented for creating liposomal images [39]. The cryo–TEM is the most used method to provide useful information regarding liposome lamellarity such as their bilayer thickness and inter-bilayer distance [40].

Other techniques for lamellarity determination include Small-Angle X-ray Scattering (SAXS) [41,42]. The basic principles of SAXS are similar to those of light scattering although working at different wavelengths (λ) and differing for the contrast generated: generally, SAXS uses λ around one Å and measures differences in electron density allowing for the extraction of in-depth structural information. A source emits an X-ray beam that interacts with the electrons of the sample and is scattered; the detector measures the radiation coming from the sample in a certain range of angles. The detected scattering pattern is characteristic of the nanostructures of the sample and can be used to determine many important structural parameters such as particle size, shape, and internal structure [43–45]. However, SAXS can highlight fine structural information related to the bilayers but is not able to differentiate the presence of vesicular or linear bilayers.

Entrapment efficiency

EE is calculated as the percentage of the amount of drug inside liposomes (entrapped drug), compared with the total amount of drug used in liposome preparation (entrapped and non-entrapped drug). The removal of the free drug (non-entrapped) could be realized with exclusion chromatography based on the differences in size (liposome versus free drug), gravitation or centrifugation, dialysis membrane with an appropriate cut-off, and ultracentrifugation [11]. The EE evaluation can be realized through indirect or direct methods. The amount of drug entrapped into liposomes can be measured indirectly by assessing the non-entrapped drug concentration and subtracting this concentration from the total drug concentration used in a liposome preparation. The direct measure can be realized through the disruption of liposomes with organic solvent and the quantification of the released material with UV–Vis, fluorescence spectroscopy, enzyme or protein-based assays, HPLC, LC-MS, and GC–MS, [11,46].

The formulation of a nanocarrier presumes the attainment of a high value of EE, since it avoids the wastage of the entrapped active ingredient, enhancing the clinical efficacy of the nanoformulation [12].

1.2. Lipid-based nanocarriers to overcome skin barrier

Among the various types of drug delivery, the use of nanocarriers for topical application continues to grow. The skin appears a reliable route of drug delivery for different reasons. With transdermal delivery, the drug molecules can reach the bloodstream, triggering systemic effects; on the other hand, topical delivery can regulate a localized action on the skin, involving minimal systemic absorption. This is very attractive for the treatment of skin diseases, such as skin cancer, psoriasis, and fungal infections [44]. Another advantage is the improvement of the bioavailability of drugs that are unstable in the gastrointestinal tract and/or suffering hepatic first-pass metabolism. Moreover, the skin represents a large and accessible surface area for drug administration. In addition to drug administration, the use of nanocarriers for topical application concerns also cosmetics. Anyway, the complex architecture of the skin makes molecules' penetration and permeation difficult.

Skin structure and permeation routes

The primary function of the skin is to provide the body with a protective interface from the external environment (e.g. microorganisms, temperature, among others) through its complex stratified structure. From the inside to the outside, the deepest layer is the *hypodermis*, consisting mainly of adipose tissue. The middle layer is the *dermis*, a connective tissue containing fibroblasts, nerve endings, blood and lymphatic vessels, adnexal structures (such as hair shafts, sweat glands, and sebaceous glands), the fibrous proteins collagen and elastin, which allow for skin's strength and flexibility, respectively, and an interfibrillar gel of glycosaminoglycans, salts, and water. The outermost layer is the *epidermis*, a stratified squamous epithelium without vascularization, responsible for the barrier function of the skin and which contains four to five layers depending on its location:

- *stratum basalis*, the closest layer to the dermis; it is mitotically active and contains stem cells, melanocytes, and keratinocytes that from this layer evolve and travel outward to create the remaining layers;
- *stratum spinosum*, containing several layers of cells tightly connected by desmosomes to resemble spines architecturally;
- *stratum granulosum*, containing several layers of cells rich in lipid-rich granules; in this layer, cells begin to immortalize and lose their nuclei, as they move away from the nutrients located in the deeper tissue;
- *stratum lucidum*, only existing in the thick skin of soles and palms and consists of mostly immortalized cells;
- *stratum corneum*, which serves as a protective overcoat and is the outermost layer of the epidermis. The stratum corneum comprises 15–20 layers of corneocytes, cells rich in packed keratin and lipids but poor in water content [12,44,47] The flattened and cornified dead cells of this layer represent the final evolution of the keratinocytes produced at the basal layer and pushed upwards the surface of the skin by newly produced keratinocytes. While travelling to the skin surface, keratinocytes gradually differentiate, losing cell organelles and nuclei, and creating tightly packed corneocytes. These cells are connected by desmosomes and embedded in an intercellular lipid-rich matrix made mostly of ceramide and neutral lipids (cholesterol and fatty acids) organized in lipid bilayers [43]. This lipid organization forms a semi-crystalline gel and liquid crystal domains that play an essential role in the barrier property of the stratum

corneum and that makes difficult molecules permeation [43,44]. The main routes to pass the stratum corneum are:

- the *dermal appendage routes* that include permeation through the sweat glands and across the hair follicles with their associated sebaceous glands;
- the *transdermal routes* where compounds permeate across the intact, unbroken stratum corneum. In this last case, there are two possible micro pathways, the *intercellular route*, a continuous but tortuous way through the lipids surrounding the cells, and the *transcellular route* through the keratinocytes and then across the intercellular lipids (Fig. 3).

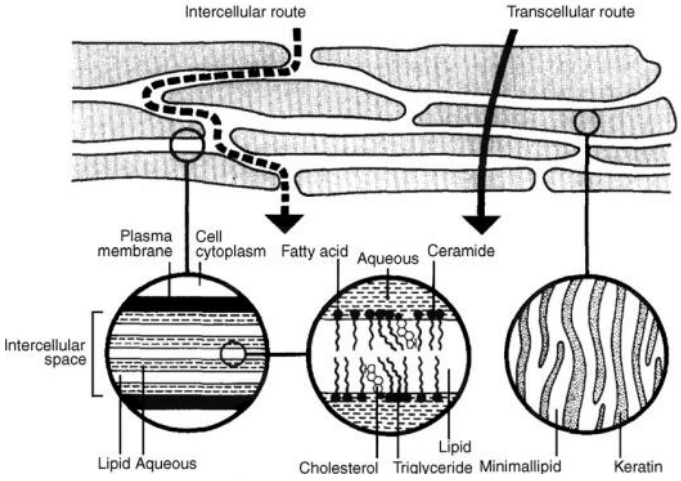

Figure 3. Simplified structure of the stratum and the possible drug permeation pathways through intact stratum corneum. Adapted from El Maghraby et al., 2008 [43].

All molecules traverse by a combination of all three routes, the relative importance of which will vary depending on their physicochemical characteristics [12,43,44].

Many compounds do not possess the physicochemical criteria (i.e. low molecular weight, adequate lipophilicity (log Po/w ≅ 1-3), low melting point) to permeate passively the skin in therapeutic quantities thus limiting the topical and transdermal market. The development of technologies to enhance delivery into the skin has been a major research focus for over half a century [12,48].

Nanocarrier for skin applications

The most common nanocarriers used in skin delivery methods are *liposomes*. As described in section 1.1, liposomes can carry molecules with different physicochemical properties. However, the role of

the liposome in skin drug delivery systems is still a great source of debate. Although several authors suggest that liposomes are suitable candidates for transdermal delivery, the majority of research has shown that conventional liposomes cannot penetrate deeply into the skin layers, remaining confined to the most superficial space of the epidermis and reaching deeper tissues only if the skin has been previously damaged [49]. Some physico-chemical characteristics seem to facilitate the penetration of conventional liposomes, such as application in the gel phase, use of cutaneous lipids for the preparation of vesicles, increased membrane fluidity by decreasing the amount of cholesterol or changing properties, such as size, charge, and lamellarity. However, most liposomes accumulate on the surface of the stratum corneum [49]. Moreover, serious inconveniences of liposomes are the hydrolysis, oxidation, and rancidity of phospholipids used, which affect the storage and the bioavailability of drugs [50,51].

Intensive research has been devoted to the development of new classes of lipid vesicles (Fig. 4). In the 1970s, L'Oreal discovered non-ionic surfactant vesicles called *niosomes* [52]. Firstly developed for cosmetic use, these vesicles have been explored in the pharmaceutical field. Niosomes are structurally similar to liposomes, being bilayered unilamellar or multilamellar vesicles composed of self-assembled non-ionic surfactants in an aqueous medium. The amphiphilic nature of the system ensures the main advantages reported for liposomes, such as the entrapment of both hydrophilic and hydrophobic drugs as well as their biodegradability. The interaction with skin is similar for liposomes and niosomes. However, the presence of non-ionic surfactants instead of phospholipids guarantees the physical and chemical stability of the system and easy formulation with low-cost and large-scale production [50,51].

New vesicular carriers have been developed by introducing some additives (edge activators) to the classic composition of liposomes for the creation of deformable, elastic, and flexible liposomes. An edge activator is generally a surfactant namely an amphiphilic molecule able to intercalate into lamellar structures, destabilizing lipid bilayer in the right measure to increase their deformability by lowering the interfacial tension [44]. Among them, t*ransfersomes*, a registered trademark by the German company IDEA AG, were the first and one of the most successful carriers for molecules skin delivery. Introduced in 1992 by Cevc and Blume [53], the typical characteristic of these vesicles

is determined by the addition of a single-chain surfactant as an edge-activator, such as sodium cholate, sodium deoxycholate, Span, Tween, dipotassium glycyrrhizinate, and polysorbic acid. These compounds can destabilize the lipid bilayers resulting in ultra-deformable vesicle formation able to cross the skin [50]. This is mainly attributable either to their typical flexible structure and the hydrostatic gradient of the skin, with the upper layers of the skin lower hydrated than the epidermal layers. Deformable liposomes, driven by the water gradient in the deeper skin layers, can deform and cross the channels between the cells of the stratum corneum, crossing the epidermis, reaching the dermis, and eventually, the systemic circulation [44,50].

Meanwhile, in 2000, Touitou et al. developed *ethosomes* by introducing ethanol into the phospholipid vesicle [54]. The most important feature of ethanol in the formulation is the ability to act as a penetration enhancer, promoting skin permeation in depth or directly into the systemic circulation. Firstly, ethanol increases lipid membrane permeability by disturbing the organization of the stratum corneum. Secondly, ethanol provides a soft and malleable structure to vesicles, decreases their size, increases their stability over time, and the entrapment efficiency of either hydrophilic or lipophilic compounds; moreover, it donates a negative surface charge to the system, preventing the vesicles aggregation and drug leakage [50].

Drawing on the discovery that the elasticity of the bilayer is a significant factor for effective skin delivery, a series of molecules have been tested as penetration enhancers (PE, such as propylene glycol, glycerol, oleic acid, etc.) producing very versatile systems called Penetration Enhancer containing Vesicles (PEVs) [55–61].

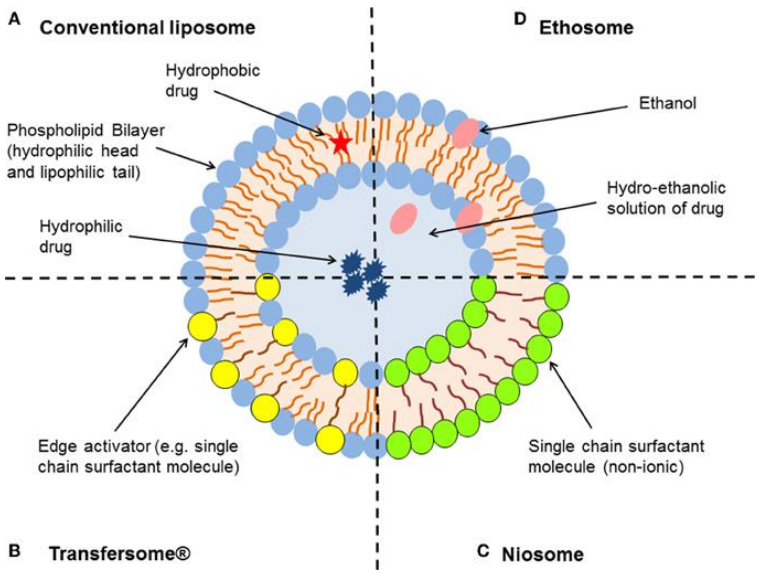

Figure 4. Schematic representation of the different types of lipid-based vesicular delivery systems. Adapted from Hua, 2015 [62].

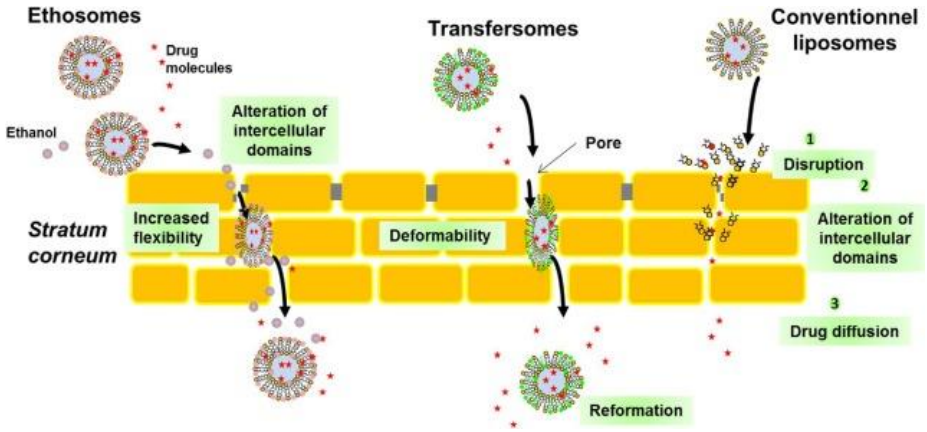

Figure 5. Schematic representation of the main permeation mechanisms of lipid-based vesicles. Adapted from Sala et al. 2018 [63].

1.3. Topical delivery of phytochemicals

Recently, also thanks to nanotechnological breakthroughs, there has been intensive growth of phytocompounds-based formulations for topical applications mainly in the cosmetic market. The cosmetic industry is a huge and dynamic sector of the world economy that, due to the public stringent concerns about beauty and skin care, is always pursuing the best technological products [12].

The plant kingdom produces a large diversity of compounds with different biological functions that find applications in sectors such as the food, pharmaceutical, and cosmetic industries. In addition, the

industrial interest in using green molecules has greatly increased to pursue the ecology and sustainability criteria [64]. Nowadays, phytochemicals are important protagonists in research. They include mostly a group of bioactive compounds naturally found in plants and commonly known as secondary metabolites such as alkaloids, phenolic compounds, and terpenoids [65]. Phytochemicals play important roles in the adaptation of plants to their environment, at the same time provide health benefits for humans. Several authors reported many biological activities, namely antioxidant, anti-inflammatory, antimicrobial, etc. However, these advantageous features cannot be fully exploited due to unfavourable physicochemical or pharmacokinetic characteristics. The main hindrances to the dermal delivery of phytochemicals appear to be their chemical instability and vulnerability to environmental conditions, alongside the potential discrepancy with the bio-pharmaceutical requirements for this route of application. The high miscibility in the aqueous phase, the low lipid solubility, and the high molecular weight have a crucial impact on the poor penetration across lipid-rich biological membranes, such as the skin barrier, leading to low bioavailability [66–68]. The inclusion of active pharmaceutical ingredients in lipid-based nanocarriers is the contemporary approach to overcoming problems such as poor solubility, stability, and permeation, and improving their dermal/transdermal delivery [69–71].

Examples of nanocarriers for phytochemicals reported in the literature are presented in table 1, and in the next paragraphs, there is a description of the plants chosen for active material production and subsequent lipid vesicle formulation.

Nanocarrier	**Phytocompounds**	**Phytocompounds activity/function**
Liposomes	Curcumin	Anticancer
	Ascorbic acid	Anti-oxidant
	Aloe vera extract	Wound-healing Moisturizing Anti-aging
Niosomes	Ellagic acid	Anti-oxidant Skin-whitening
	Curcumin	Anti-oxidant Anti-aging Moisturizing Anticancer Antibacterial Anti-inflammatory Wound-healing
	Resveratrol	Anti-inflammatory skin-whitening

		Anti-acne Anti-aging
Ethosomes	Rutin	Antioxidant Photoprotection Venotonic
	Ursolic acid	Anti-oxidant Anti-inflammatory Antimicrobial Cytotoxic Anti-aging Cellular renewal
Transferosomes	Baicalin	Anti-inflammatory
Cubosomes	Capsain	Anti-inflammatory
Phytosomes	*Citrus auranticum* and *Glycyrrhiza glabra* extracts	Anti-oxidant Anti-aging
	Quercetin	Anti-oxidant Anti-inflammatory
Nanoemulsions	Pomegranate peel extract	Photoprotection
	Resveratrol	Anti-inflammatory Skin-whitening Anti-acne Anti-aging
	Betulin	Anti-cancer
Nanocrystals	Quercetin	Anti-oxidant Anti-inflammatory Photoprotection
Polymeric nanoparticles	α-mangostin	Anti-acne
	Rutin	Anti-oxidant Photoprotection Venotonic
Solid lipid nanoparticles	Auraptene	Anti-inflammatory
	Resveratrol	Anti-oxidant Anti-inflammatory Anti-acne
	Quercetin	Anti-inflammatory
	Luteolin	Anti-oxidant Cellular protection Photoprotection
Nanostructured lipid carriers	Silymarin	Anti-oxidant Photoprotection Immunomodulatory
	Ursolic acid	Anti-inflammatory
Carbon Nanotubes	Curcumin	Anti-oxidant Anti-cancer
Fullerenes	Ascorbic acid	Photoprotection
Dendrimers	Silibinin and Epigallocatechin-3-gallate	Anti-inflammatory Wound healing

Table 1. Examples of nanocarriers reported in the literature as phytocompounds-based nano-cosmeceuticals. Adapted from Santos et al. 2019 [12].

1.3.1. *Myrtus communis* L.

Myrtus communis L., commonly referred to as myrtle, is an evergreen shrub belonging to the Myrtaceae family. Myrtle is widely distributed in the Mediterranean area and presents round blue-

black berries extremely rich in seeds and traditionally used for many purposes. Berry extracts are known for various biological activities [72–79]. The broad spectrum of biological activities associated with myrtle is ascribed to many isolated components. Phytochemical analysis has revealed its richness in phenolic compounds, including phenolic acids, flavan-3-ols, and anthocyanins. Moreover, essential oils and polyunsaturated fatty acids have been detected [80–85]. One of berry extracts' best-known actions is their antioxidant effects [86]. Some studies have highlighted their inhibitory activity against enzymes linked to neurodegenerative diseases [87], beneficial effects on gastrointestinal disorders [88–90], ability to reduce streptozotocin-induced oxidative stress in diabetic rats [91], and wound-healing properties [92]. These properties can all be related to myrtle extract's antioxidant activity.

1.3.2. *Prunus spinosa* L.

Prunus spinosa L. is a perennial deciduous plant growing as a thorny bush or small tree in uncultivated areas of different countries among them the Mediterranean. Also known as blackthorn or sloe, it belongs to the Rosaceae family and its fruit is a small, spherical, bluish-black drupe with a yellow-greenish pulp and a characteristic astringent flavour that determines consume after processing into jams, jellies, juices, tea, and alcoholic beverages; recently studied as natural food colourants [93–97]. In European tradition, blackthorn has been known as a medicinal plant for its diuretic, laxative, anti-spasmodic, anti-microbial, and anti-inflammatory properties. Blackthorn fruits were recommended i.e. in the treatment of various inflammation-related disorders within the gastrointestinal and urinary tracts, respiratory system, and topically in oral and pharyngeal mucosa inflammation. Moreover, the fruit was used to treat metabolic diseases (including diabetes and obesity), and circulatory system disorders [93,96,98–102]. More recently, many studies found also beneficial effects on the wound healing process [102,103], cytotoxic activity on some cancer cell lines [94,100,104,105], and selective growth inhibition of some potentially pathogenic bacteria strains [96]. All these properties can be attributed to the high levels of phenolic acids and flavonoids, including anthocyanins, flavonols, and flavones, found in *P. spinosa* berries [94,96,100,106].

1.3.3. *Ceratonia siliqua* L.

Ceratonia siliqua L., carob, is an evergreen tree that belongs to the Leguminosae family, widely cultivated in Mediterranean countries [107]. Traditionally, carob has been used to produce animal feed. Nowadays, agricultural and industrial sectors exploit carob fruit and its primary products (i.e., flour, powder, and syrup) to develop a variety of foods and beverages [108].

The fruit is a brown pod with an elongated and compressed shape of varying dimensions and a wrinkled surface that becomes leathery when ripe. The pods are mainly made up of sweet edible pulp with a leathery outer layer (pericarp) and a softer inner area (mesocarp), rich in hard seeds [109].

Carob pulp contains a wide range of biologically active compounds [110]. Generally, carob pods have a high sugar content (40–60%, e.g. sucrose, glucose, maltose, and fructose), relatively low content of lipids (0.4–0.8%), and protein (3–4%), but some essential amino acids (namely aspartic, glutamic acids) as well as ω-3 and ω-6 fatty acids (namely oleic, linoleic and α-linolenic acids). Moreover, this fruit contains a high amount of low-calorie dietary fibres (cellulose, hemicelluloses, and lignin), minerals (calcium, phosphorus, and potassium), and different kinds of phenolic compounds [108,111]. The phenolic content is mainly represented by gallic acid; the other phenolic compounds are myricetin rhamnocyte, quercetin rhamnocyte, methyl gallate, cinnamic acid, and myricetin glycoside. Furthermore, it is known that the *C. siliqua* pod is one of the important sources of the bioactive component pinitol [109,112,113].

Carob pods show significant pharmacological activities (anti-inflammatory anti-bacterial, anti-diabetic, anti-hypercholesterolemic, hepatoprotective, neuroprotective, and nephroprotective) [107,110,114–116]. Traditional medicine used carob pods widely for the treatment of human gastrointestinal diseases. Several studies showed that carob pods could be useful for the attenuation of processes that are related to various chronic diseases, such as type 2 diabetes, obesity, and metabolic syndrome [117]. They exert beneficial effects on dyslipidemia and interfere with glucose absorption mechanisms [118–120].

1.3.4. *Amoracia rusticana* L.

Armoracia rusticana L., also known as horseradish, is a perennial crop belonging to the Brassicaceae family [121]. It originates from the temperate eastern parts of Europe but is cultivated nowadays in many regions of the world and is valued for its fleshy root. Horseradish shows a root system composed of a long main root, cylindrical or tapered, and several lateral roots. The roots show a brown outer skin and a fleshy white interior; they are inodorous but release a short-lasting pungent and intensive odour when cut [121,122]. Due to their hot and piquant flavour and aromatic and penetrating smell, horseradish roots are a traditional spice for many foods all over the world [122]. Moreover, horseradish represents a rich source of health-promoting phytochemicals. Horseradish is rich in glucosinolates (sinigrin, glucobrassicin, neoglucobrassicin, and gluconasturin) that provide the characteristic flavour and aroma [123,124]. The roots also contain ascorbic acid (vitamin C), a very strong antioxidant, and a few amounts of flavonoids such as kaempferol and quercetin also known for antioxidant properties [124].

Horseradish roots have been reported to support and strengthen the body's defences due to their high natural vitamin C content [125]. For their anti-bacterial activities, horseradish roots have been used for treating infections of the upper respiratory airway and uncomplicated urinary tract infections as well as a remedy for headaches and pain associated with rheumatism due to their strong antioxidant and anti-inflammatory properties [125–134].

Traditionally, this plant was used for crop protection and many reports confirm that the plant produces a range of substances with potential insecticidal effects as well as antifungal action, which allow its use as a natural and preservative agent [135–139].

Figure 6. Plants used for extract preparation. (A) Berries of Myrtus communis L., (B) berries of Prunus spinosa L., (C) pods of Ceratonia siliqua L., (D) roots of Armoracia rusticana L.. Adapted from [140].

2. Aims of the research

This research project aims to evaluate the formulation of plant extracts in lipid-based nanocarriers as a tool to overcome some drawbacks related either to the difficult permeation route that is the skin or to the nature of plant compounds.

Topical drug delivery has gained increasing importance in the health field and different research teams have introduced a variety of innovative systems to improve this process. Phospholipid vesicles are one of the most successful vehicles for active compounds, due to their ability to load hydrophobic or hydrophilic compounds improving their aqueous solubility and protecting from degradation, and to interact with biological membranes improving the payload bioavailability.

These vehicles can improve the therapeutic efficacy of natural molecules or plant extracts, taking into account that their promising health benefits are limited by instability and low bioavailability.

The plant extracts studied in this project have been prepared from common plants in the Mediterranean area, using various plant parts, characterized for quali-quantitative composition and antioxidant or antibacterial activities, and incorporated in different kinds of phospholipid vesicles for topical applications. The extracts preparation and their subsequent formulation in phospholipid vesicles were realized without the utilization of hazardous solvents.

The phospholipid vesicles were characterized in terms of size, polydispersity index, surface charge, encapsulation efficiency, morphology, storage stability, and capacity to preserve the typical antioxidant activity of each extract. The biocompatibility of these vesicles was assessed in different cellular models to ensure their safety and asses their antioxidant effects.

3. Materials and methods

3.1. Plant extracts' preparation

The plants chosen for the study belong to four different families quite common in the Mediterranean area. The extraction process was performed through the conventional method of maceration in a green solvent that is ethanol or its mixture with water, and subsequent sonication (Sonorex Super RK 100/H sonicator Bandelin electronic, Berlin, Germany). The solvent was removed by vacuum distillation (Büchi Rotavapor R-114, City, Switzerland). Specific details are reported below for each extract.

3.1.1. *Myrtus communis* L.

Purple myrtle (*Myrtus communis* L.) berries were randomly collected in Monte Arcosu (Sardinia, Italy) in December 2020. The berries were gently cleaned before being ground in a mortar, macerated with ethanol 96% (1:1, w/v), and incubated twice for 30 min under sonication at 15 ± 2 °C. The supernatant was separated, and the berries were manually pressed to recover more liquid. Afterwards, the same quantity of ethanol 96% was poured on the exhausted berries and the procedure was repeated. The supernatants were joined, filtrated using a strainer, and then concentrated by vacuum distillation until the alcohol was eliminated. The obtained extract was stored at -20 °C and later used for liposome preparation.

3.1.2. *Prunus spinosa* L.

The fruits of *Prunus spinosa* L. were collected fully ripened in the Marmo Platano area (Basilicata, Italy) in December 2021. The berries were gently cleaned and ground in a mortar with ethanol 70% (1:2, w/v), sonicated for 30 min at room temperature, and macerated for 24 h. After filtration through paper filters, the same quantity of ethanol 70% was poured on the exhausted sample and the procedure was repeated twice. The supernatants were joined, filtrated using a strainer, and then concentrated by vacuum distillation. The obtained extract was stored at -20 °C and later used for the preparation of phospholipid vesicles.

3.1.3. *Ceratonia siliqua* L.

Carobs (*Ceratonia siliqua* L.) were collected in the Arco Ionico Metapontino area (Basilicata, Italy) in 2019. The carobs were cut into small pieces and let dry for 72 h. Subsequently, the samples were ground in a food processor to produce a fine powder and sieved through a stainless-steel mesh. The carob powder obtained from the whole ripe carobs was macerated with ethanol 70% (1:2, w/v), sonicated for 30 min at room temperature, and macerated for 24 h. After filtration through paper filters, the same quantity of ethanol 70% was poured on the exhausted sample, and the procedure was repeated twice. The supernatants were joined, filtrated using a strainer, and then concentrated by vacuum distillation. The obtained extract was stored at -20 °C and used for the preparation of phospholipid vesicles.

3.1.4. *Armoracia rusticana* L.

Horseradish roots (*Armoracia rusticana* L.) were collected in Oliveto Lucano (Basilicata, Italy) in 2019. The plant samples were cleaned with distilled water and dried with paper towels. The roots were cut into small pieces, left to dry for 72 h, ground into fine powder through a food processor, and sieved through a stainless-steel mesh. The obtained powder was macerated with ethanol 70% (1:2, w/v), sonicated for 30 min at room temperature, and macerated for 24 h. After filtration through paper filters, the same quantity of ethanol 70% was poured on the exhausted sample and the procedure was repeated for twice. The supernatants were joined, filtrated using a strainer, and then concentrated by vacuum distillation. The obtained extract was stored at -20 °C and used for the preparation of phospholipid vesicles.

3.2. Extract characterization

3.2.1. HPLC-PDA

A preliminary characterization of plant extracts through HPLC-PDA was performed to detect the most abundant compounds. For the HPLC-PDA analysis, stock standard solutions were prepared solubilizing the plant extracts in a MeOH:H_2O 80:20 (v/v) mixture (plant–solvent ratio 1:50 w/v); the working standard solutions were prepared to dilute them 1:1 (v/v) with H_3PO_4 0.22 M.

The analyses were performed using a modified HPLC-PDA method [141]. A 1260 Infinity II HPLC system (Agilent Technologies, Cernusco sul Naviglio, MI, Italy) fitted with a pump module G7111A, an autosampler module G7129A, a thermostatted HPLC column compartment G7116A (30 ± 1 °C), and a G4212B photodiode array detector was used. The separation was obtained with a Kinetex EVO C18 column (150×4.60 mm, 2.6 µm, Phenomenex, Casalecchio di Reno, BO, Italy) using 0.22 M phosphoric acid (solvent A) and acetonitrile (solvent B) as mobile phase, at a constant flow rate of 0.8 mL/min. The gradient (v/v) was generated decreasing from 100% solvent A to 80% in 20 min, to 70% in 35 min, to 0% in 45 min, and then remaining stable up to 50 min; finally, the gradient get to 100% solvent A and stay stable 5 min before the following injection. The injection volume was 10 µL. The chromatograms and spectra were elaborated with an OpenLab V. 2.51 data system (Agilent Technologies, Cernusco sul Naviglio, MI, Italy), and polyphenols were detected and quantified according to the main classes: anthocyanins at 520 nm, flavonols at 360 nm, hydroxycinnamic acids at 313 nm, and hydroxybenzoic acids at 280 nm, as well as tryptophan.

The individual components were identified by comparing the retention time and UV-VIS spectra of pure commercial standards. After the identification, quantitative analyses of single compounds were performed. The calibration curves for commercial standards were plotted with the method of the external standard, correlating the peak area with the concentration by means of the least-squares method, with a coefficient of determination (r^2) > 0.999 in the range of 10–1000 µg/L for all the compounds.

3.2.2. High-Resolution LC-ESI-QTOF-MS-MS Analysis

A qualitative investigation of the plant extracts was performed by an ion mobility QTOF LC/MS system using a 1290 Infinity II UPLC equipped with an autosampler (G7167B), a quat pump (G7120A), a column comp (G7116B) and 6560 IM-QTOF (Agilent Technologies Inc., Palo Alto, CA, USA). Overall instrument performances were tested before analysis using an Agilent tuning solution mix (G1969-85000), and during the analysis, two reference masses at *m/z* 112.9855 and *m/z* 966.0007 were continuously infused into the system for constant mass correction. The electrospray ionization (ESI) source in negative ion mode was used to perform all the experiments and the optimized source parameters were the follows: drying gas at 300 °C with a flow of 5 L/min, sheath gas at 250 °C at a

flow rate of 12 L/min, nebulizer at 45 psi, capillary voltage set to 3500 V with a nozzle voltage of 500 V. The automatic acquisition MS/MS experiments were carried out by applying a formula to determine the collision energy by linear interpolation calculated according to the following equation: collision energy = [slope (5) × *m/z* of precursor mass]/100 + Offset (2). The mass spectra were acquired by full range acquisition covering the *m/z* range of 40-1300.

Chromatographic separation was performed on a Kinetex EVO C18 column (150 × 2.1 mm, 1.7 µm 100 Å, Phenomenex, Castel Maggiore, BO, Italy) maintained at 55 ± 1 °C. The mobile phase consisted of a combination of solvent A (0.1% formic acid) and solvent B (acetonitrile + 0.1% formic acid) at a flow rate of 0.3 mL/min. The gradient elution was as follows: 0–20 min (99–80 % A), 20–35 min (80–70% A), 35–40 min (70–1% A), 40–45 min (1–1% A), 45–46 min (1–99% A) and 46–50 min (99–99% A). The injection volume was 4 µL.

Data acquisition and processing were done using a MassHunter Workstation Acquisition software v. B.09.00. (Agilent Technologies, Santa Clara, CA, USA). ESI/QTOF MS data were then analyzed using the molecular feature extraction algorithm of the MassHunter Workstation Qualitative Analysis software v. 10.0 (Agilent Technologies, Santa Clara, CA, USA). The tentative identification and analysis of LC-MS/MS of the metabolites were carried out using the MassHunter METLIN metabolite PCDL database B.08.00 (Agilent Technologies) and Sirius® software version 4.7.4 to predict fragmentation and molecular formulae [142,143].

3.3. Vesicle preparation

Initially, investigational experiments of pre-formulation were performed. For each extract, the aim was to formulate lipid vesicles of small size (with a mean diameter <100 nm), with a high homogeneity level (PDI <0.3), and without extract precipitation.

Different kinds of phospholipids (Lipoid S75, Phospholipon90G, lecithin in granules) have been used, at different concentrations (120, 150, and 180 mg/mL with 20 mg/mL extract), in various dispersant media (deionized water or phosphate buffered saline (PBS) pH 7.4), in the presence or absence of penetration enhancer (ethanol and propylene glycol at 10% and 20%).

The best conditions found for the preparation of conventional liposomes (Lip) and/or penetration enhancers containing vesicles (PEVs) will be indicated for each extract. For the preparation of

conventional liposomes, the phospholipids and the plant extracts were weighed in a glass vial and sonicated in a dispersant medium with a Soniprep 150 (MSE Crowley, London, UK). For the PEVs preparation, a penetration enhancer like propylene glycol (PG) or ethanol (Et) was added along with phospholipid and the extract to the dispersant medium. For a proper comparison, empty vesicles were prepared according to the same procedure as the extract-loaded liposomes or PEVs, but without the extract.

3.3.1. *Myrtus communis* L. vesicles

The myrtle extract was encapsulated in conventional liposomes prepared with Lipoid S75 (fat-free soybean phospholipids with 70% phosphatidylcholine; S75, Lipoid GmbH, Ludwigshafen, Germany). 180 mg of S75 and 20 mg of myrtle extract were sonicated in 1 mL of PBS, pH 7.4 (10 cycles of 5 sec on/2 sec off + 5 cycles 2 sec on/2 sec off; 13 µm of probe amplitude).

	Phospholipid	**Extract**	**Dispersant medium**
Lip	S75 180 mg	20 mg	PBS 1 mL
Empty lip	S75 180 mg		PBS 1 mL

Table 2. Composition of the M. communis L. extract formulations.

3.3.2. *Prunus spinosa* L. vesicles

For the blackthorn extract, conventional liposomes and PG-PEVs were prepared with soy lecithin in granules (a mixture of polar phospholipids and glycolipids; Galeno srl, Comeana, Prato, Italy). Liposomes were prepared with 180 mg of soy lecithin and 20 mg of extract in 1 mL of deionized water (obtained with a MilliQ RG system, Millipore, Bedford, MA, USA) and sonicated (10 cycles of 5 sec on/2 sec off + 5 cycles 2 sec on/2 sec off; 13 µm of probe amplitude). PG-PEVs were prepared according to the same protocol as for liposomes, but with the addition of 10% v/v PG.

	Phospholipid	**Extract**	**Penetration enhancer**	**Dispersant medium**
Lip	Lecithin 180 mg	20 mg		water 1 mL
Empty lip	Lecithin 180 mg			water 1 mL
PEVs	Lecithin 180 mg	20 mg	100 µL PG	water 1 mL
Empty PEVs	Lecithin 180 mg		100 µL PG	water 1 mL

Table 3. Composition of the P. spinosa L. extract formulations.

3.3.3. *Ceratonia siliqua* L. vesicles

The carob extract was formulated in conventional liposomes prepared with Phospholipon90G (>90% phosphatidylcholine; P90G; Lipoid GmbH, Ludwigshafen, Germany). 150 mg of P90G and 20 mg of carob extract were sonicated in 1 mL of deionized water (13 cycles of 5 seconds on/2 seconds off + 5 cycles 2 sec on/2 sec off; 13 µm of probe amplitude).

	Phospholipid	**Extract**	**Dispersant medium**
Liposomes	P90G 150 mg	20 mg	water 1 mL
Empty liposomes	P90G 150 mg		water 1 mL

Table 4. Composition of C. siliqua L. extract formulations.

3.3.4. *Armoracia rusticana* L. vesicles

Conventional liposomes and Et-PEVs were prepared with horseradish extract. For liposome preparation, 180 mg of S75 and 20 mg of horseradish extract were sonicated in 1 mL of deionized water (10 cycles of 5 sec on/2 sec off + 6 cycles 2 sec on/2 s off; 13 µm of probe amplitude). Et-PEVs were prepared according to the same protocol as for liposomes, but with the addition of 10% v/v Et.

	Phospholipid	**Extract**	**Penetration enhancer**	**Dispersant medium**
Lip	S75 180 mg	20 mg		water 1 mL
Empty lip	S75 180 mg			water 1 mL
PEVs	S75 180 mg	20 mg	100 µL Et	water 1 mL
Empty PEVs	S75 180 mg		100 µL Et	water 1 mL

Table 5. Composition of A. rusticana L. extract formulations.

3.4. Vesicle characterization

The vesicle dimensions, size distribution of particles, surface charge, entrapment efficiency, and long-term stability are the main parameters analyzed to assess whether the prepared vesicles are good vehicles for the topical delivery of plant extracts. The specific methodology was described below.

3.4.1. Size, zeta potential, and stability

The average diameter, polydispersity index, and zeta potential of the phospholipid vesicles were

measured by DLS and ELS techniques, described in section 1.1.2. The samples were properly diluted (1:100) with their respective dispersant medium and analyzed by using a Zetasizer nano-ZS (Malvern Panalytical, Worcestershire, UK) that uses Non-Invasive Back-Scatter (NIBS) technology. The speckle pattern produced by illuminating the particles with a laser working at 633 nm and 10mW is observed. The scattering intensity at a specific angle fluctuating with time is detected using a sensitive avalanche photodiode detector (APD). Measurement angles were 13° and 173°. For zeta potential measurements, the instrument uses the technology M3-PALS for signal processing, based on a multi-frequency measurement of phase analysis light scattering. All analyses were done in triplicate at 25 °C. The stability assessment was realized by evaluating over time the size, polydispersity index, and zeta potential of the samples kept at 4°C, as described in the literature [144,145].

3.4.2. Morphology

The direct observation of the samples by cryo-TEM allowed confirming lipid vesicle formation and knowing their morphology. For *M. communis* liposomes, vesicle dispersion (5 µL) was placed on a glow-discharged holey carbon grid and then blotted against filter paper. The obtained thin film was vitrified by plunging the grid (100% humidity, room temperature) into ethane kept at its melting point with liquid nitrogen, using a Vitrobot (FEI Company, Eindhoven, The Netherlands). The vitrified film was transferred to a Tecnai F20 TEM (FEI Company) by using a cryo-transfer (Gatan, Pleasanton, CA, USA) for sample observation. Images were acquired at 200 kV and at –170/–175 °C, using low-dose imaging conditions not exceeding 20 $e^{-}/Å^{2}$, with a 4096 × 4096 pixel CCD Eagle camera (FEI Company).

The *P. spinosa* PEVs, *C. siliqua* liposomes, and *A. rusticana* PEVs, were observed with cryo TEM (model JEOL-2011 TEM; JEOL, USA) with a similar procedure: a droplet of the sample (3.9 µL) was applied on a holey carbon grid, which was then blotted and plunge-frozen into the precooled liquid ethane (-180 °C) with Leica EM GP cryo preparation chamber (Leica, USA). The sample was then embedded in a thin layer of vitreous ice to protect it from radiation damages and to preserve the structure of the vesicles. Experiments were carried out under 200 kV acceleration voltage energy.

3.4.3. Entrapment efficiency

The entrapment efficiency (EE), a measure of the amount of extract incorporated into the vesicles during formulation, was calculated with the direct measurement of the target compounds of each extract through HPLC. Particularly, the EE was calculated as the percentage of the compounds detected in dialyzed *vs*. non-dialyzed vesicles, according to the following formula (1):

$$\mathrm{EE} = \frac{(\text{quantity of the compound in dialyzed vesicles})}{(\text{quantity of the compound in non-dialyzed vesicles})} \text{ x } 100 \quad (1)$$

The non-incorporated extract components were removed from the vesicle dispersions through dialysis. Each sample (1 mL) was loaded into Spectra/Por® tubing (12,000–14,000 Da MWCO; Spectrum, DG Breda, The Netherlands) previously rinsed in water, and dialyzed in water (2 L), under gentle stirring, for 2 h. Non-dialyzed and dialyzed vesicles were disrupted by diluting (1:100) with methanol and analyzed by HPLC–PDA, according to the same procedure described in the 3.2.1 section.

3.4.4. Small-Angle X-ray Scattering

Small Angle X-ray Scattering (SAXS) measurements were carried out using an S3-MICRO (Hecus X-ray systems GMBH Graz, Austria) coupled to a GENIX-Fox 3D X-ray source (Xenocs, Grenoble) working at 50 kV and 1 mA. This source provides a detector-focused X-ray beam with λ=0.1542 nm Cu K_α line with more than 97% purity and less than 0.3% K_β. Transmitted scattering was detected by using a PSD 50 Hecus. The temperature was controlled by means of a Peltier TCCS-3 Hecus and the diffraction patterns were recorded at 25°C. The vesicular dispersions were loaded in a flow-through glass capillary of 1 mm diameter and 10 μm wall thickness. The SAXS scattering curves are shown as a function of the scattering vector modulus (2):

$$q = \left(\frac{4\pi}{\lambda}\right) * \sin\left(\frac{\theta}{2}\right) \quad (2)$$

where θ is the scattering angle and λ the wavelength. The q values with this setup ranged from 0.01 to 0.6 $Å^{-1}$. The scattering vector was calibrated by measuring a standard silver behenate sample. All the scattering curves were recorded every 20 min up to 2 h, with subsequent calculation of the electron distance distribution. SAXS patterns were analyzed using a home-made fitting procedure based on a Gaussian description of the bilayers and using a Levenberg-Marquardt minimization scheme [146–150].

For the figures, the sum of all curves was used, plotting the scattering intensity *I* as a function of the scattering vector *q*. A raw electron density profile was calculated and then fitted with an electron density model (Gaussian profile), taking the results as input parameters for further calculations. The electron density profile ρ(z) was modeled as a function of distance z from the center of the bilayer, given by a summation of two Gaussians, each representing the polar head group and the methyl terminus, respectively (fig. 7).

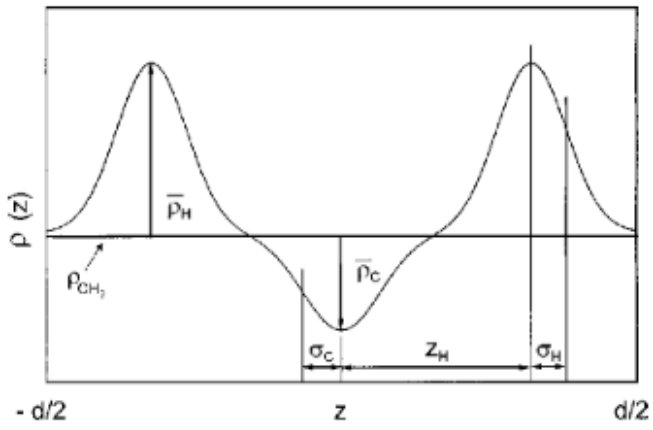

Figure 7. Electron density profile model ρ(z) as a function of distance z from the center of the bilayer, given by a summation of two Gaussians. Adapted from Pabst et al. [147].

The main parameters obtained were:

- *d* that is the repetition distance between lamellae;

- η or Caillé parameter that is related to the bilayer flexibility;

- *N* that is the number of correlated lamellae;

- Z_H that is the polar head distance to the center of the bilayer;

- σ_H that is the polar head amplitude;

- σ_C that is the methyl groups segregation.

3.5. Evaluation of biological activity

The biological activities tested are related to the antioxidant and antimicrobial potency of the plant extracts. Furthermore, the safety of the formulations (biocompatibility) was assayed *in vitro* in different cell lines along with the free extract (20 mg/mL in ethanol:water 70:30 v/v) and empty vesicles.

3.5.1. Biocompatibility evaluation

The biocompatibility of the extracts and their nanoformulations (for blackthorn, carob, and horseradish) was preliminarily tested through the evaluation of hemolytic activity on erythrocytes, one of the most widely cell membrane model systems [151]. Then, their safety was assayed through representative skin cells with some differences among the four plant samples.

Myrtle samples were tested in 3T3-L1 fibroblasts (ATCC® CL-173™). For the other plant formulations, three different cell lines were selected and obtained from Celltec UB (University of Barcelona), two representatives of keratinocytes and one other representative of fibroblasts:

- immortal human keratinocytes (HaCaT);
- squamous carcinoma keratinocytes (A431);
- murine Swiss albino fibroblasts (3T3).

Cells were grown in Dulbecco's Modified Eagle's Medium (DMEM, 4.5 g/L glucose) supplemented with 10% (v/v) FBS, 1% (v/v) L-glutamine solution (200 mM), and 1% (v/v) penicillin-streptomycin solution (10,000 U/mL penicillin and 10 mg/mL streptomycin) at 37 ºC and 5% CO_2. Cells were cultured in 75 cm^2 culture flasks and were routinely split using trypsin-EDTA (ethylenediaminetetraacetate) solution (170,000 U/L trypsin and 0.2 g/L EDTA) when cells are approximately 80% confluent. The cells were seeded into 96-well plates and the biocompatibility of samples was tested under different experimental conditions:

- for myrtle samples, 3T3-L1 cells were exposed to myrtle aqueous solution or myrtle liposomes, previously diluted to reach the required doses of myrtle (0.1, 1.0 and 10 µg/well), for 5 and 24 h; cells viability was tested through MTT;
- for all other samples, HaCaT, A431, and 3T3 cells were exposed to free extract solution or their lipid formulations, previously diluted to reach the required doses (0.1, 5, 10, 15, and 20 µg/well), for 24 h; MTT was performed to determine the concentration-dependent cell viability response.

For comparative purposes, empty vesicles were tested at the same dilutions as the free extract solutions or vesicle dispersions.

3.5.1.1. Hemolytic activity

The erythrocytes were isolated from rabbit blood samples, washed three times in PBS at pH 7.4, and resuspended in the same buffer solution at a cell density of approximately 10^9 cells/mL.

The hemolytic activity evaluation was carried out using the procedure described in the literature [152]. The samples were resuspended in a total volume of 1 mL with PBS buffer and 25 μL of the prepared erythrocyte suspension. The test was performed for different concentrations of all samples, extract solutions and nanoformulations, and for the controls, 100% hemolysis (erythrocytes in Milli-Q water) and 0% hemolysis (erythrocytes in PBS buffer). The samples were incubated at room temperature, under stirring for 10 min, and then centrifuged (5 min at 10,000 rpm). The hemolysis (%) was calculated by comparing the absorbance at 575 nm of the supernatant with that of controls. Unfortunately, the vesicle formulations dispersed in PBS buffer solution showed turbidity, which increased absorbance values regardless of cell disruption. For a more accurate evaluation of data, the absorbance at 575 nm was measured for each sample solubilized in PBS buffer before the addition of erythrocytes. The difference in absorbance values with and without erythrocytes was used for the evaluation of the hemolytic activity.

3.5.1.2. MTT

The MTT assay relies on the mitochondrial activity of live cells to convert yellow tetrazolium salt (2,5-Diphenyl-3,-(4,5-dimethyl-2-thiazolyl) tetrazolium bromide - MTT), into insoluble purple formazan, detectable via spectrophotometry.

Cells (3T3 and HaCaT cells at 1×10^5 cells/mL, A431 cells at 5×10^4 cells/mL) were incubated for 24 h under 5% CO_2 at 37ºC into a 96-well plate. Then, the spent medium was removed, and cells were incubated for 24 h with the samples to be tested, previously diluted in DMEM medium supplemented with 5% FBS. The medium was removed and 100 μL of MTT (5 mg/mL in PBS), diluted 1:10 in culture medium without phenol red and absence of FBS, were added to the cells. The plates were incubated for 3 h, after which the medium was removed. Thereafter, 100 μL of dimethylsulfoxide (DMSO) was added to each well to dissolve the purple formazan crystals. Plates were then placed in a microtiter-plate shaker for 5 min at room temperature to help the total dissolution. Then, the

absorbance of the resulting solutions was measured at 550 nm using a Bio-Rad 550 microplate reader (Hercules, California, USA). The effect of each treatment was calculated as the percentage of tetrazolium salt reduction by viable cells against the untreated cell control (cells with medium only). For myrtle samples, the fibroblasts 3T3 (5×10^4 cells/well) were incubated with MTT (0.5 mg/mL) for 3 h at 37 °C. The medium was removed, and a DMSO:isopropanol (10:90, v/v) mixture was added to the cells to dissolve the purple formazan crystals. The dye released from the cells was quantified by reading the absorbance at 540 nm with a Multiskan EX multi-plate reader. The assay was performed with a few differences between the samples following standardized protocols of the two laboratories where the tests were performed.

3.5.2. Antioxidant assays

The antioxidant power of the plant extracts was examined using the spectrophotometric tests DPPH and FRAP. Once settled the volume of free extract able to scavenge the DPPH radical or to reduce ferric ions to ferrous ions, the analyses were carried out both for the free extracts and the nanoformulated forms to evaluate if the antioxidant property of each extract was preserved after the encapsulation process. The tests were performed also for empty vesicles for a more accurate results interpretation. Moreover, antioxidant activity was evaluated by monitoring Reactive Oxygen Species (ROS) levels in cells treated with myrtles samples and exposed to a radical generator (2,20-azobis(2-methylpropionamidine) dihydrochloride, AAPH); for the other plant nanoformulations, antioxidant properties were assayed as the capacity to protect cells from hydrogen peroxide (H_2O_2) induced oxidative stress.

3.5.2.1. DPPH

The DPPH analysis allows the determination of the antioxidant power of the samples by monitoring the reduction reaction of the DPPH free radical (1,1-diphenyl-2-picrylhydrazyl). The unpaired electron of the DPPH radical absorbs strongly at 517 nm and exhibits an intense deep purple color in the solution. In assays, the radical is neutralized by accepting either a hydrogen atom or an electron from an antioxidant species (or reducing agents) during which, it is converted into a reduced form (DPPH or DPPH-H) at the end of the process, and the initial color gradually

decolorizes into pale yellow. The decrease in absorbance is proportional to the antioxidant charge of the sample.

Each sample was added to a DPPH methanolic solution of 25 µM and incubated at room temperature in the dark for 30 min. The color change of the solutions is monitored through light adsorbed to 517 nm. The antioxidant activity (AA) of the samples was calculated according to Equation (3):

$$\text{AA}\ (\%) = \left(\frac{A_{DPPH} - A_{sample}}{A_{DPPH}}\right) \text{x}\ 100 \quad (3)$$

The results were expressed also as Trolox Equivalents (TEs). The TE values (µg TE/mL solution) were calculated by using a calibration curve (Trolox concentration range: 0-1000 µg/mL).

3.5.2.2. FRAP

The ferric ion reducing antioxidant power or FRAP is based on the reduction of the Fe^{3+}-TPTZ chemical (iron-2,4,6-tripyridyl-S-triazine complex), under acidic conditions, to the intense blue-colored ferrous complex Fe^{2+}-TPTZ, that causes an increase in absorbance. FRAP reagent is prepared by mixing 0.3 mM TPTZ and 20 mM $FeCl_3 \cdot 6H_2O$ in 0.2 M acetate buffer (pH 3.6).

The sample is added to a 2 mL FRAP reagent and incubated at room temperature for 4 min in the dark; the absorbance was read at 593 nm. The results, expressed as µg Fe^{2+} equivalents/mL solution, were calculated by using a calibration curve ($FeSO_4$ concentration range: 13.9−2317 µg/mL).

3.5.2.3. Assessment of ROS and cell morphology

For myrtle formulations, antioxidant activity was evaluated by monitoring ROS levels production in cells treated with myrtles samples and exposed to AAPH. The 3T3-L1 cells were incubated with the samples alone or the samples and 500 µM AAPH, and the endogenous or chemically induced cellular ROS were detected. Particularly, the fibroblasts were seeded into a 96-well blackened fluorescence plate (5×10^4 cells/well) and incubated with 5-(and-6)-chloromethyl-20,70-dichlorodihydrofluorescein diacetate, acetyl ester (CM-H_2DCF-DA;) (5 µM/well) for 60 min, at 37 ºC, in the dark. The cells were rinsed with 1× PBS to remove CM-H_2DCF-DA and treated according to the following experimental conditions:

- cells unexposed (negative control) or exposed to 500 µM of AAPH, the peroxyl radical generator used as a positive control, for 4 and 23 h;

- cells exposed to myrtle aqueous solution or myrtle liposomes, previously diluted to reach the required dose of myrtle (10 µg/well), for 1 h and co-incubated with 500 µM AAPH for a further 4 h.

ROS production was detected by measuring the increase in fluorescence with a microplate reader. Fluorescence was measured by excitation at 495 nm and emission at 527 nm, using a Varian Cary Eclipse Spectrophotometer (Variant/Agilent Technologies, Santa Clara, CA, USA). The experiment was repeated at least three times independently, each time in quadruplicate. To assess cell morphology, 3T3-L1 cells, untreated or incubated with 500 µM AAPH, or co-incubated with 500 µM AAPH and myrtle aqueous solution, empty or myrtle liposomes for 5 h were examined under a Primo Vert inverted microscope (Carl Zeiss Microscopy GmbH, Jena, Germany).

3.5.2.4. Protection from H_2O_2-induced oxidative stress

For blackthorn, carob, and horseradish formulations, their antioxidant properties were assayed as the capacity to protect cells from hydrogen peroxide (H_2O_2) induced oxidative stress. The HaCaT, A431, and 3T3 cells were pre-treated with the samples and then treated with 2 mM H_2O_2. Then, the cell viability was measured by MTT. Particularly, the cells were seeded into 96-well plates (3T3 and HaCaT cells at 1×10^5 cells/mL, A431 cells at 5×10^4 cells/mL) and incubated with samples (10 µg/well) for 19 h. After their removal, 2 mM H_2O_2, a relatively stable ROS, was added to the pre-treated cells and control cells (positive control) for a further 3 h. Cells unexposed to samples and H_2O_2 were used as a negative control. Cell viability was assayed by MTT as described in section 3.5.1.2. The protective capacity (PC %) of each tested sample was calculated according to the following formula (4):

$$\text{PC (\%)} = \frac{\text{Cell viability in treated group} - \text{Cells viability in stressed control}}{\text{Cells viability in the stressed control}} \text{ x } 100 \qquad (4)$$

3.5.3. Antibacterial activity

Antibacterial activity was assayed by using eight bacterial strains typical of surfaces and skin. Microorganisms were *Bacillus subtilis* ATCC6633, *Staphylococcus epidermidis* ATCC12228, *Staphylococcus aureus* ATCC6538, *Listeria monocytogenes* ATCC15313, *Enterococcus faecalis* ATCC29212, *Escherichia coli* ATCC25922, *Acinetobacter baumannii* ATCC19606, and *Klebsiella aerogenes* ATCC13048. Antimicrobial activity was assessed *in vitro* using the determination of the minimum inhibitory concentration (MIC) values by the broth microdilution method [153,154]. Muller Hinton broth, prepared according to the manufacturer's instructions by dissolving 21 g of powder in 1 L of distilled water with a final pH of 7.3, was used as bacterial growth and dilution medium.

Initially, the free extract solutions were tested. Different dilutions of these samples in Muller Hinton broth were prepared to achieve a concentration range in the microtiter plates from 4 to 16000 μg/mL. 40 μL of the nutrient broth culture of each bacterial strain was added to achieve a final microorganism density of ca. 10^6 colony forming units/mL. Medium with and without bacterial inoculum was used as growth and sterility controls, respectively. The MIC value was determined as the lowest concentration of extract solution that inhibits visible growth of the microorganism in dilution wells after 24 h of incubation at 37 °C. The bacteria growth in the wells was confirmed also with resazurin, a deep blue-colored solution used as an indicator of cellular metabolic ability: resazurin solution (20 μL of 0.1 mg/mL) diffuses through cell membranes and it is metabolically reduced by viable cells to the pink-colored product, resorufin [155]. The MIC value and a higher concentration were plated on agar Muller Hinton plates. The plates were incubated for 24 h at 37 °C for the determination of the minimum bactericidal concentration (MBC) which is the lowest concentration that kills 99.9% of the inoculum.

4. Results

4.1. *Myrtus communis* L.

4.1.1. Quali-quantitative determination of phenolic compounds in the extract

The HPLC–DAD qualitative evaluation of the major phenolic compounds in the myrtle extract showed the purple myrtle berries' typical composition [86,156]. The most abundant polyphenolic compounds were anthocyanins (delphinidin, cyanidin, malvidin 3-*O*-glucosides, petunidin-3-*O*-glucoside, and peonidin-3-*O*-glucoside: 122.41 ± 0.10, 81.81 ± 1.60, 139.41 ± 1.40, 115.01 ± 1.60, and 84.61 ± 0.40 μg/L, respectively) and two flavonoids, myricetin derivatives (myricetin-3-*O*-galactoside and myricetin-3-*O*-rhamnoside: 208.60 ± 2.10 and 207.40 ± 3.30 μg/L, respectively) (Figure 8). Ellagic acid was also detected in the chromatogram at 280 nm (17.10 ± 1.20 μg/L), along with several galloyl derivatives, including gallic acid (87.50 ± 6.80 μg/L).

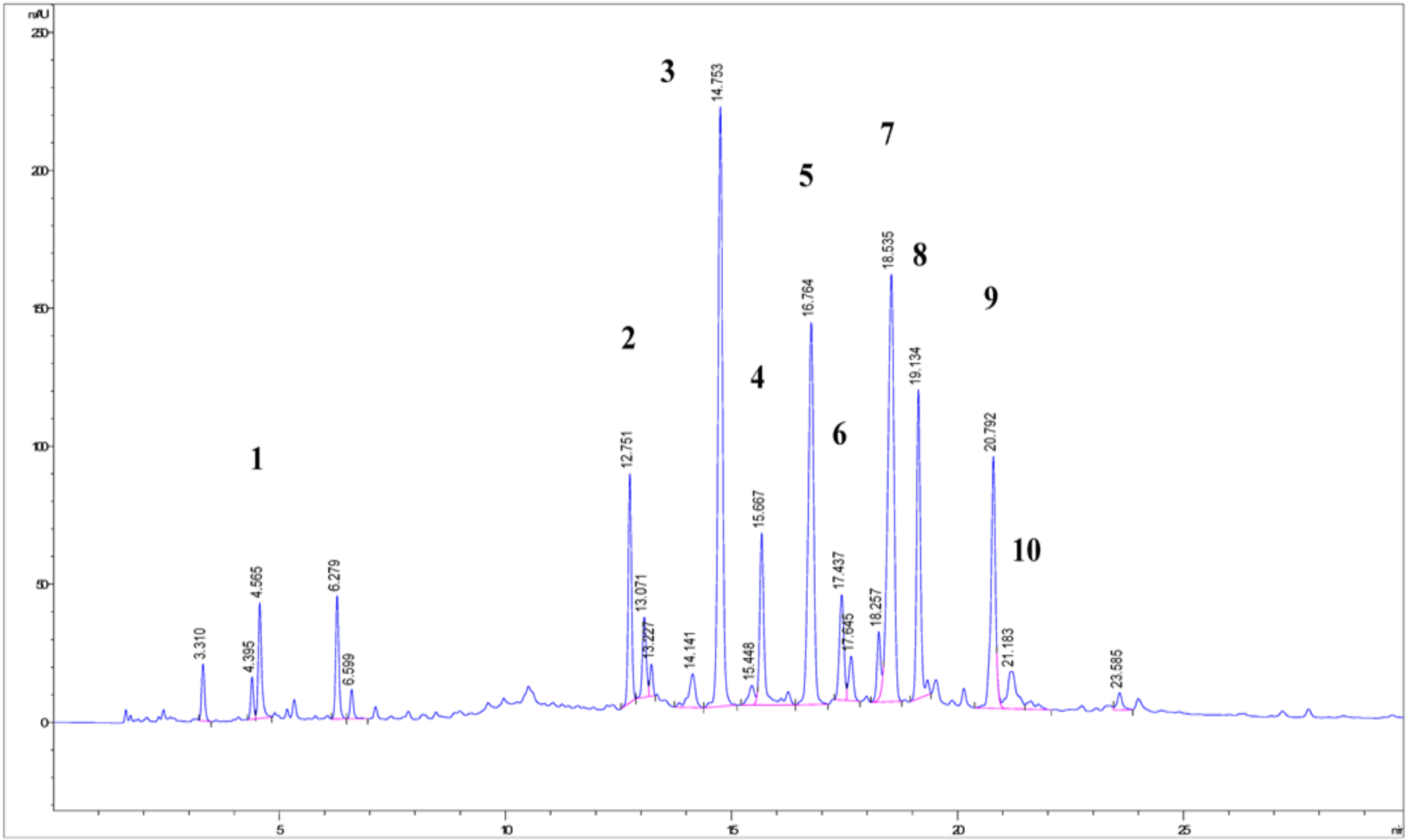

Figure 8. HPLC–DAD chromatogram of myrtle berry extract at λ = 280 nm. Chromatographic conditions are described in the text. Peaks identification is given in Table 7.

4.1.2. Vesicles characterization

Myrtle formulations were characterized in terms of mean diameter, polydispersity, and zeta potential through DLS and ELS measurements, shape and lamellarity through cryo-TEM observation, and efficiency encapsulation with direct measurements of many compounds though HPLC–DAD.

4.1.2.1. Size, zeta potential, and storage stability

The light-scattering results showed that the empty liposomes were 95 nm in diameter, monodispersed (PDI 0.20), and negatively charged (-10 mV). The extract's loading significantly increased the vesicles' mean diameter, although they remained small (around 100 nm), whereas the polydispersity index and zeta potential values were unaltered. The stability of the liposomal formulations was evaluated by monitoring the extract precipitation, the mean diameter, the polydispersity index, and the zeta potential during storage at 4 ºC. No signs of significant alterations were detected (Table 6).

	Liposomes		**Empty Liposomes**	
	Day 0	***Day 21***	***Day 0***	***Day 21***
Mean diameter (nm ± SD)	*102.00 ± 5.6	103.00 ± 1.00	95.00 ± 4.60	97.00 ± 3.90
Polidispersity index (± SD)	0.22 ± 0.02	0.21 ± 0.01	0.20 ± 0.03	0.22 ± 0.02
Zeta potential (mV ± SD)	-10.00 ± 0.80	-11.00 ± 0.70	-10.00 ± 1.10	-11.00 ± 1.20

*Table 6. Characteristics of myrtle formulations. Each value represents the mean ± SD (n> 10). * Values statistically different (p< 0.01) from empty liposomes at day 0.*

4.1.2.2. Morphology

The formation of vesicular structures characterized by their small size was confirmed by cryo-TEM observation. Figure 9 shows spherical, oligolamellar vesicles at around 100 nm in diameter, which aligns with the light scattering data.

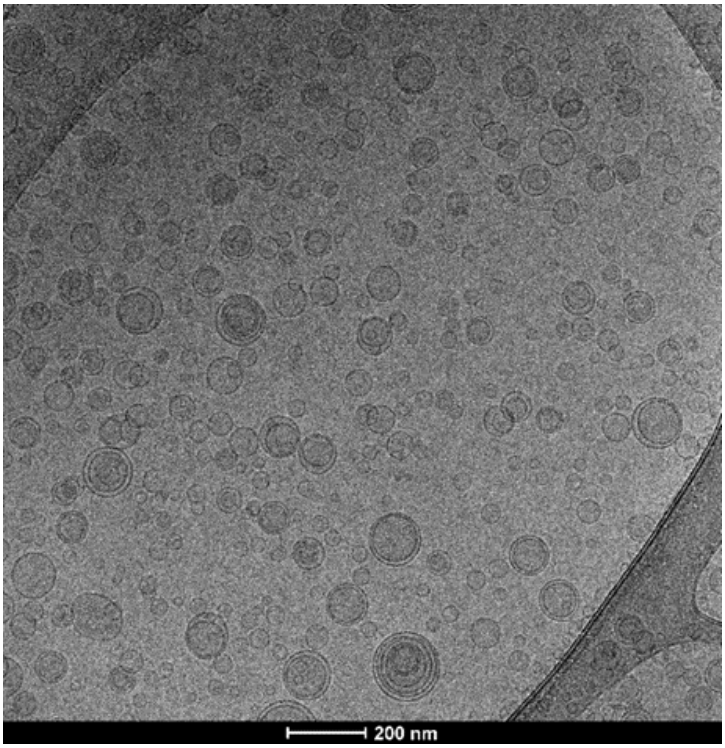

Figure 9. Myrtle liposomes through cryo-TEM observation.

4.1.2.3. Entrapment efficiency

The entrapment efficiency of the liposomes was calculated based on the amount of ten targeted phenolic compounds identified in the myrtle extract and detected in the dialyzed and non-dialyzed dispersions. The liposomes entrapped high amounts of extract; the entrapment efficiency was at least 71.4% (for myricetin-3-*O*-galactoside) and over 95% for most of the anthocyanins (Table 7).

Peaks	Compounds	EE %
1	Gallic acid	90.4 ± 0.7
2	Gallic acid derivative *	89.7 ± 1.2
3	Delphidin-3-*O*-glucoside	95.4 ± 0.6
4	Cyanidin-3-*O*-glucoside	96.2 ± 0.1
5	Petunidin-3-*O*-glucoside	96.8 ± 1.4
6	Peonidin-3-*O*-glucoside	96.9 ± 1.1
7	Malvidin-3-*O*-glucoside	85.5 ± 4.3
8	Myricetin-3-*O*-galactoside	71.4 ± 2.3
9	Myricetin-3-*O*-rhamnoside	84.0 ± 4.4

10	Ellagic acid	78.7 ± 5.3

*Table 7. Entrapment efficiencies (EE%) of the main phenolic compounds identified in myrtle extract. * Dosed with the calibration curve for gallic acid. Data are given as the mean ± SD (n= 4).*

4.1.3. Evaluation of biological activity

The safety of myrtle samples and their antioxidant power were tested. The colorimetric tests DPPH and FRAP showed that the prominent antioxidant activity of myrtle extract was retained after the nanoformulation. *In vitro* analyses of fibroblasts demonstrated the safety of myrtle liposomes at the tested doses and ROS-levels measurements confirmed the high antioxidant activity.

4.1.3.1. Biocompatibility – MTT

The absence of cytotoxic effects of the liposome formulations was evaluated using 3T3-L1 fibroblasts for viability after 5 and 24 h of exposure to increasing doses of myrtle extract (Figure 10). After 5 h, slight cytotoxicity (~10-20% mortality) was induced with all doses of the myrtle solution, even though it was not statistically significant compared with the untreated control cells. In contrast, this effect was not detected in the cells treated with myrtle liposomes, which appeared to prevent the inner toxicity of the myrtle extract. The same trend was observed after 24 h of treatments, confirming the positive impact of the nanoformulation.

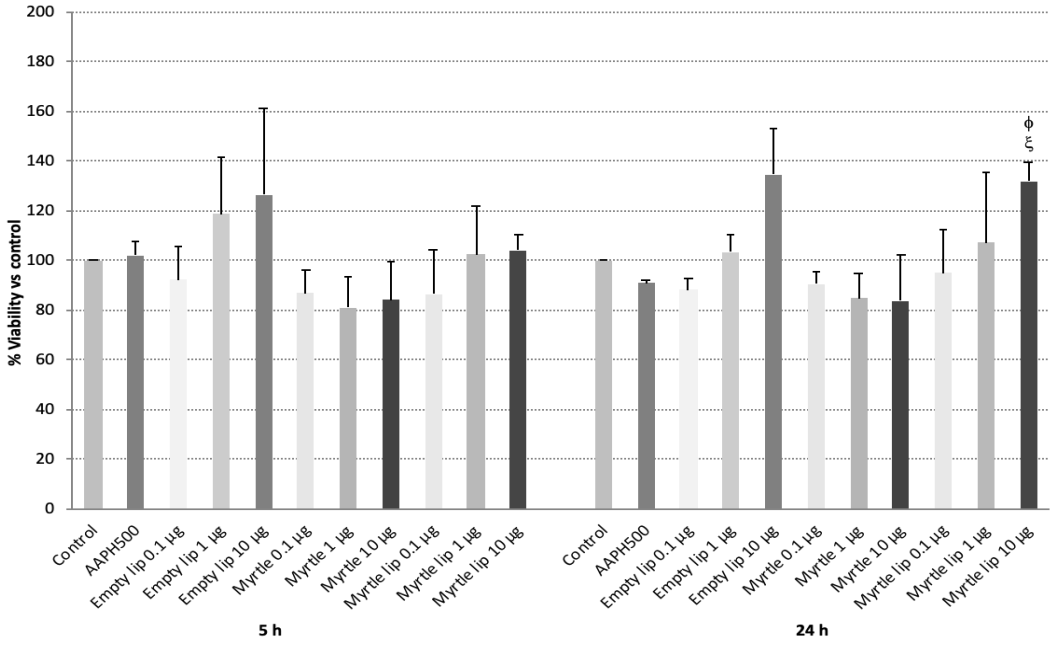

Figure 10. Viability of 3T3-L1 cells upon exposure to empty liposomes, myrtle solution, and myrtle liposomes for 5 h and 24 h. Data are expressed as means ± standard error (SE); n=3; φ $p<0.05$ vs. myrtle solution 1 µg; ξ $p<0.05$ vs. myrtle solution 10 µg. AAPH was tested for subsequent antioxidant tests.

4.1.3.2. Biocompatibility – endogenous ROS production

The safety of the myrtle liposomes was also assessed as the absence of endogenous ROS production. As shown in Figure 11, after 5 h of exposure to the formulations of fibroblasts, none of them induced the formation of free radicals. The values were statistically similar (p>0.05) to untreated control cells and statistically different (p<0.05-0.005) from cells treated with AAPH, a known radical generator. It must be pointed out that 500 μM AAPH induced a significant increase in ROS levels without affecting the viability of the cells compared to the control (Figures 10 and 11). After 24 h of exposure, the myrtle solution triggered ROS production to a slight extent, yet statistically different from control levels (p<0.05), and this effect was mitigated by the incorporation in liposomes (Figure 11).

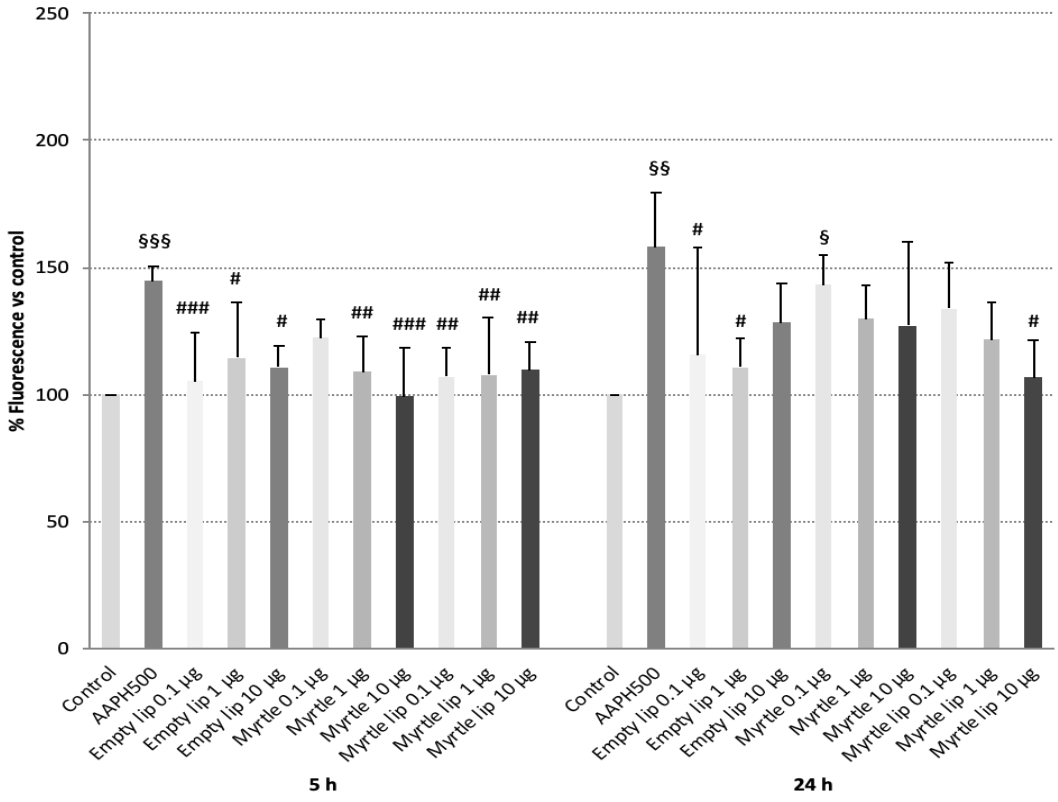

Figure 11. Effects of 500 μM AAPH, empty liposomes, myrtle solution, and myrtle liposomes on ROS production in 3T3-L1 cells after 5 and 24 h of incubation. Data are expressed as means ± SD; n=3. # p<0.05 vs. 500 μM AAPH; ## p<0.01 vs. 500 μM AAPH; ### p<0.005 vs. 500 μM AAPH; § p<0.05 vs. control (i.e., cells without AAPH); §§ p<0.01 vs. control; §§§ p<0.005 vs. control.

4.1.3.3. Antioxidant activity – DPPH, FRAP

The antioxidant activity of the myrtle formulations was estimated as a function of their radical scavenging and ferric reducing abilities (Table 8). 10 µL of the myrtle solution scavenged the DPPH radical completely (AA 96%), corresponding to 344 µg/mL of Trolox equivalents. Given the presence of phosphatidylcholine, empty vesicles possess a slight antioxidant activity (AA 39%). The level of antioxidant activity for the myrtle liposomes was slightly lower than the myrtle solution, with a statistically significant difference. Nevertheless, the antioxidant activity was greater than 90%, corresponding to 326 µg/mL of Trolox equivalents (Table 8).

The results of the FRAP assay showed that the myrtle solution had a reducing power corresponding of 1867 µg/mL of ferrous equivalents; myrtle liposomes displayed similar values, with no statistically significant differences. In addition, the empty liposomes showed a slight reducing power (Table 8).

	DPPH assay		**FRAP assay**
	AA (%)	***TE (µg Trolox equivalents/mL)***	***FE (µg Fe^{2+} equivalents/mL)***
Free extract solution	96.0 ± 1.4	344.0 ± 22.0	1867.0 ± 32.0
Lip	*91.0 ± 0.8	326.0 ± 17.0	1831.0 ± 70.0
Empty lip	39.0 ± 7.4	137.0 ± 19.0	602.0 ± 46.0

*Table 8. In vitro antioxidant activity of myrtle formulations. For the DPPH assay, results are expressed as AA (%) and TE (µg Trolox equivalents/mL solution); for the FRAP assay, results are expressed as FE (µg Fe^2 equivalents/mL solution) and reported as the mean ± SD of at least three separate experiments, each performed in triplicate. * statistically different values ($p<0.01$) from the myrtle solution.*

4.1.3.4. Antioxidant activity – reduction of chemical induced-ROS levels

The antioxidant activity of the myrtle formulations was analyzed in AAPH-stressed fibroblasts as a function of their ability to reduce ROS levels using DCFH-DA, a cell-permeable dye sensitive to the cellular redox state. In light of the results reported above on cell viability and endogenous ROS production, the higher dose of myrtle was evaluated (Figure 12).

After 5 h of treatment with the myrtle solution, a marked decrease in AAPH-induced ROS levels was detected ($p<0.05$ vs. 500 µM AAPH). When the myrtle extract was delivered using liposomes, a further reduction was apparent ($p<0.01$ vs. 500 µM AAPH), and the basal ROS levels were

restored (*p*=ns vs. control). Furthermore, the results displayed the contribution provided by the nanosystem to the antioxidant activity of the myrtle formulation. Given their phospholipid content, empty liposomes exerted a minimum anti-ROS effect (Figure 12), and their carrier capabilities facilitated the transport of the myrtle bioactive compounds through the cell membrane. This resulted in a superior efficacy of the liposomal formulation.

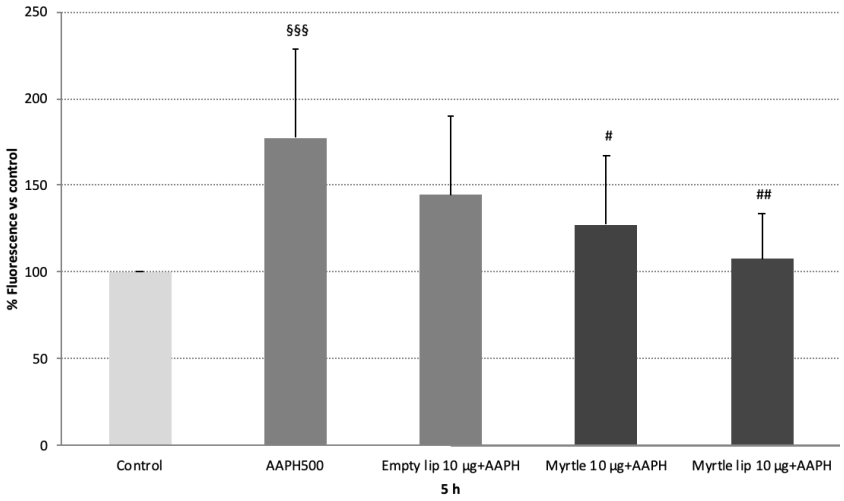

Figure 12. Anti-ROS effect of empty liposomes, myrtle solution, and myrtle liposomes on 3T3-L1 cells stressed with AAPH (500 μM). Data are expressed as means ± SD; n=3. §§§ p<0.005 vs. control (i.e., cells without AAPH); # p<0.05 vs. 500 μM AAPH; ## p<0.01 vs. 500 μM AAPH.

The evaluation of cell morphology confirmed these results. Figure 13 shows a slight reduction in the number of cells in cells treated with the myrtle solution, similar to what was observed in AAPH-stressed cells. In contrast, the AAPH-stressed cells treated with myrtle liposomes displayed features similar to non-stressed control cells.

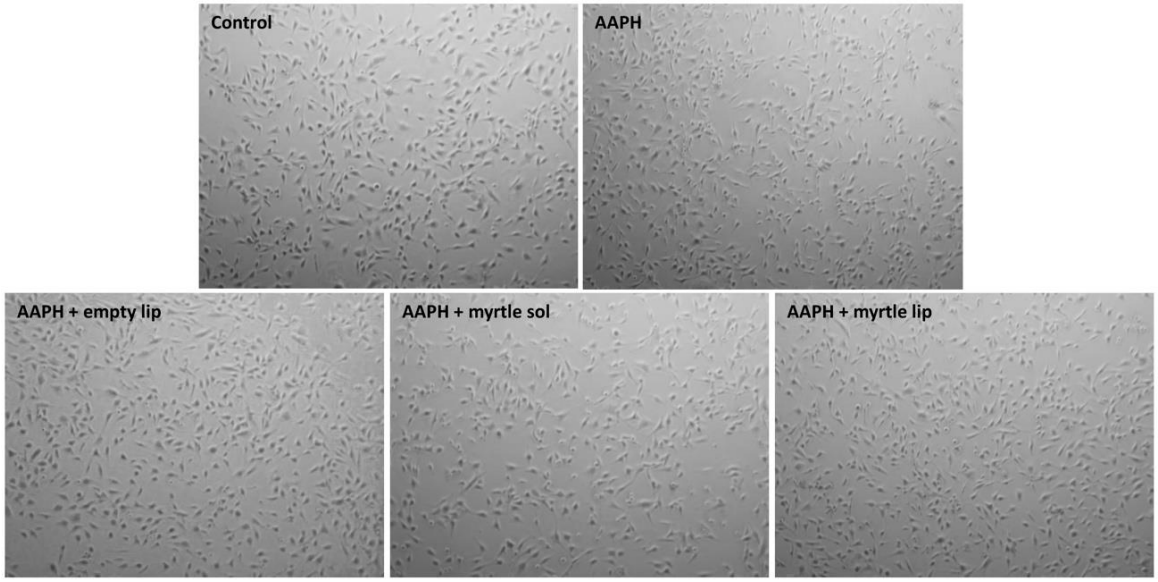

Figure 13. Representative microscope images of untreated 3T3-L1 cells in comparison with cells stressed with 500 μM AAPH or stressed with AAPH and treated with empty liposomes, myrtle solution, and myrtle liposomes for 5 h.

4.2. *Prunus spinosa L.*

4.2.1. Quali-quantitative determination of phenolic compounds in the extract

The extract obtained from *P. spinosa* fruits was qualitatively analysed by (HR) LC-ESI-QTOF MS/MS in negative ion mode, and targeted phenolic compounds were quantified by HPLC-DAD analysis.

The negative LC-MS profile highlighted the presence of a large group of compounds corresponding to the deprotonated molecular ions of different phenolic derivatives, mainly hydroxycinnamic acid and flavonoid derivatives (Figure 14). Individual components were identified by comparison of their *m/z* values in the total compound chromatogram (TCC) profile with those described in the literature (Table 9). Moreover, by comparing experimental MS/MS spectra with fragmentation patterns reported in the literature for the same analytes or with the fragmentation patterns and spectra reported in a public repository of mass spectral data [143,157], 24 compounds were identified. Table 9 reports the identified compounds, listed according to their retention times, the chemical formula derived by accurate mass measurement, MS/MS results, the references used for identification and the identification confidence levels [158].

Compounds **2-5** and **9-12** were identified as hydroxycinnamic derivatives. Peaks **2** and **5** were identified as caffeoylquinic acid isomers, due to the $[M-H]^-$ at *m/z* 353.0885 and a fragment at *m/z* 191.0532 (loss of a quinic acid unit) [159,160]. By comparison with pure standards, the two peaks were attributed to 3-*O*-caffeoylquinic acid (neochlorogenic acid) and 5-*O*-caffeoylquinic acid (chlorogenic acid), respectively. Peaks **3** and **9** were tentatively attributed to coumaroylquinic acids due to the $[M-H]^-$ at *m/z* 337.0940, and more precisely peak **3** to 3-*p*-coumaroylquinic acid for the characterizing fragment at *m/z* 163.0403 [159,160], and peak **9** to 4-*p*-coumaroylquinic acid for the characterizing fragment at *m/z* 173.0461 [159,160]. Peak **4**, with $[M-H]^-$ *m/z* 367.1043 and a fragment at *m/z* 193.0516, was tentatively attributed to 3-*O*-feruloylquinic acid [159,160]. Compounds **10** and **11**, with $[M-H]^-$ *m/z* 335.0773 corresponding to $C_{16}H_{16}O_8$, and MS/MS product ions at *m/z* 179.0352, 135.0448, and 161.0247, were tentatively attributed to caffeoylshikimate isomers [161]. Peak **12**, with $[M-H]^-$ *m/z* 381.1186 and a fragment at *m/z* 161.0246, was tentatively attributed to ethyl caffeoylquinate (ethyl chlorogenate) [162]. These last three compounds were not previously detected in *P. spinosa* fruits.

Table 10 reports the quantitative data of targeted phenolic compounds detected in *P. spinosa* extract. 3-*O*-caffeoylquinic (neochlorogenic) acid was the most represented hydroxycinnamic derivative and phenolic compound as well (2.38 ± 0.02 mg/g), followed by other quinic acid derivatives, such as 3-*p*-coumaroylquinic acid (0.13 ± 0.00 mg/g), 5-*O*-caffeoylquinic (chlorogenic) acid (0.13 ± 0.00 mg/g), and 3-*O*-feruoilquinic acid (0.07 ± 0.00 mg/g).

Other two compounds (**1** and **6**), not previously detected in *P. spinosa* fruits, were tentatively attributed to benzyl and benzoic derivatives. Compound **1**, with $[M-H]^-$ *m/z* 329.0877 and a fragment at *m/z* 167.0349, was tentatively attributed to vanillic acid-*O*-glucopyranoside [163]. This compound was the only hydroxybenzoic acid dosed by HPLC-DAD, and its amount was 0.12 ± 0.00 mg/g (Table 10). Compound **6**, with $[M-H]^-$ *m/z* 461.1302 and a fragment at *m/z* 121.0295, was tentatively attributed to a hydroxybenzoyl-hexosyl-hexoside compound [164]. Compounds **7** and **8**, with $[M-H]^-$ *m/z* 447.1508 corresponding to $C_{19}H_{28}O_{12}$ and two characterizing fragment at *m/z* 71.0141 and 101.0242, were tentatively attributed to isomeric forms of barlerin (8-*O*-acetylshanzhiside methyl ester) [165], an iridoid already detected in *P. spinosa* leaves [166].

Compounds **13-24** were identified as flavonoid derivatives, namely glycosides derivatives of quercetin, by the diagnostic $[M-H]^-$ ions shown in (HR) ESI-MS and MS/MS analysis in negative ion mode, compared with literature data. By comparison with pure standards, compounds **14**, **15** and **22** were attributed to quercetin-3-*O*-rutinoside (rutin), quercetin-3-*O*-glucoside and quercetin-3-*O*-rhamnoside (quercitrin), respectively. These compounds were previously reported in *P. spinosa* fruits [159,160]. Interestingly, other two compounds (**13** and **21**) showed the same $[M-H]^-$ at *m/z* 609.1458 corresponding to $C_{27}H_{30}O_{16}$ and the two characterizing fragments at *m/z* 300 and 301 of quercetin-3-*O*-rutinoside. Thus, compounds **13** and **21** were tentatively attributed to quercetin disaccharides derivatives containing rhamnose and a hexose [159,160]. Compound **17** showed a fragmentation pattern very similar to that of quercetin-3-*O*-glucoside: comparison with quercetin-3-*O*-galactoside retention time excluded the hypothesis that it could be this compound, and it was attributed to a quercetin hexoside. Compound **16**, with $[M-H]^-$ *m/z* 595.1303 and a fragment at *m/z* 121.0295, was tentatively attributed to a quercetin disaccharides derivative containing a pentoxide (probably xylose or arabinose) and a hexose (probably glucose or galactose), as previously reported by Guimarães et

al. [160] and Mikulic-Petkovsek [159]. Compounds **18**, **19** and **20**, with the same $[M-H]^-$ at *m/z* 433.0773 corresponding to $C_{22}H_{18}O_{11}$, were attributed to different quercetin pentosides, and quercetin 3-*O*-arabinoside (guaijaverin or reinutrin) was previously detected in *P. spinosa* fruits [159,160]. Finally, compounds **23** and **24,** with $[M-H]^-$ at *m/z* 505.0992 and $[M-H]^-$ at *m/z* 651.1561 corresponding to $C_{23}H_{22}O_{13}$ and $C_{29}H_{32}O_{17}$, respectively, were attributed to acetyl derivatives of quercetin hexoside (**23**) and quercetin hexosyl-rhamnoside (**24**). These two compounds were already identified by Guimarães et al.[160].

Quercetin-3-*O*-rutinoside (**14**) was the most abundant flavonol (0.74 ± 0.00, mg/g), followed by quercetin-3-*O*-rhamnoside and quercetin-3-*O*-glucoside (Table 10). The sum of quercetin pentosides (0.49 ± 0.03 mg/g) accounted for 37% of total flavanols, with compound **20** contributing for 60% of this amount. These findings were in accordance with literature data, where high amounts of quercetin-3-*O*-rutinoside and quercetin pentosides were detected in *P. spinosa* extracts [160].

HPLC-DAD analysis showed the presence of four anthocyanins that were not detected by (HR) LC-ESI-QTOF MS/MS in negative mode (Figure 15). The four anthocyanins (**A1**, **A2**, **A3** and **A4**) were identified by comparison with literature data [159,160] and pure standards, and resulted to be cyanidin-3-*O*-rutinoside, cyanidin-3-*O*-glucoside, peonidin-3-*O*-rutinoside, and peonidin-3-*O*-glucoside, respectively. The most abundant anthocyanin was cyanidin-3-*O*-rutinoside (0.74 ± 0.03 mg/g), followed by peonidin-3-*O*-rutinoside and cyanidin-3-*O*-glucoside with very similar amounts (0.44 ± 0.01 and 0.43 ± 0.01 mg/g, respectively), and finally peonidin-3-*O*-glucoside (0.11 ± 0.00 mg/g) (Table 10).

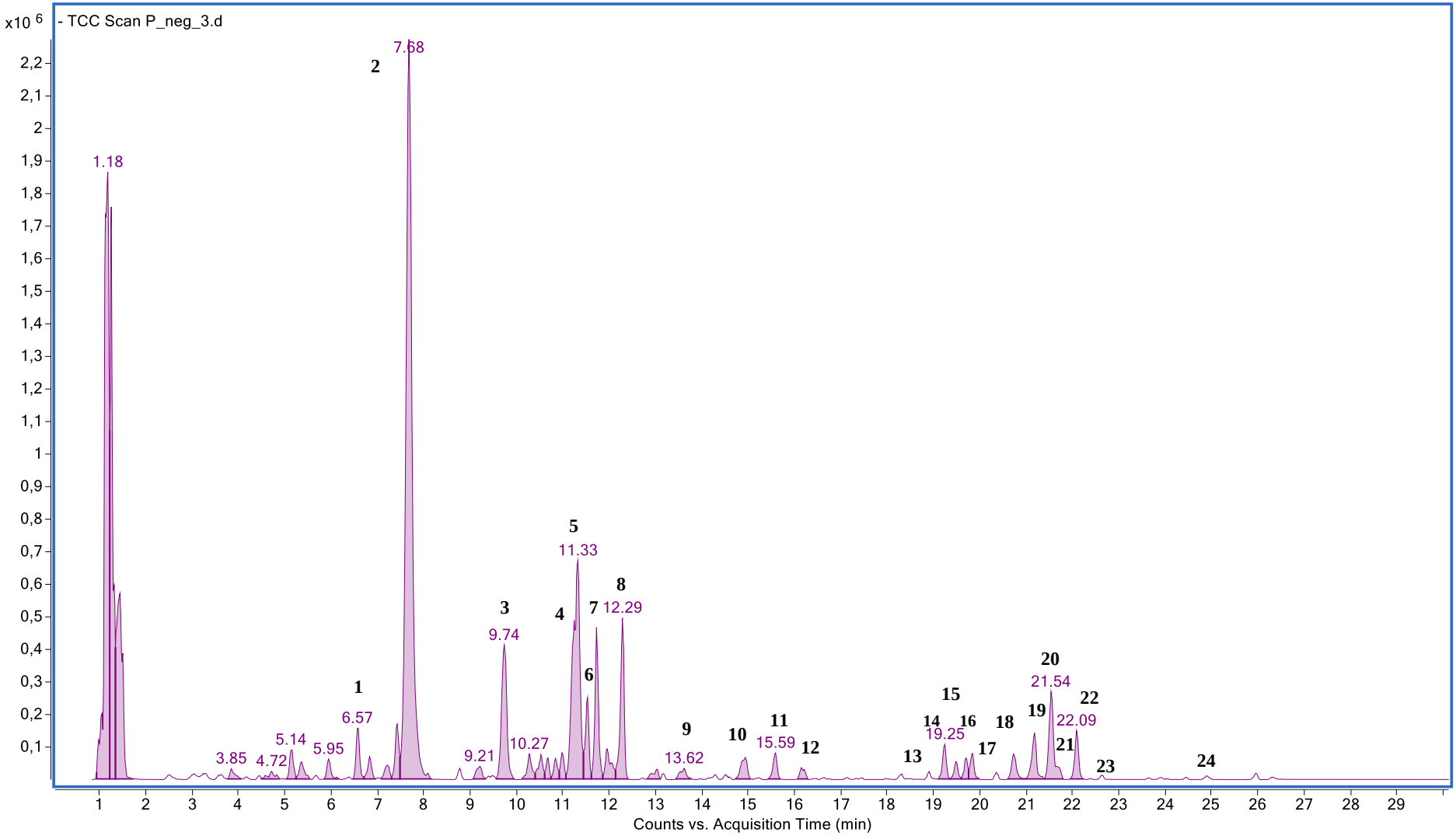

Figure 14. (HR) LC-ESI-Orbitrap MS Total Compound Chromatogram of P. spinosa fruit extract acquired in negative ion mode. Chromatographic conditions are described in the text. Peaks identification is given in Table 9.

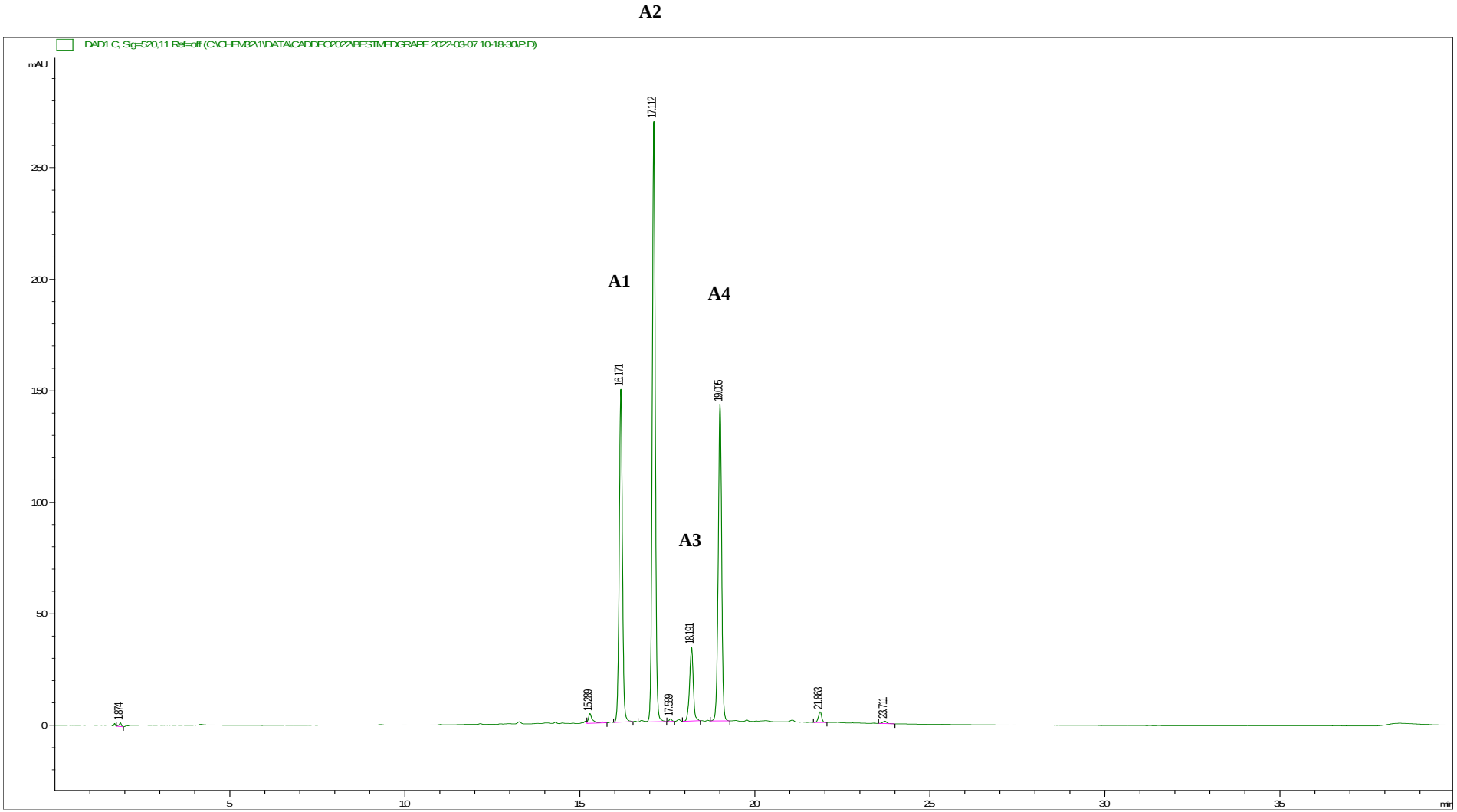

Figure 15. HPLC-DAD chromatogram of P. spinosa fruit extract at λ = 520 nm. Chromatographic conditions are described in the text. Peak identification is given in Table 10.

Compound n°	Rt min	Identity	[M-H]$^-$ *m/z*	molecular formula	Δ ppm	MS/MS* *m/z*	References	Level$^\#$
1	6.59	vanillic acid-*O*-glucopyranoside	329.0877	$C_{14}H_{18}O_9$	-0.2134	167.0349(100)	[163]	2
2	7.68	3-*O*-caffeoylquinic acid	353.0885	$C_{16}H_{18}O_9$	-0.3257	179.0353(53)/191.0563(100)	[159,160,163]	1
3	9.74	3-*p*-coumaroylquinic acid	337.0940	$C_{16}H_{18}O_8$	-0.2511	163.0403(100)/119.0504(48)	[159,160,163]	2
4	11.18	3-*O*-feruloylquinic acid	367.1043	$C_{17}H_{20}O_9$	-0.4858	193.0516(100)/134.0372(77)	[159,160,163]	2
5	11.33	5-*O*-caffeoylquinic acid	353.0884	$C_{16}H_{18}O_9$	0.5943	179.0347(55)/191.0561(100)	[160,163]	1
6	11.55	hydroxybenzoyl-hexosyl-hexoside	461.1302	$C_{19}H_{26}O_{13}$	-0.4844	121.0295(100)	[163,164]	3
7	11.73	barlerin isomer I	447.1508	$C_{19}H_{28}O_{12}$	-0.7799	71.0141(100)/101.0242(41)	[163,165]	3
8	12.29	barlerin isomer II	447.1508	$C_{19}H_{28}O_{12}$	-0.7799	101.0242(100)/ 71.0146(46)	[163,165]	3
9	13.62	4-*p*-coumaroylquinic acid	337.0940	$C_{16}H_{18}O_8$	-0.2511	173.0461(100)/163.0403(32)	[159,160,163]	2
10	14.94	caffeoylshikimic acid isomer I	335.0773	$C_{16}H_{16}O_8$	0.0590	179.0352(100)/135.0448(75)/161.0247(43)	[161,163]	3
11	15.59	caffeoylshikimic acid isomer II	335.0773	$C_{16}H_{16}O_8$	0.1590	161.0247(100)/135.0448(20)/179.0339(15)	[161,163]	3
12	16.21	ethyl caffeoylquinate	381.1186	$C_{18}H_{22}O_9$	-0.5058	161.0246(100)	[162,163]	3
13	18.89	quercetin hexosyl-rhamnoside	609.1468	$C_{27}H_{30}O_{16}$	0.6916	300.0272(100)/301.0344(39)/343.0440(21)	[160,163]	2
14	19.25	quercetin-3-*O*-rutinoside	609.1458	$C_{27}H_{30}O_{16}$	-0.3084	300.0269(100)/301.0342(60)/343.0458(17)	[159,160,163]	1
15	19.48	quercetin-3-*O*-glucoside	463.0886	$C_{21}H_{20}O_{12}$	0.4004	300.0270(100)/301.0322(41)	[159,160,163]	1
16	19.70	quercetin pentosyl-hexoside	595.1303	$C_{26}H_{28}O_{16}$	-0.1584	300.0280 (100)/301.0322(15)/415.0632(12)	[159,160,163]	2
17	19.83	quercetin hexoside	463.0879	$C_{21}H_{20}O_{12}$	-0.2996	300.0260(100)/301.0363(37)	[160,163]	2

18	20.73	quercetin pentoside	433.0773	$C_{20}H_{18}O_{11}$	-0.3349	300.0277(100)/301.0366(37)	[160,163]	2
19	21.18	quercetin pentoside	433.0779	$C_{20}H_{18}O_{11}$	-0.3249	300.0280(100)	[159,163]	2
20	21.54	quercetin pentoside	433.0784	$C_{20}H_{18}O_{11}$	0.7651	300.0274(100)/301.0354(72)	[159,163]	2
21	21.68	quercetin hexosyl-rhamnoside	609.1457	$C_{27}H_{30}O_{16}$	-0.4084	301.0360(100)/300.0255(98)	[159,163]	2
22	22.09	quercetin-3-*O*-rhamnoside	447.1006	$C_{21}H_{20}O_{11}$	0.0427	300.0267(100)/301.0351(71)	[159,160,163]	1
23	22.63	quercetin acetyl hexoside	505.0992	$C_{23}H_{22}O_{13}$	0.3318	300.0261(100)/271.0227(30)	[160,163]	2
24	25.96	quercetin acetyl hexosyl-rhamnoside	651.1561	$C_{29}H_{32}O_{17}$	-0.5137	301.0349(100)/300.0267(50)/609.1430(15)	[160,163]	2

Table 9. Compounds identification by (HR) LC-ESI-QTOF MS/MS in P. spinosa fruit extract. [*] *in brackets the relative intensity;* [#] *according to Blaženović, 2018* [158].

Compound	Peak	*P. spinosa* L. extract (mg/g dr)	
		Mean	± SD
Total Anthocyanins		**1.72**	**0.05**
cyanidin-3-*O*-glucoside	A1	0.43	0.01
cyanidin-3-*O*-rutinoside	A2	0.74	0.03
peonidin-3-*O*-glucoside	A3	0.11	0.00
peonidin-3-*O*-rutinoside	A4	0.44	0.01
Total Flavonols		**1.33**	**0.01**
quercetin-3-*O*-rutinoside	14[§]	0.31	0.00
quercetin-3-*O*-glucoside	15[§]	0.06	0.00
quercetin-3-*O*-rhamnoside	22[§]	0.12	0.00
quercetin pentosides [a]	(18, 19, 20) [§]	0.49	0.00
Other quercetin derivatives [a]	(13,16,17,21,23,24) [§]	0.35	0.00
Total Hydroxycinnamic acids		**2.72**	**0.02**
3-*O*-caffeoylquinic acid	2[§]	2.38	0.02
3-*p*-coumaroylquinic acid [b]	3[§]	0.13	0.00
3-*O*-feruoilquinic acid [c]	4[§]	0.07	0.00
5-*O*-caffeoylquinic acid	5[§]	0.13	0.00
Total Hydroxybenzoic acids		0.12	0.00
vanillic acid-*O*-glucopyranoside [d]	1[§]	0.12	0.00
Total polyphenols		**5.92**	**0.08**

Table 10. Concentration of targeted phenolic compounds detected in P. spinosa extract (mg/g of dried extract (dr), mean ±SD; n = 3). [a] expressed as quercetin-3-O-glucoside equivalents; [b] expressed as p-coumaric acid equivalents; [c] expressed as ferulic acid equivalents; [d] expressed as vanillic acid equivalents; [§] peak number as reported in Table 9.

4.2.2. Vesicles characterization

Blackthorn extract formulations were characterized in terms of mean diameter, polydispersion, and zeta potential through DLS and ELS measurements. A deeper structural characterization was realized through SAXS analyses, while entrapment efficiency was calculated by direct measurements of some phenolic compounds through HPLC–DAD analysis.

4.2.2.1. Size, zeta potential, and storage stability

For blackthorn extract formulations, the liposomes' mean diameter was less than 100 nm, significantly larger than their corresponding empty vesicles, although both appeared monodispersed and negatively charged (Tab. 11). The addition of PG to the formulation, produced vesicles significantly smaller in diameter than liposomes (86 *vs* 94 nm), but with similar

characteristics of polydispersity and surface charge (Tab. 11). Also for PEVs, the extract's loading significantly increased the vesicles' mean diameter, keeping unaltered polydispersity and zeta potential values (Tab. 11).

The stability of the lipid formulations was evaluated by monitoring the possible extract precipitation, the mean diameter, the polydispersity index, and the zeta potential during storage at 4ºC. No signs of significant alterations were detected after 1 month of storage (Table 11).

	Lip		**Empty Lip**	
	Day 0	***Day 30***	***Day 0***	***Day 30***
Mean diameter (nm ± SD)	*94.00 ± 2.00	96.00 ± 1.50	70.00 ± 2.60	74.00 ± 5.00
Polidispersity index (± SD)	0.19 ± 0.01	0.19 ± 0.01	0.19 ± 0.03	0.17 ± 0.01
Zeta potential (mV ± SD)	-48.00 ± 1.40	-44.00 ± 2.70	-46.00 ± 2.30	-48.00 ± 2.90

	PEVs		**Empty PEVs**	
	Day 0	***Day 30***	***Day 0***	***Day 30***
Mean diameter (nm ± SD)	*,**86.00 ± 6.40	98.00 ± 6.70	59.00 ± 3.30	64.00 ± 0.80
Polidispersity index (± SD)	0.21 ± 0.02	0.19 ± 0.03	0.21 ± 0.03	0.19 ± 0.01
Zeta potential (mV ± SD)	-47.00 ± 1.70	-46.00 ± 0.40	-47.00 ± 1.10	-47.00 ± 2.40

*Table 11. Characteristics of blackthorn formulations. Each value represents the mean ± SD (n> 10). * Values statistically different (p< 0.01) from corresponding empty vesicles. ** Values statistically different (p< 0.05) from liposomes.*

4.2.2.2. Entrapment efficiency

Nine phenolic compounds identified in *P. spinosa* extract were quantified in the non-dialysed and dialysed formulations and used to determine the entrapment efficiency (Table 12). Liposomes gave higher values than PG-PEVs with entrapment efficiencies >96% and >82% for anthocyanins and for flavonols, respectively. Interestingly, although hydroxycinnamic acids were highly represented in the extract, they were entrapped into the vesicles with less efficiency. This selectivity could be related to the hydrophilicity/polarity of compounds.

Peak	Compound	EE % ± SD	
		Lip	***PEVs***
2	3-*O*-caffeoylquinic acid	33.6 ± 3.4	24.2 ± 1.4
4	3-*O*-feruoilquinic acid[a]	35.3 ± 4.3	28.2 ± 1.7
5	5-*O*-caffeoylquinic acid	38.0 ± 3.4	28.2 ± 1.5
A1	cyanidin-3-*O*-glucoside	98.6 ± 0.9	84.9 ± 1.7
A2	cyanidin-3-*O*-rutinoside	96.3 ± 0.9	74.4 ± 1.7
A4	peonidin-3-*O*-rutinoside	97.0 ± 0.5	77.4 ± 0.9
14	quercetin-3-*O*-rutinoside	82.6 ± 6.1	64.5 ± 3.2
15	quercetin-3-*O*-glucoside	85.1 ± 7.8	72.8 ± 1.7
20	quercetin pentoside [b]	87.5 ± 7.5	70.7 ± 4.8

Table 12. Entrapment efficiencies (EE%) of the main phenolic compounds identified in blackthorn extract. [a] expressed as ferulic acid equivalents; [b] expressed as quercetin-3-O-glucoside equivalents. Data are given as mean ± standard deviation (n = 4).

4.2.2.3. Morphology

The formation of vesicular structures characterized by their small size was confirmed by cryo-TEM observation, for PEVs. Figure 16 shows spherical and elongated unilamellar vesicles at around 100 nm in diameter, which aligns with the light scattering data.

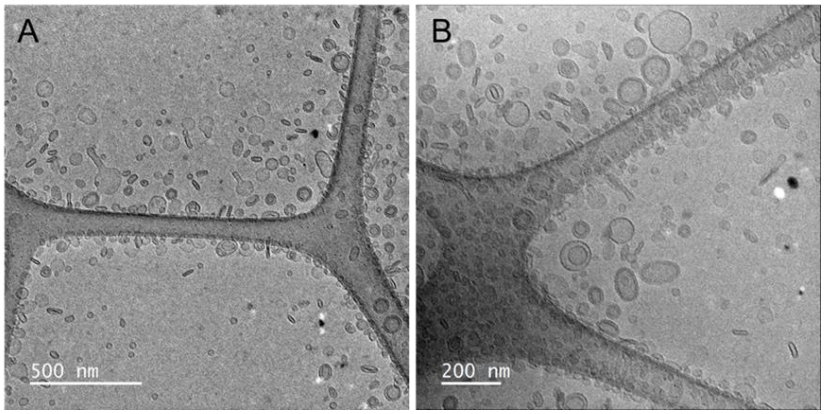

Figure 16. Cryo-TEM images of P. spinosa PG-PEVs. Two magnifications are shown: 15,000 x (A) and 20,000 x (B).

4.2.2.4. Small-Angle X-ray Scattering

Further insights into the morphology and lamellar arrangement of the vesicles were gained by SAXS, a well-established technique for the study of self-assembling nanostructures. The SAXS patterns of conventional liposomes and PG-PEVs are shown in Fig. 17 and 18, together with the fits of the lamellar model, and suggest that the electronic density profile was typical of bilayers as described in the literature. The main parameters obtained from the fits are listed in Table 13.

All the vesicles were unilamellar structures (N=1).

Z_H, that is the distance between the polar heads and the bilayer centre, slightly increased with extract loading, especially in liposomes; there were no differences between PEVs with or without extract, but the presence of PG reduced Z_H value compared with conventional liposomes.

The polar head region dimension, expressed by σ_H, slightly increased in liposomes with extract loading. The PG in PEVs increased σ_H value compared with liposomes, but there were no differences between empty or loaded PG-PEVs.

σ_C, related to the segregation of terminal methyl groups at the centre of bilayer, seemed to increase with extract loading in liposomes and to be unaffected in PEVs. Although mathematically different, the effect of these values is similar, and can be explained by the lack of a minimum in the Gaussian profile: high or low values both correspond to the lack of segregation. However, it must be considered that the value of χ^2, the parameter indicating the similarity of the fit used for the sample (must be close to 1) was 6.36, 5.07, 3.42, and 3.72 respectively for liposomes, empty liposomes, PEVs, and empty PEVs (worse than for the other cases).

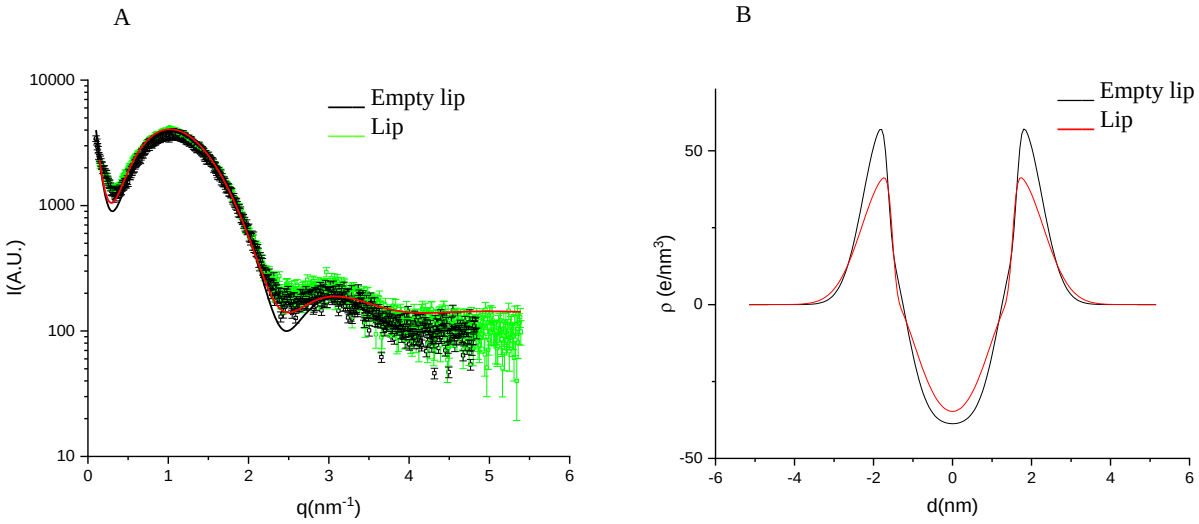

Figure 17. (A) SAXS profiles of empty and P. spinosa loaded liposomes. The lines correspond to the best fit of Gaussian bilayer models. (B) Electron density profiles corresponding to the best fits of empty and P. spinosa loaded liposomes.

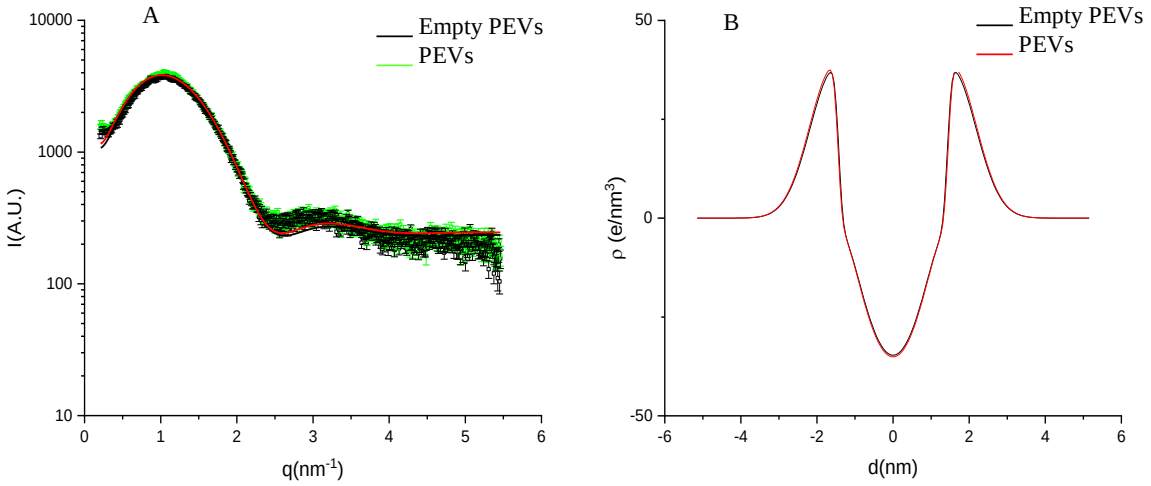

Figure 18. (A) SAXS profiles of empty and P. spinosa loaded PEVs. The lines correspond to the best fit of Gaussian bilayer models. (B) Electron density profiles corresponding to the best fits of empty and P. spinosa loaded.

	Lip	**Empty lip**	**PEVs**	**Empty PEVs**
χ^2	6.36	5.07	3.42	3.72
N	1.00	1.00	1.00	1.00
Z_H *(Å)*	18.40 ± 0.50	17.27 ± 0.50	15.49 ± 0.50	15.29 ± 0.50
σ_H *(Å)*	5.91 ± 0.50	5.30 ± 0.50	6.43 ± 0.50	6.47 ± 0.50
σ_C *(Å)*	17.73 ± 10.00	$4.62 * 10^{-5}$ ± 1.00	$4.27 * 10^{-4}$ ± 1.00	$4.27 * 10^{-4}$ ± 1.00

Table 13. Selected fitting parameters and derived parameters for SAXS curves of P. spinosa formulations.

4.2.3. Evaluation of biological activity

Initially, the biocompatibility of blackthorn samples was determined through the hemolytic activity evaluation on erythrocytes, and then through the absence of cytotoxic effects on skin layer cells. The antioxidant activities were tested through DPPH test; it was not possible to assay blackthorn samples with FRAP test for solubility problems in the reagent. Moreover, the antioxidant power was studied as the capacity to reduce H_2O_2 induced oxidative stress on fibroblasts and keratinocytes. In addition, the antibacterial power of *P. spinosa* extract was assayed.

4.2.3.1. Biocompatibility – hemolityc activity

Initially, the free extract solution was tested from 200 to 2000 µg/mL and no relevant activity was seen (data not shown). For this reason, two high concentrations (1 and 2 mg/mL) were assayed for each sample.

The intrinsic turbidity of the nanoformulations dispersed in PBS buffer complicated the interpretation of the results. However, all samples showed a clear, low erythrocyte-disrupting ability: although the samples dissolved in the buffer showed an initially whitish aspect, after the treatment the erythrocytes harvested had still a red coloration indicating that most of the cells were intact (Fig. 19).

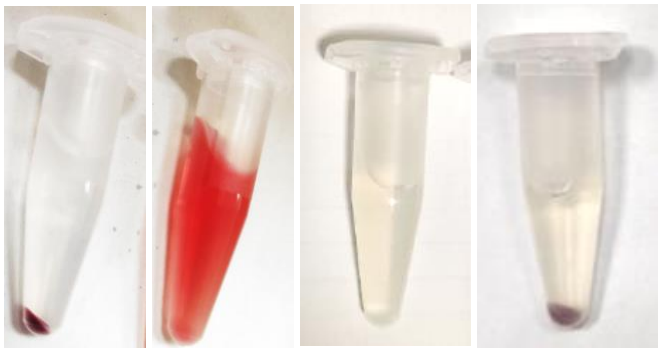

Figure 19. Appearance of some assayed samples. In order from left, control 0% haemolysis, control 100% haemolysis, nanoformulated extract without erythrocytes, and nanoformulated extract with erythrocytes.

The hemolytic activity was lower than 3% for each tested sample and the results are shown in Table 14.

At the concentration of 1 mg/mL, each sample tested showed a hemolytic activity less or equal to 2%, but the differences were not statistically significant between free and nanoformulated forms.

At the concentration of 2 mg/mL, the hemolytic activity of the free extract was 2.6% approximately; this value was lowered to 1.2% for the liposomal form (not statistically significant) and to 0.7% for PG-PEVs with statistical significance.

For both concentration, empty vesicles had a hemolytic activity approximately between 0.5 – 1.0 %.

	Hemolysis (% ± SD)	
Sample\Concentration	*1 mg/mL*	*2 mg/mL*
Free extract	2.00 ± 0.32	2.61 ± 0.71
Lip	0.66 ± 0.46	1.20 ± 0.62
Empty lip	0.51 ± 0.46	* 0.47 ± 0.19
PEVs	0.66 ± 0.52	* 0.65 ± 0.06
Empty PEVs	1.01 ± 0.02	* 0.74 ± 0.07

*Table 14. Hemolytic activity of P. spinosa L. nanoformulations. Data are expressed as means ± standard deviation (SD); n = 3; * p < 0.05 vs. free extract solution 2 mg/mL.*

Moreover, some results found in the literature, although regarding aqueous extract obtained from in *P. spinosa* berries, highlighted a hemolysis inhibition on human erythrocytes when in oxidative stress condition [96] and an inhibition capacity of the oxidative hemolysis on cells blood from healthy sheep [97].

4.2.3.2. Biocompatibility - MTT

The blackthorn extract in the free form had not shown any toxicity at all the concentrations and in all the cell lines tested (Fig. 20, 21, 22).

For 3T3 fibroblasts, the value of cell viability was similar between the free extract and nanoformulated forms (liposomes or PEVs), with some statistically relevant differences between the concentrations tested (Fig. 20), and not statistically different from control cells (100% viability; Fig. 20). For the empty formulations, a different trend between liposomes and PEVs was observed: for high concentrations (> 10 µg in the well), empty liposomes were toxic, while empty PEVs showed high values of cells viability also for high concentrations (Fig. 20).

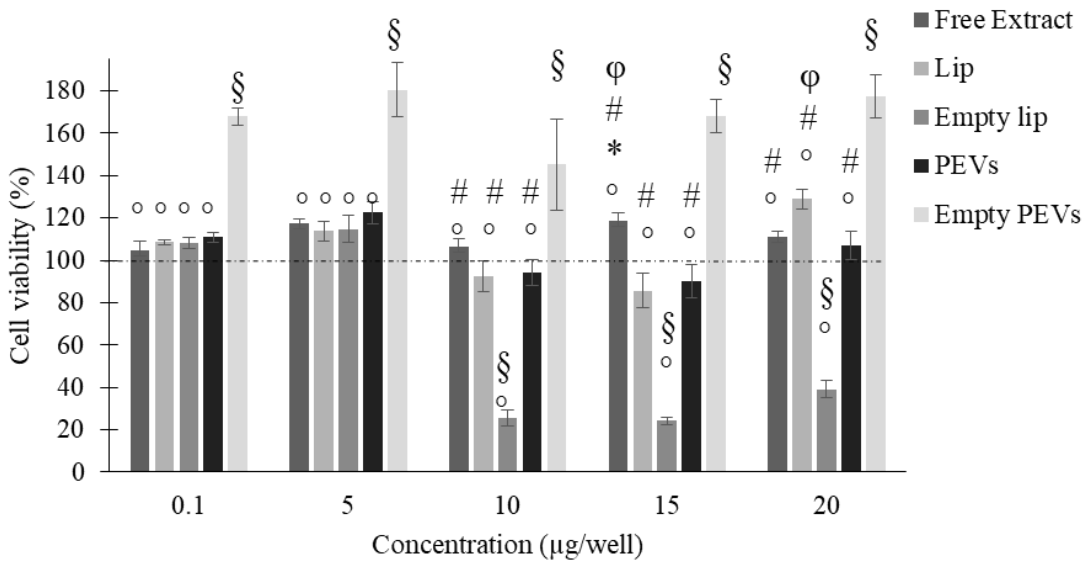

*Figure 20. Viability of 3T3 upon exposure to P. spinosa samples for 24 h. Data are expressed as means ± standard error (SE); n=2 independent experiments; § p<0.01 vs. control group (cells untreated, 100% viability, not shown in the graph); * p<0.05 vs lip; # p<0.01 vs. empty lip; ° p<0.01 vs. empty PEVs; φ p<0.05 vs PEVs.*

In the case of normal HaCaT keratinocytes, there were no relevant differences among the samples, but again empty PEVs showed higher values of cells viability than other samples for all concentrations (Fig. 21).

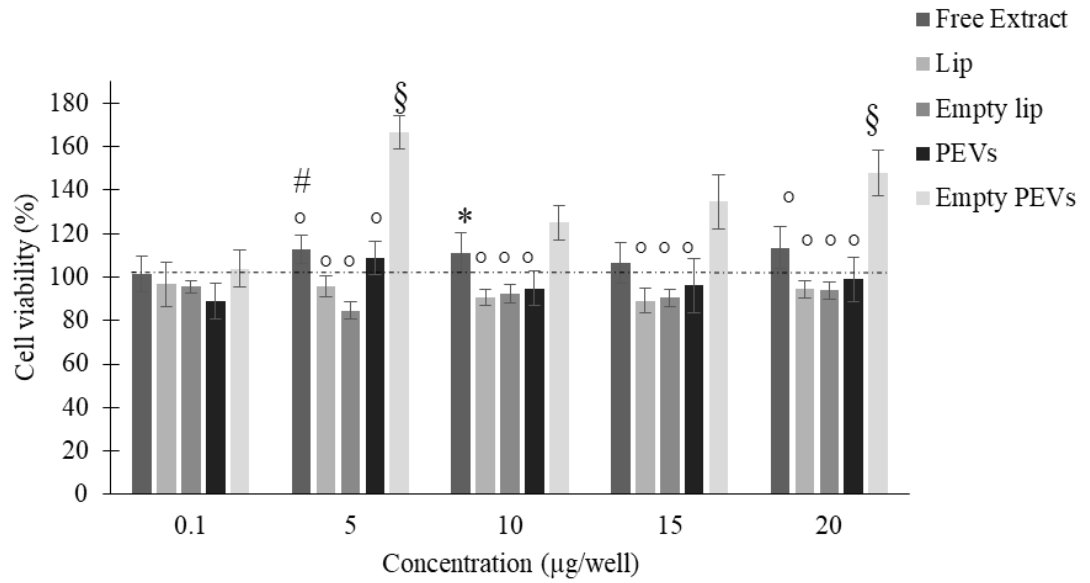

*Figure 21. Viability of HaCaT upon exposure to P. spinosa samples for 24 h. Data are expressed as means ± standard error (SE); n=2 independent experiments; § p<0.01 vs. control group (cells untreated, 100% viability; not shown in the graph); * p<0.05 vs lip; # p<0.05 vs. empty lip; ° p<0.01 vs. empty PEVs.*

When the tumoral A431 keratinocytes were considered the same trend was observed (Fig.22).

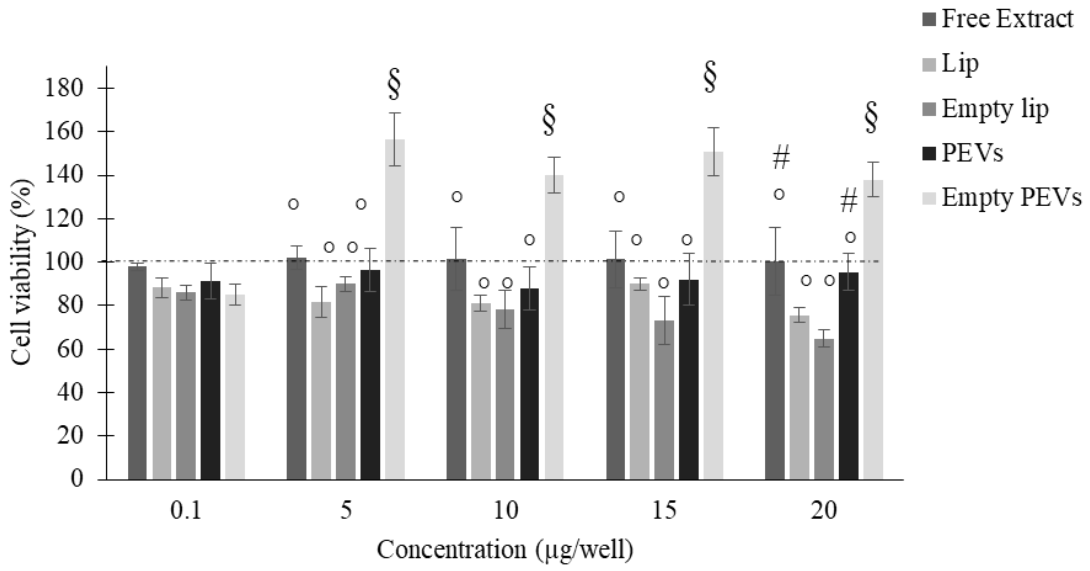

Figure 22. Viability of A431 upon exposure to P. spinosa samples for 24 h. Data are expressed as means ± standard error (SE); n=2 independent experiments; § p<0.01 vs. control group (cells untreated, 100% viability; not shown in the graph); # p<0.05 vs. empty lip; ° p<0.01 vs. empty PEVs.

4.2.3.3. Antioxidant activity – DPPH

The antioxidant activity of the blackthorn formulations (5 µL) was estimated as a function of their radical scavenging activity. The blackthorn solution scavenged the DPPH radical markedly (85%; Table 15), corresponding to 983 µg/mL of Trolox equivalents. The level of antioxidant activity for the blackthorn liposomes and PEVs was lower than the blackthorn solution, with a statistically significant difference and nevertheless, the antioxidant activity was approximately 70% and 78% respectively corresponding to approximately 840 µg/mL of Trolox equivalents (Table 15). Given the presence of phosphatidylcholine, empty vesicles possessed a slight antioxidant activity as well (Tab. 15).

	DPPH assay	
	AA (%)	***TE (µg Trolox equivalents/mL)***
Free extract solution	85.0 ± 1.7	983.0 ± 11.5
Lip	*,§ 70.0 ± 2.4	*,§ 846.0 ± 39.5
Empty lip	13.0 ± 0.7	75.0 ± 6.3
PEVs	$^{*,\#,\circ}$ 78.0 ± 0.8	$^{\#,\circ}$ 835.0 ± 5.6
Empty PEVs	17.0 ± 0.9	115.0 ± 7.8

*Table 15. In vitro antioxidant activity of blackthorn formulations. The results of DPPH assay are expressed as AA (%) and TE (µg Trolox equivalents/mL) and reported as the mean ± SD of at least three separate experiments, each performed in triplicate. * values statistically different (p<0.01) from the free extract solution. § values statistically different (p<0.01) from the empty liposomes. ° values statistically different (p<0.01) from the liposomes. # values statistically different (p<0.01) from the empty PEVs.*

4.2.3.4. Antioxidant activity - cells protection from chemically induced oxidative stress

The antioxidant capabilities of *P. spinosa* samples in protecting cells from hydrogen peroxide induced oxidative stress were investigated. In light of the results reported above on cells viability, for all sample 10 µg in each well was used. Fig. 23 shows that a 3 h treatment with 2 mM H_2O_2 reduced significantly the viability of 3T3 fibroblasts (42%) compared with untreated cells (100% viability). Free extract treated cells showed slow inhibitory activity (2%) of oxidative stress. Unfortunately, none of the formulations was able to counteract the damage induced by H_2O_2.

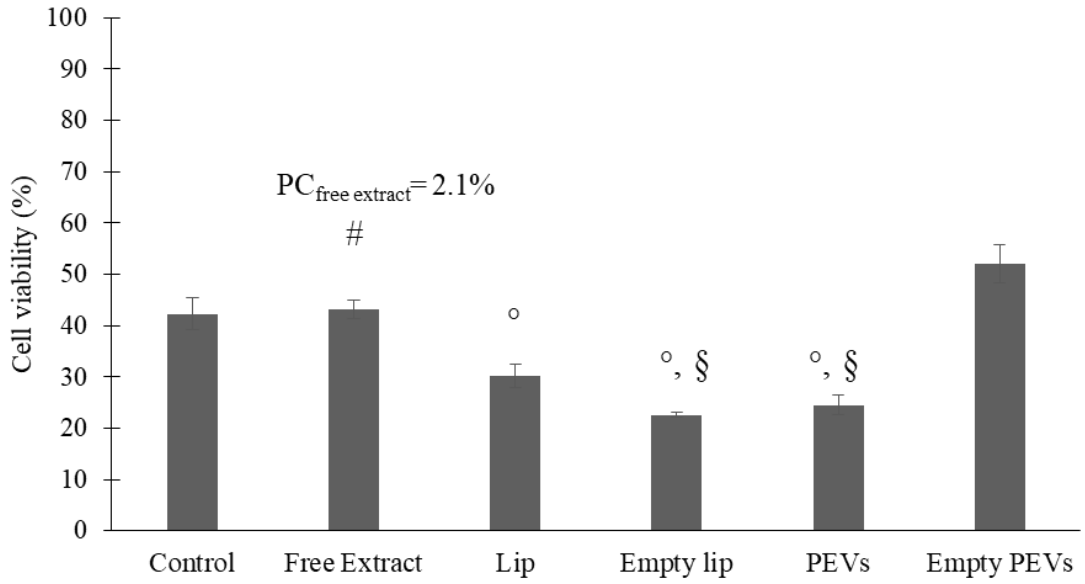

Figure 23. Viability of 3T3 upon pre-treatment with P. spinosa samples and subsequent exposure to H_2O_2 2 mM. Data are expressed as means ± standard error (SE); n=2 independent experiments; § p<0.05 vs. control group (cells without

pre-treatment); # p<0.05 vs. empty lip; ° p<0.05 vs. empty PEVs. All samples were different from control cells without pre-treatment and H_2O_2 exposure (100% viability). When present, the PC% is also expressed.

The fig. 24 shows that a 3 h treatment with 2 mM H_2O_2 reduced significantly the viability of HaCaT keratinocytes (41%) compared with control cells (100%). Free extract treated cells showed an inhibitory activity (14%) of oxidative damage, while the nanoformulated extract was not as effective.

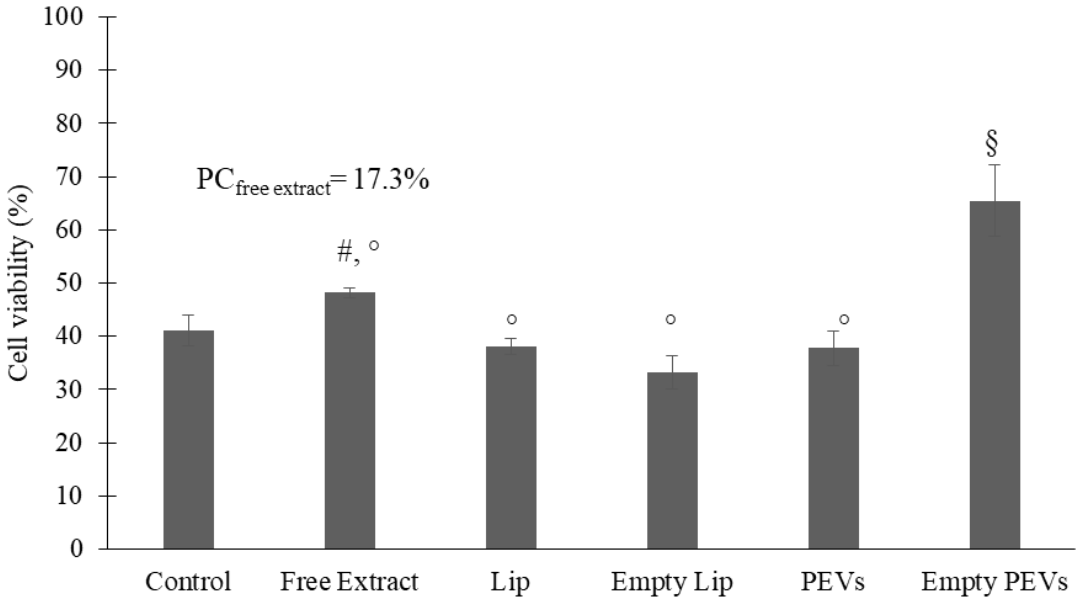

Figure 24. Viability of HaCaT upon pre-treatment with P. spinosa samples and subsequent exposure to H_2O_2 2 mM. Data are expressed as means ± standard error (SE); n=2 independent experiments; § p<0.05 vs. control group (cells without pre-treatment); # p<0.05 vs. empty lip; ° p<0.05 vs. empty PEVs. All samples were different from control cells without pre-treatment and H_2O_2 exposure (100% viability). When present, the PC% is also expressed.

Fig. 25 demonstrates that a 3 h treatment with 2 mM H_2O_2 reduced significantly the viability of A431 tumoral keratinocytes (56%) compared with control cells (100%). Free extract treated cells showed a slow inhibitory activity (3%) of oxidative damage, similarly to extract loaded PEVs, while extract loaded liposomes were more effective (15%).

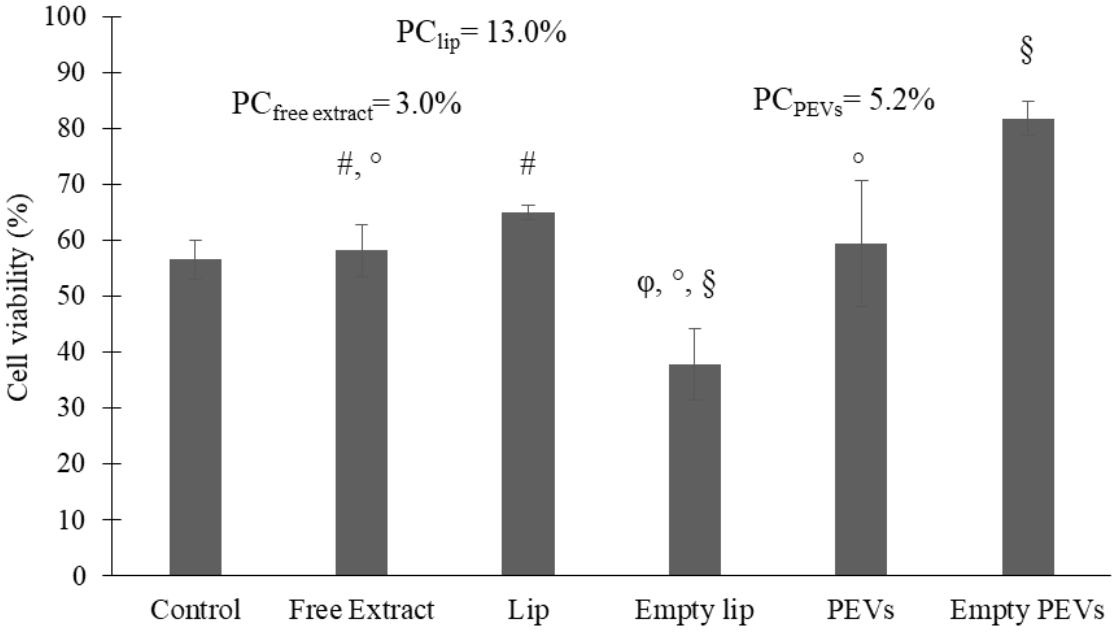

Figure 25. Viability of A431 upon pre-treatment with P. spinosa samples and subsequent exposure to H_2O_2 2 mM. Data are expressed as means ± standard error (SE); n=2 independent experiments; § p<0.05 vs. control group (cells without pre-treatment); # p<0.05 vs. empty lip; ° p<0.05 vs. empty PEVs; φ p<0.05 vs. PEVs. All samples were different from control cells without pre-treatment and H_2O_2 exposure (100% viability). When present, the PC% is also expressed.

4.2.3.5. Antibacterial activity

The antibacterial activity was evaluated against a panel of Gram-positive and Gram-negative bacteria clinically relevant. The intrinsic coloration of free extract solution hindered the turbidity visualization and the shifting colour due to the metabolization of resazurin for MIC values determination. The clearest results were those from the plate's interpretation, which evaluates the bacterial growth or inhibition for MBC values determination.

The *P. spinosa* extract showed antibacterial activity against *S. aureus* and *S. epidermidis*. More precisely, MIC and MBC are 16 mg/mL for both strains (Fig. 26).

Sabatini et al. described the antibacterial activity of *P. spinosa* ethanol extract against *S. aureus* with a similar MBC value (17.44 mg/mL). Moreover, the authors found a wider antimicrobial activity of this extract defining it as a promising antimicrobial compound of natural origin [167]. No previous data are found for inhibitory activity against *S. epidermidis*. It was not possible to assay the two vesicular formulations because MIC and MBC values were approximately the same concentrations as used for liposome/PEVs preparation (20 mg/mL).Therefore, no more dilutions with bacteria medium could be performed (as required by the protocol described in the previous

chapter, for appropriate bacteria growth). Our formulations had an extract concentration of 20 mg/mL, which is above the MIC and MBC values, so it is reasonable to assume that they would have antibacterial activity.

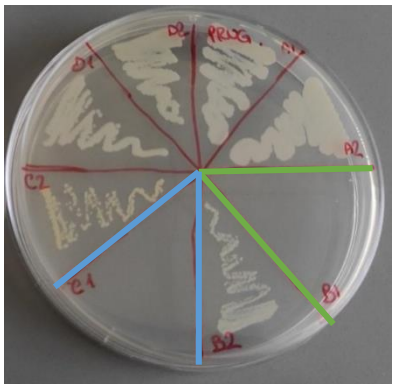

Figure 26. Antibacterial activity of P. spinosa extract (16 mg/mL) against Staphylococcus epidermidis (B1, in green) and Staphylococcus aureus (C1, in blue).

4.3. *Ceratonia siliqua L.*

4.3.1. Qualitative determination of active compounds in the extract

C. siliqua L. fruits extracts showed a high content of gallic acid and its derivatives (Figure 27). According to literature data [111], most of them are galloyl glucose derivatives. Some flavonols were also detected with quercetin derivative being the most abundant.

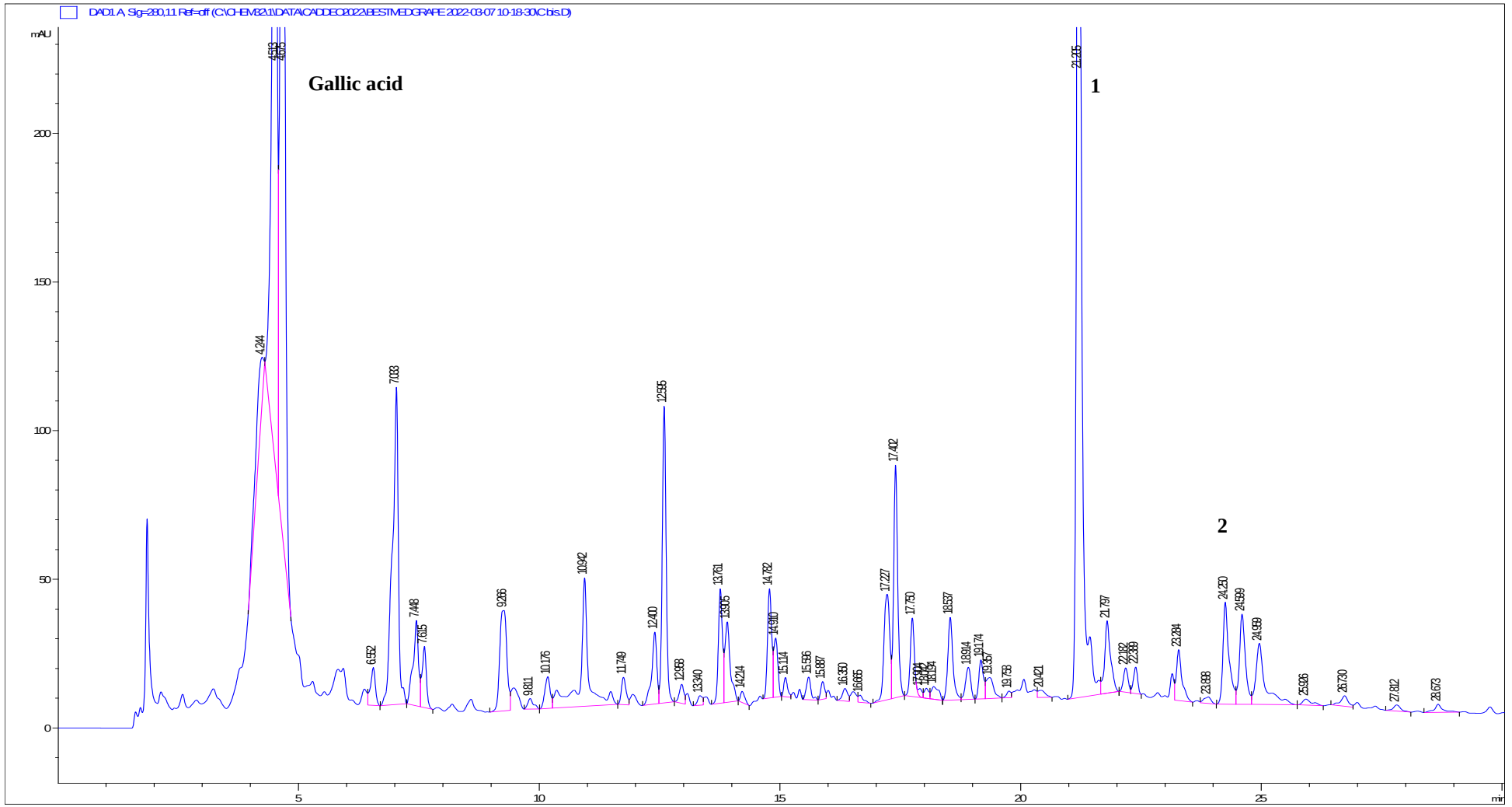

Figure 27. HPLC-DAD chromatogram of Ceratonia siliqua L. fruit extract at λ = 280 nm. Chromatographic conditions are described in the text. Peak identification is given in Table 17.

4.3.2. Vesicles characterization

Carob liposomes were characterized in terms of mean diameter, polydispersity, zeta potential through DLS and ELS measurements, morphology and lamellarity through cryo-TEM and SAXS, and efficiency encapsulation with direct measurements of some compounds though HPLC–DAD.

4.3.2.1. Size, zeta potential, and storage stability

Liposomes loaded with carob extract were approximately of 100 nm and significantly larger in mean diameter than empty liposomes (73 nm; Table 16). Polidispersity index and zeta potential values for carob liposomes were 0.27 and -13 mV, respectively, and similar to those measured for empty liposomes. The stability of the nanoformulations was evaluated by monitoring the extract precipitation, the mean diameter, the polydispersity index, and the zeta potential during storage at 4ºC. No signs of significant alterations were detected after 30 days (Table 16).

	Lip		**Empty Lip**	
	Day 0	***Day 30***	***Day 0***	***Day 30***
Mean diameter (nm ± SD)	*107.00 ± 3.80	105.00 ±3.20	73.00 ± 2.00	83.00 ± 6.30
Polidispersity index (± SD)	0.27 ± 0.01	0.26 ±0.01	0.31 ±0.03	0.41 ± 0.02
Zeta potential (mV ± SD)	-13.00 ± 2.80	-17.00 ±2.90	-18.00 ± 2.70	-22.00 ±3.70

*Table 16. Characteristics of carob formulations. Each value represents the mean ± SD (n> 10). * Values statistically different (p< 0.01) from empty vesicles.*

4.3.2.2. Entrapment efficiency

Two targeted phenolic compounds were quantified in the liposomes (Table 17). The formulation was capable of loading a high amount of extract, as the entrapment efficiency was 97.1 ± 6.3 % for the gallic acid derivative and 91.2 ± 7.7% for the quercetin derivative.

Peak	**Compounds**	**EE %**
1	Gallic acid derivative [a]	97.1 ± 6.3
2	Quercetin derivative [b]	91.2 ± 7.7

Table 17. Entrapment efficiency (EE %) of the main phenolic compounds identified in carob extract .[a] Dosed with the calibration curve for quercetin-3-glucoside. [b] Dosed with the calibration curve for quercetin-3-glucoside. Data are given as the mean ± SD (n= 4).

4.3.2.3. Morphology

The formation of vesicular structures characterized by their small size was confirmed by cryo-TEM observation. Figure 28 shows spherical and elongated oligolamellar vesicles at around 100 nm in diameter, which aligns with the light scattering data.

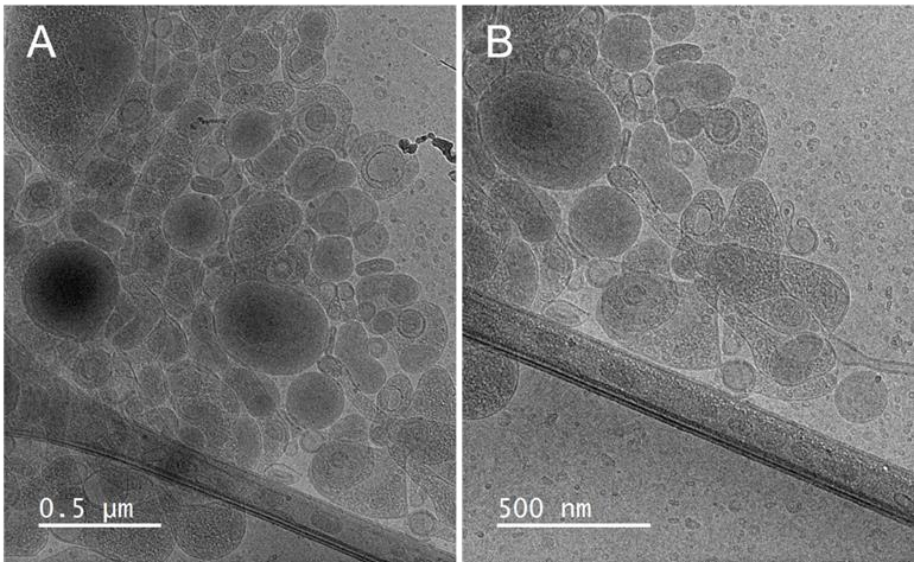

Figure 28. Cryo-TEM images of C. siliqua liposomes. Two magnifications are shown: 12,000 x (A) and 15,000 x (B).

4.3.2.4. Small-Angle X-ray Scattering

A deeper structural characterization of liposomes was gained by SAXS analysis. The SAXS patterns of liposomes are shown in Fig. 29, together with the fits of the lamellar model (χ^2=1.75 e 1.61): they were typical of bilayered structures.

The main parameters obtained from the fits are listed in Table 18.

The results suggest that the carob extract induced in liposomes some multilamellar arrangement in structures with a small number of correlated layers (N=1.29) at a repetition distance of ~62 Å and η=0.23.

The distance between the polar heads and the bilayer center (Z_H) slightly increased with extract loading.

The polar head (σ_H) and methyl (σ_C) amplitude slightly decreased in liposomes with the extract loading, however the differences were small for graphic visualization.

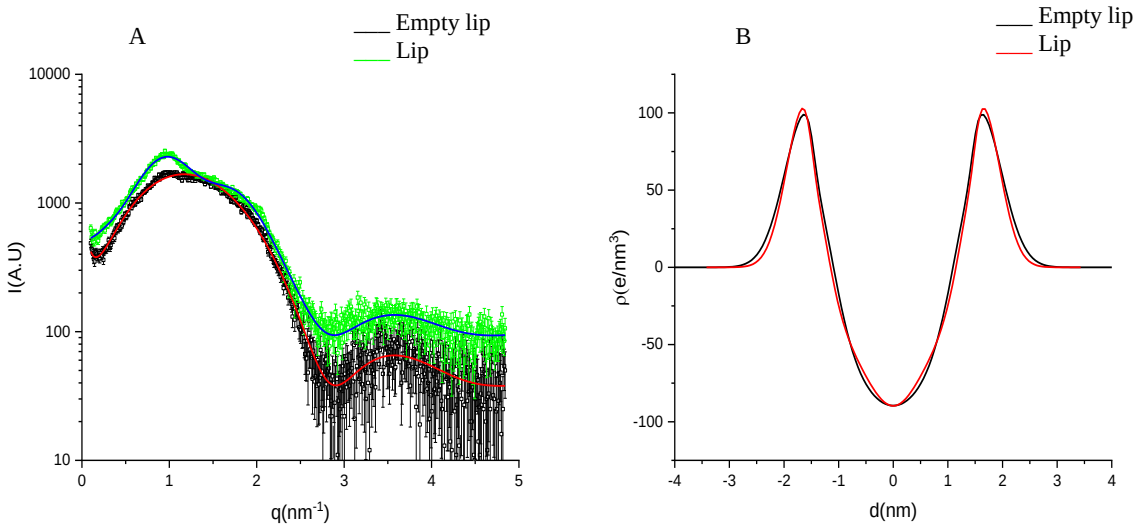

Figure 29. (A) SAXS profiles of empty and loaded liposomes of C. siliqua. The lines correspond to the best fit of Gaussian bilayer models. (B) Electron density profiles corresponding to the best fits of empty and loaded liposomes of C. siliqua.extract.

	Liposomes	**Empty liposomes**
X^2	1.75	1.61
N	1.29	1.00
d (Å)	62.16	/
η_1	0.23	/
Z_H (Å)	16.05 ± 0.50	15.60 ± 0.50
σ_H (Å)	3.44 ± 0.50	4.16 ± 0.50
σ_C (Å)	5.19 ± 0.50	7.48 ± 0.50

Table 18. Selected fitting parameters and derived parameters for SAXS curves of C. siliqua formulations.

4.3.3. Evaluation of biological activity

Also in this case, the biocompatibility of samples was assayed as hemolityc activity evaluation on erythrocytes and as absence of cytotoxic effects on fibroblasts and keratinocytes. The antibacterial activity was tested against a panel of common bacteria. Moreover, the antioxidant power was studied through DPPH and FRAP colorimetric tests and as capacity to reduce H_2O_2-induced oxidative stress on fibroblasts and keratinocytes.

4.3.3.1. Biocompatibility - hemolityc activity

As in the case of *P. spinosa* L. formulations, initially, the free extract solution was tested from 200 to 2000 µg/mL and no relevant activity was seen (data not shown). For this reason, the concentrations 1 and 2 mg/mL were assayed for each sample. All samples showed a low erythrocyte-disrupting ability: despite the whitish aspect of superrnatants (as for *P. spinosa* samples), the erythrocytes harvested after the treatment had still a red coloration indicating that most of the cells were intact (Fig. 19 in the section 4.2.3.1.). More precisely, the hemolytic activity was lower than 5% without statistically significant differences between free and nanoformulated forms. The results are shown in Tab. 19.

	Hemolysis (% ± SD)	
Sample\Concentracion	*1 mg/mL*	*2 mg/mL*
Free extract	1.68 ± 0.70	1.55 ± 1.07
Lip	2.39 ± 2.89	0.94 ± 1.33
Empty lip	1.42 ± 1.14	3.73 ± 1.92

Table 19. Hemolytic activity of C.siliqua L. formulations. Data are expressed as means ± standard deviation (SD); n = 3; Differences are not statistically significant.

No previous data were found in literature about the hemolytic activity of carob extract except the protective action of an aqueous extract on human erythrocytes from hypotonic solution-induced hemolysis [110].

4.3.3.2. Biocompatibility - MTT

The treatment of the three cell lines with carob extract, in free solution or nanoformulated in liposomes, at the tested concentrations, was not toxic for cells, as expressed by MTT results.

For 3T3 fibroblasts, the MTT results showed a slight reduction in viability for cells treated with free extract solution; anyway, the values were never lower than 86%. After treatment with extract in liposomal form, the viability cell values were approximately the same as for the control cells. Also empty liposomes did not show toxicity, at the tested concentrations and no statistically relevant difference was highlighted among the different groups (Fig. 30).

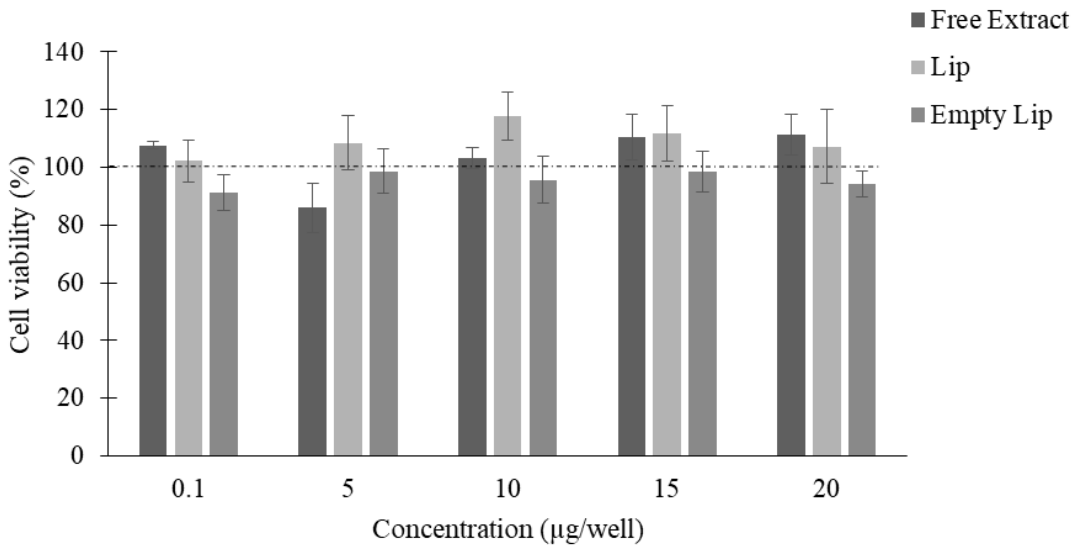

Figure 30. Viability of 3T3 upon exposure to C. siliqua samples for 24 h. Data are expressed as means ± standard error (SE); n=2 independent experiments; no differences statistically relevant among the different samples and among the control group (100% viability; not shown in the graph).

In the case of normal HaCaT keratinocytes, the same results were obtained: the cells showed viability values always higher than 80% when treated with free extract solution or liposomes, both with the same trend of proliferation with increasing concentrations and without statistically relevant differences. In no case, empty liposomes showed toxicity (Fig. 31).

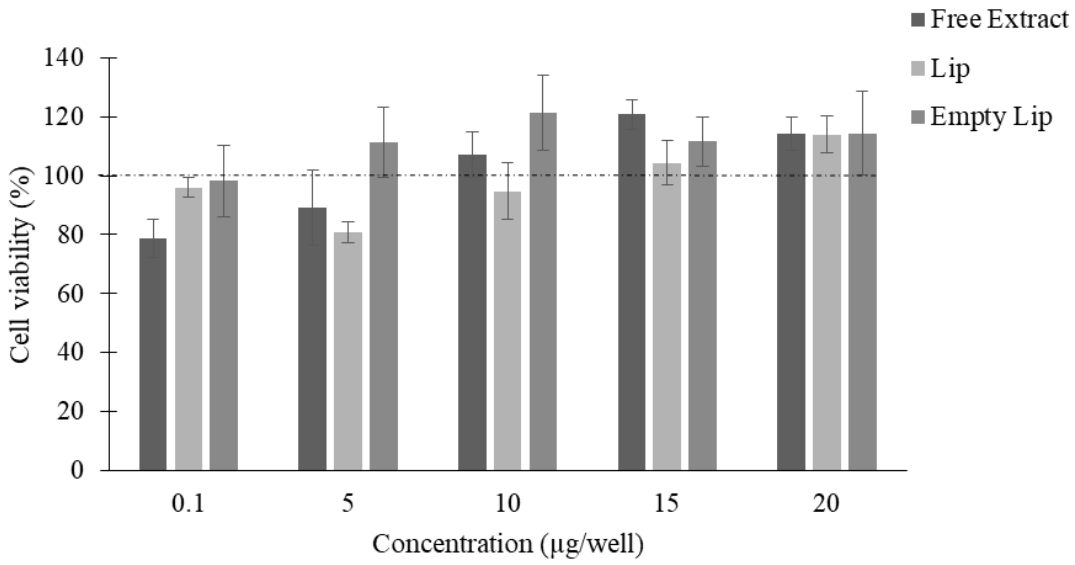

Figure 31. Viability of HaCaT upon exposure to C. siliqua samples for 24 h. Data are expressed as means ± standard error (SE); n=2 independent experiments; no differences statistically relevant among the different samples and among the control group (100% viability; not shown in the graph).

For the tumoral A431 keratinocytes, there was a statistically relevant difference between free extract solution and liposomes; particularly, cell viability was slightly affected by liposomal treatment, but the lower value was approximately to 80% (Fig. 32). The MTT test was performed also in cells treated with empty liposomes. The results confirmed that the nanocarriers were not toxic to cells.

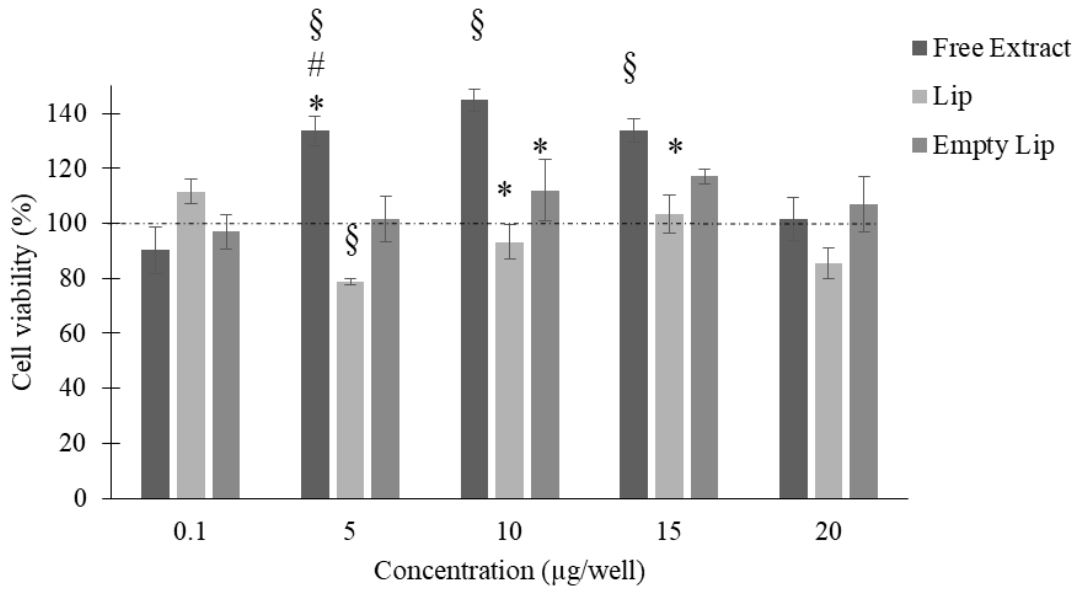

*Figure 32. Viability of A431 upon exposure to C. siliqua samples for 24 h. Data are expressed as means ± standard error (SE); n=2 independent experiments; no differences statistically relevant among the different samples and among the control group (100% viability; not shown in the graph); § p<0,05 vs. control group (cells without pre-treatment); * p<0,05 vs lip; # p<0,05 vs. empty lip.*

4.3.3.3. Antioxidant activity – DPPH, FRAP

The antioxidant activity of the carob formulations was estimated as a function of their radical scavenging and ferric reducing abilities (Table 20). The carob solution scavenged the DPPH radical almost completely (92%, corresponding to ~469 µg/mL of Trolox equivalents). The level of antioxidant activity for the carob liposomes was slightly higher than the carob solution, without statistically significant difference. Given the presence of phosphatidylcholine, empty liposomes possessed a moderate antioxidant activity (40%; Table 20).

The results of the FRAP assay showed that the carob solution and carob liposomes had a strong reducing power of ~2000 µg/mL of ferrous equivalents without statistic relevant differences. In addition, the empty liposomes showed a slight reducing power (Table 20).

These findings confirm that the antioxidant activity of the carob extract was retained in the vesicle formulation.

	DPPH assay		**FRAP assay**
	AA (%)	***TE (µg Trolox equivalents/mL)***	***FE (µg Fe2+ equivalents/mL)***
Free extract solution	92.0 ± 4.2	469.0 ± 14.1	2139.0 ± 257.0
Lip	95.0 ± 1.7	*486.0 ± 10.5	1995.0 ± 253.0
Empty lip	40.0 ± 4.1	220.0 ± 18.2	687.0 ± 99.0

*Table 20. In vitro antioxidant activity of carob formulations. For the DPPH assay, results are expressed as AA (%) and TE (µg Trolox equivalents); for the FRAP assay, results are expressed as FE (µg Fe^{2+} equivalents/mL solution) and reported as the mean ± SD of at least three separate experiments, each performed in triplicate. * statistically different values ($p<0.05$) from the carob solution.*

4.3.3.4. Antioxidant activity - cells protection from chemically induced oxidative stress

The antioxidant capabilities of *C. siliqua* samples were also investigated as the ability in protecting cells from hydrogen peroxide-induced oxidative stress. A concentration of 100 µg/mL (100 µg in each well) was used for each cell pre-treatment. Figure 33 displays that treatment with 2 mM H_2O_2 reduced 3T3 viability to 38% compared to the untreated cells and that there was some protection capacity with the pre-treatment with carob samples, both for free extract and liposomes.

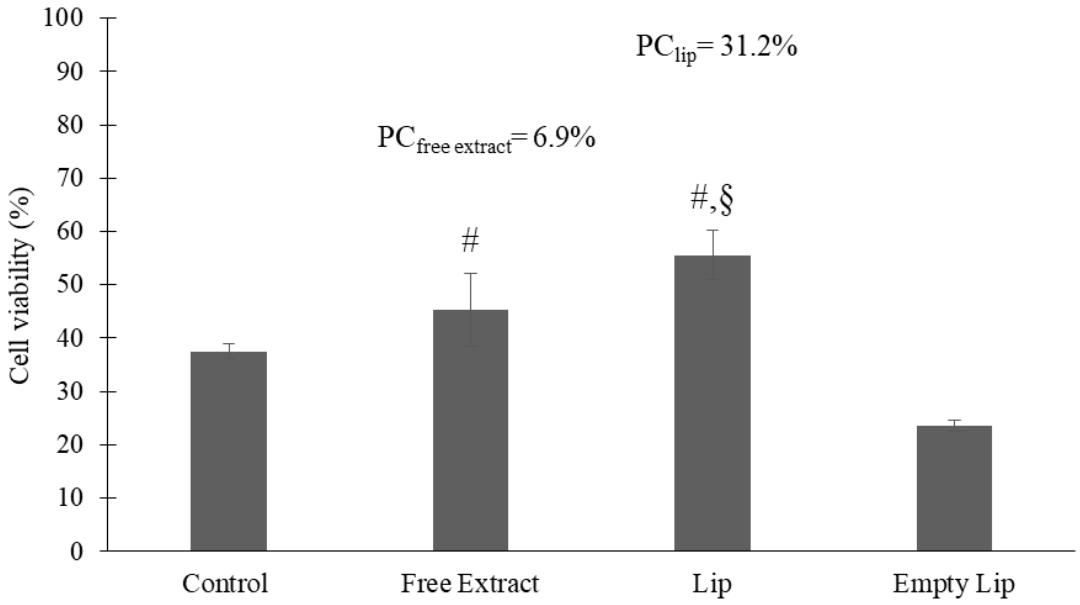

Figure 33. Viability of 3T3 upon pre-treatment with C. siliqua samples and subsequent exposure to H_2O_2 2 mM. Data are expressed as means ± standard error (SE); n=2 independent experiments; § p<0,05 vs. control group (cells without pre-treatment); # p<0,05 vs. empty lip. All samples were different from control cells without pre-treatment and H_2O_2 exposure (100% viability). When present, the PC% is also expressed.

In the case of HaCaT cells, H_2O_2 induced similar cytotoxic effect than for 3T3 cells (41%), and the pre-treatment with carob solution had a protective effect increasing cell viability to 55%. Liposomes showed a lower protection, not significantly different from the solution (Fig. 34).

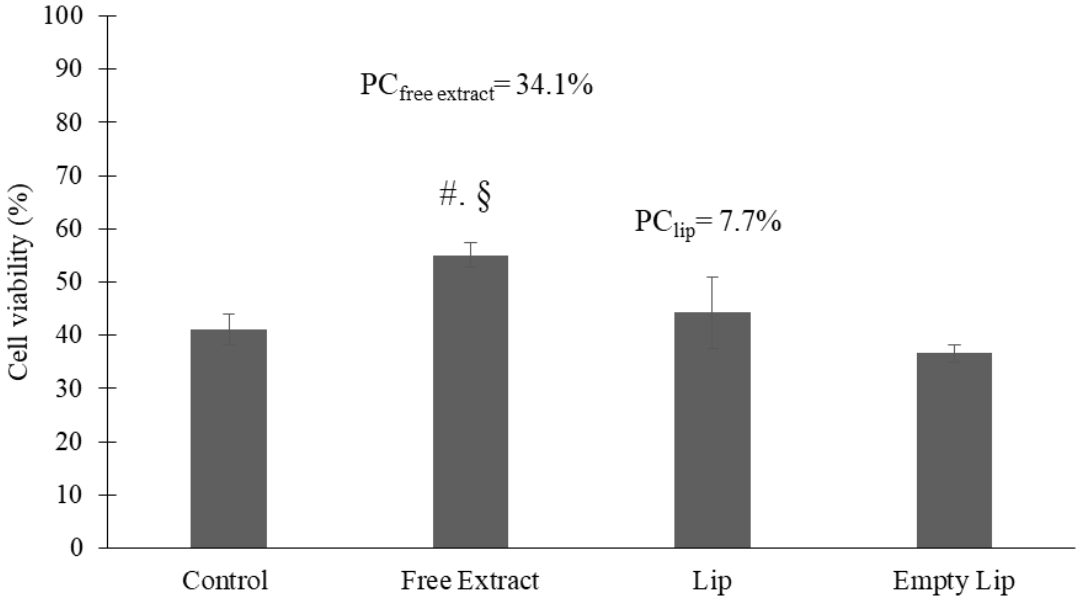

Figure 34. Viability of HaCaT upon pre-treatment with C. siliqua samples and subsequent exposure to H_2O_2 2 mM. Data are expressed as means ± standard error (SE); n=2 independent experiments; § p<0,05 vs. control group (cells without pre-treatment); # p<0,05 vs. empty lip. All samples were different from control cells without pre-treatment and H_2O_2 exposure (100% viability). When present, the PC% is also expressed.

The same trend was seen for tumoral A431 keratinocytes (Fig. 35).

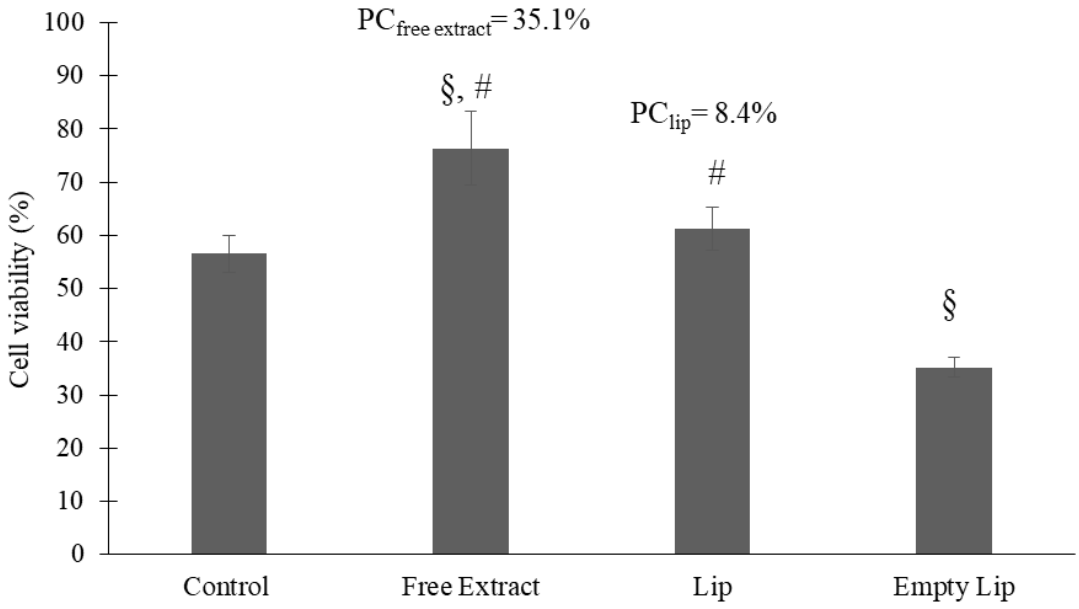

Figure 35. Viability of A431 upon pre-treatment with C. siliqua samples and subsequent exposure to H_2O_2 2 mM. Data are expressed as means ± standard error (SE); n=2 independent experiments; § p<0,05 vs. control group (cells without pre-treatment); # p<0,05 vs. empty lip. All samples were different from control cells without pre-treatment and H_2O_2 exposure (100% viability). When present, the PC% is also expressed.

4.3.3.5. Antibacterial activity

This extract did not show antibacterial activity against the tested strains. Data found in literature about its antibacterial potential for these strains, regard essential oil [168] or methanol extract from leaves [169].

4.4. *Armoracia rusticana* L.

4.4.1. Qualitative determination of active compounds in the extract

A. rusticana L. root extract showed numerous compounds, but most of them in small amounts and of difficult identification (Figure 36) [131].

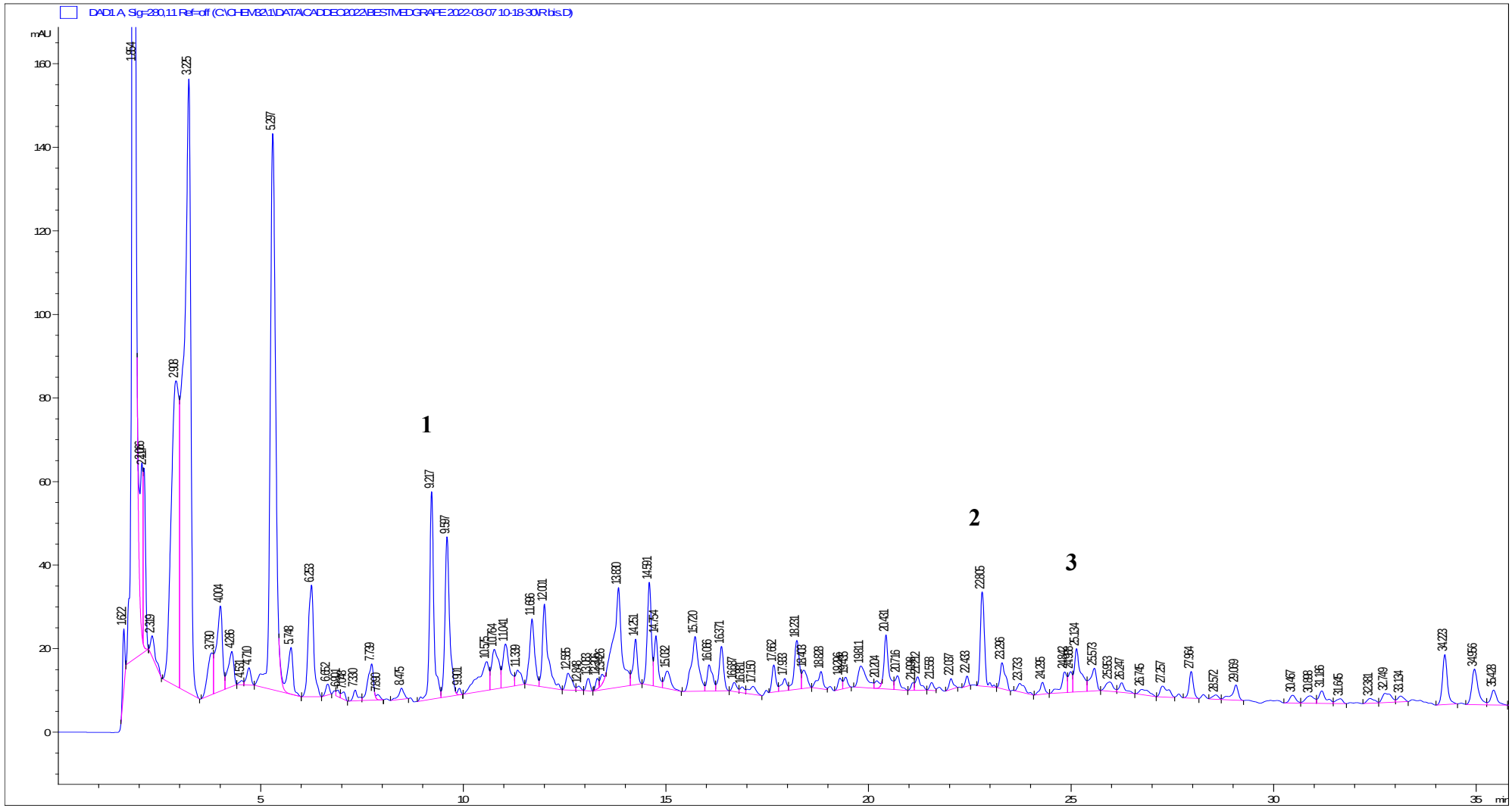

Figure 36. HPLC-DAD chromatogram of Armoracia rusticana L. roots extract at λ = 280 nm. Chromatographic conditions are described in the text. Peak identification is given in Table 22.

4.4.2. Vesicles characterization

Horseradish formulations were characterized in terms of mean diameter, polydispersity, zeta potential through DLS measurements, structural arrangements through SAXS measurements, entrapment efficiency with direct measurements of some compounds though HPLC–DAD, and storage stability.

4.4.2.1. Size, zeta potential, and storage stability

As reported in Table 21, the liposomes with horseradish extract were approximately of 80 nm in mean diameter and significantly smaller than the corresponding empty vesicles; these formulations appeared monodispersed (PDI 0.22) and with a high surface charge (ZP -68 mV). The addition of ethanol increased the mean diameter of the vesicles, wich was below 100 nm (Tab. 21). The formulations' stability was evaluated by monitoring these parameters and extract precipitation in time and by keeping the samples at 4°C.

	Lip		**Empty Lip**	
	Day 0	***Day 30***	***Day 0***	***Day 30***
Mean diameter (nm ± SD)	*84.00 ± 5.80	82.00 ± 3.80	95.00 ± 3.20	94.00 ± 1.60
Polidispersity index (± SD)	0.22 ± 0.02	0.25 ± 0.01	0.34 ± 0.02	0.37 ± 0.04
Zeta potential (mV ± SD)	-50.00 ± 2.20	-56.00 ± 2.40	-68.00 ±9.60	-71.00 ± 3.90

	PEVs		**Empty PEVs**	
	Day 0	***Day 30***	***Day 0***	***Day 30***
Mean diameter (nm ± SD)	*,**93.00 ± 7.40	97.00 ± 9.60	67.00 ± 5.10	66.00 ± 4.00
Polidispersity index (± SD)	0.23 ± 0.01	0.24 ± 0.01	0.54 ± 0.04	0.51 ± 0.06
Zeta potential (mV ± SD)	-60.00 ± 1.90	-65.00 ± 3.00	-72.00 ± 5.20	-66.00 ± 8.80

*Table 21. Characteristics of horseradish formulations. Each value represents the mean ± SD (n> 10). * Values statistically different (p< 0.01) from corresponding empty vesicles. ** Values statistically different (p< 0.05) from liposomes.*

4.4.2.2. Entrapment efficiency

Tryptophan, kaempferol-3-*O*-rutinoside and another kaempferol derivative were quantified and used to evaluate the entrapment efficiency. The two nanoformulations showed similar values of entrapment efficiency for all compounds (Table 22).

Peak	Compound	% EE	
		Lip	***PEVs***
1	Tryptophan	61.7 ± 2.1	68.1 ± 6.2
2	Kaempferol-3-*O*-rutinoside	86.1 ± 3.8	87.6 ± 4.1
3	Kaempferol derivative[a]	88.4 ± 8.4	86.7 ± 7.4

Table 22. Entrapment efficiencies (EE%) of the main phenolic compounds identified in horseradish extract. [a] Dosed with kaempferol-3-O-rutinoside calibration curve. Data are given as mean ± standard deviation (n = 4).

4.4.2.3. Morphology

The formation of vesicular structures characterized by their small size was confirmed by cryo-TEM observation, for PEVs. Figure 37 shows spherical unilamellar vesicles at around 100 nm in diameter, which aligns with the light scattering data.

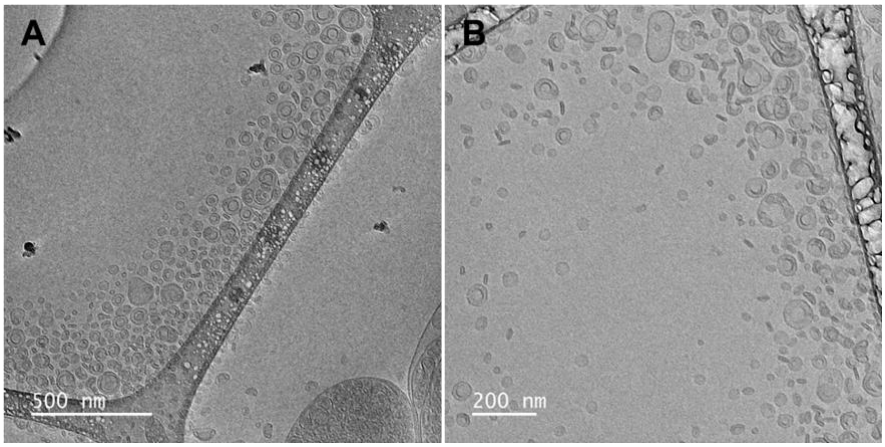

Figure 37. Cryo-TEM images of A. rusticana Et-PEVs. Two magnifications are shown: 15,000 x (A) and 20,000 x (B).

4.4.2.4. Small-Angle X ray Scattering

The SAXS patterns of liposomes and PEVs are shown in Fig. 38 and 39, together with the fits of the lamellar model, which align with the typical profile of bilayers described in the literature.

The main parameters obtained from the fits are listed in Table 23.

The results suggest that *A. rusticana* formulations had unilamellar arrangements (N=1).

Z_H, the distance between the polar heads and the bilayer centre, slightly decreased with extract loading in liposomes compared to empty liposomes. There was an opposite behavior for Et-PEVs where the extract loading increased Z_H value compared to empty Et-PEVs, although Z_H value was the same for liposomes and Et-PEVs.

The polar head region amplitude, expressed by σ_H, increased in liposomes with extract, while decreased it in Et-PEVs with the extract and a contribution from Et, compared with the corresponding empty vesicles. Compared to liposomes, Et-PEVs had a lower σ_H.

The methyl region amplitude, σ_C, decreased with the loading of the extract in liposomes but it did not affect in Et-PEVs, but for all samples these value were very small because there was not a minimum in Gaussian profile.

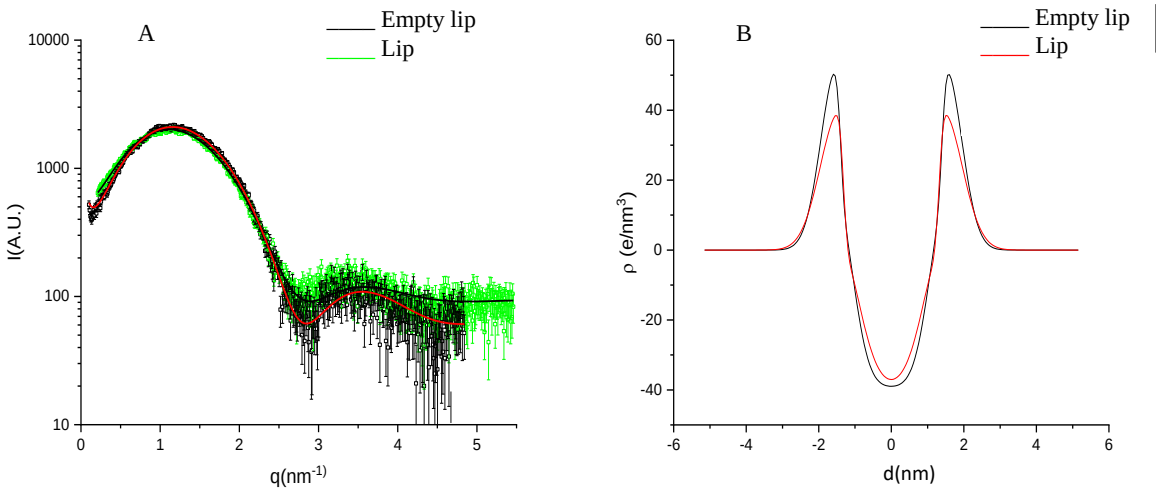

Figure 38. (A) SAXS profiles of empty and A. rusticana loaded liposomes. The lines correspond to the best fit of Gaussian bilayer models. (B) Electron density profiles corresponding to the best fits of empty and A. rusticana loaded liposomes.

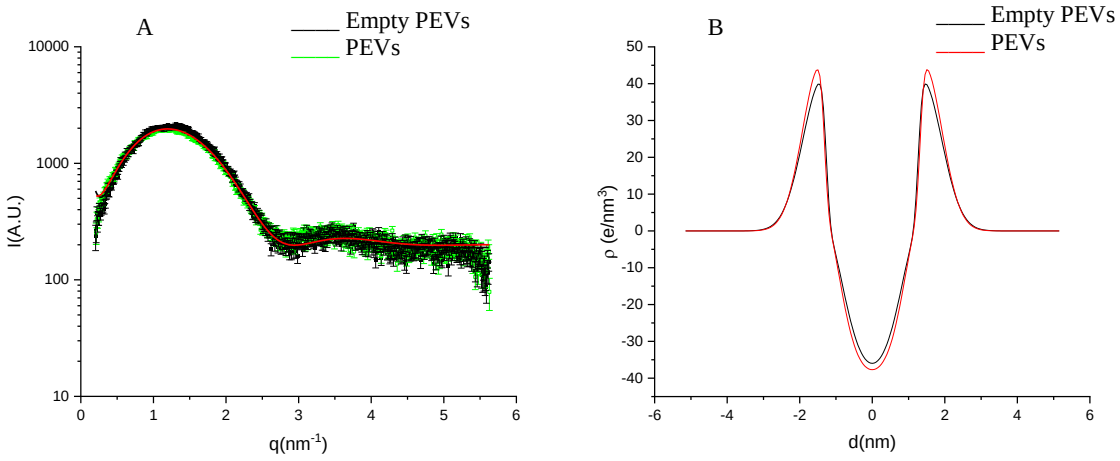

Figure 39. (A) SAXS profiles of empty and loaded PEVs of A. rusticana. The lines correspond to the best fit of Gaussian bilayer models. (B) Electron density profiles corresponding to the best fits of empty and loaded PEVs of A. rusticana extract.

	Lip	**Empty lip**	**PEVs**	**Empty PEVs**
χ^2	0.98	1.21	1.64	1.86
N	1.00	1.00	1.00	1.00
Z_H *(Å)*	14.20 ± 0.50	14.99 ± 0.50	14.20 ± 0.50	13.70 ± 0.50
σ_H *(Å)*	5.33 ± 0.50	4.44 ± 0.50	5.00 ± 0.50	5.41 ± 0.50
σ_C *(Å)*	$4.27 * 10^{-4}$ ± 1.00	$3.28 * 10^{-2}$ ± 1.00	$4.27 * 10^{-4}$ ± 1.00	$4.27 * 10^{-4}$ ± 1.00

Table 23. Selected fitting parameters and derived parameters for SAXS curves of A. rusticana formulations.

4.4.3. Evaluation of biological activity

The biocompatibility of horseradish samples was evaluated as absence of hemolityc activity *ex vivo* in erythrocytes and cytotoxicity *in vitro* in fibroblasts and keratinocytes. The antioxidant activity was assayed with the DPPH and FRAP colorimetric tests and as capacity to reduce H_2O_2-induced oxidative stress *in vitro* on fibroblasts and keratinocytes. Moreover, antibacterial activity was also tested.

4.4.3.1. Biocompatibility – hemolityc activity

As for previous samples, initially, the free extract solution was tested from 200 to 2000 µg/mL and no relevant activity was seen (data not shown). For this reason, higher concentrations (1 and 2 mg/mL) were assayed for each sample. Samples showed a different erythrocyte-disrupting ability: at the concentration of 1 mg/mL, the hemolytic activity of the free extract was 1.9 % and lowered to 0.9 % for liposomal form with statistical significance and to 1.2 % for Et-PEVs but no statistical significance from the free extract. For empty vesicles, the hemolytic activity was similar to the corresponding loaded vesicles.

At the concentration of 2 mg/mL, the hemolytic activity of the free extract increased to 16 %; this value decreased to 1.5 % in the liposomal form and to 3.2% in Et-PEVs with statistical significance. Both empty vesicles had a hemolytic activity lower than 2%. The results are shown in Tab.24.

	Hemolysis (% ± SD)	
Sample\Concentracion	*1 mg/mL*	*2 mg/mL*
Free extract	1.90 ± 0.18	16.33 ± 2.42
Lip	*0.91 ± 0.02	**1.48 ± 0.44
Empty lip	0.90 ± 0.60	**1.80 ± 0.77
PEVs	1.17 ± 0.45	**3.22 ± 0.97
Empty PEVs	*1.26 ± 0.10	**1.08 ± 0.02

*Table 24. Hemolytic activity of A. rusticana L. formulations. Data are expressed as means ± standard deviation (SD); n = 3; * $p < 0.05$ vs. free extract solution 1 mg/mL; ** $p < 0.01$ vs. free extract solution 2 mg/mL.*

4.4.3.2. Biocompatibility - MTT

The treatment of the three cell lines with carob extract, in solution or formulated in liposomes and at the tested concentrations, was not cytotoxic, as indicated by MTT results.

For 3T3 fibroblasts, the MTT results showed a slight reduction in viability for cells treated with the extract solution; nevertheless, the values were never lower than 80%. The liposomes seem to relieve the slight extract cytotoxicity showing viability values similar or higher than control cells (100% viability). The same tendency was showed for Et-PEVs; however, at the highest concentration, liposomes seemed to increase cell proliferation while Et-PEVs seemed to decrease it. For tested concentrations, empty vesicles did not show toxicity (Fig. 40).

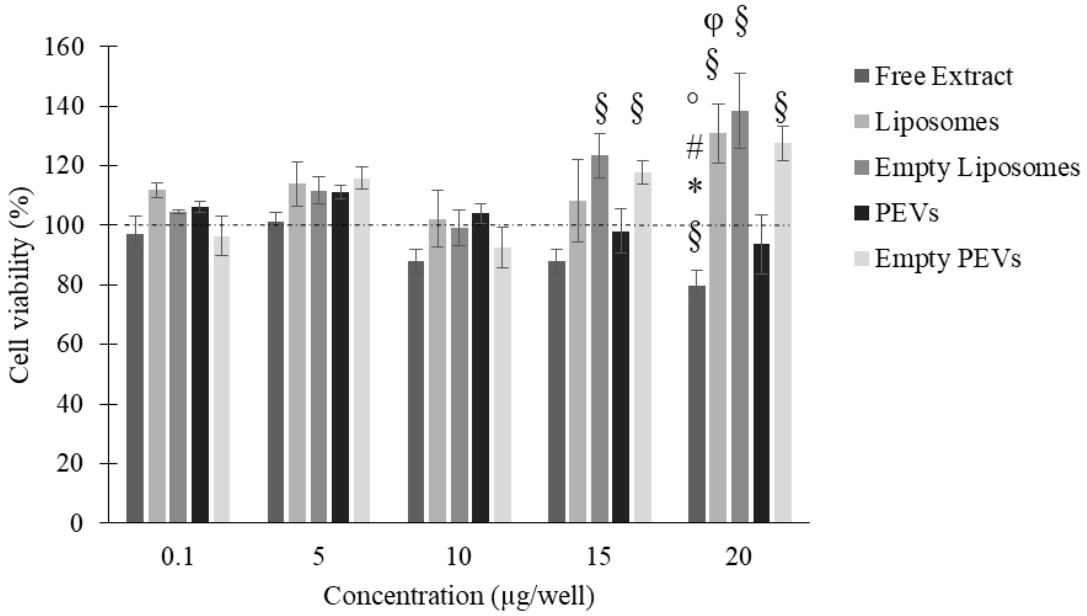

*Figure 40. Viability of 3T3 upon exposure to A. rusticana samples for 24 h. Data are expressed as means ± standard error (SE); n=2 independent experiments; § p<0.05 vs. control group (cells untreated, 100% viability; not shown in the graph); * p<0.01 vs lip; # p<0.01 vs. empty lip; ° p<0.01 vs. empty PEVs; φ p<0.05 vs PEVs.*

In the case of HaCaT cells, no particular cytotoxicity emerged, although for each concentration there was the same tendency among the different formulations, with the nanoformulated extract decreasing cell viability compared with the extract solution (Fig. 41).

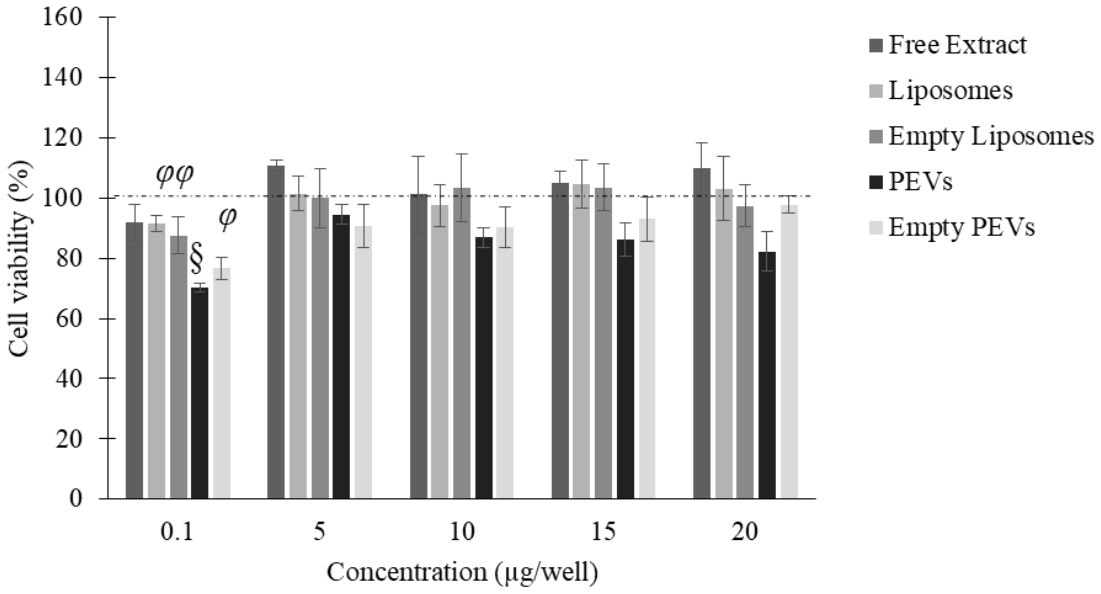

Figure 41. Viability of HaCaT upon exposure to A. rusticana samples for 24 h. Data are expressed as means ± standard error (SE); n=2 independent experiments; § p<0.05 vs. control group (cells untreated, 100% viability; not shown in the graph); φ p<0,05 vs PEVs.

When the A431 cells were considered, no particular cytotoxicity emerged as well (Fig.42).

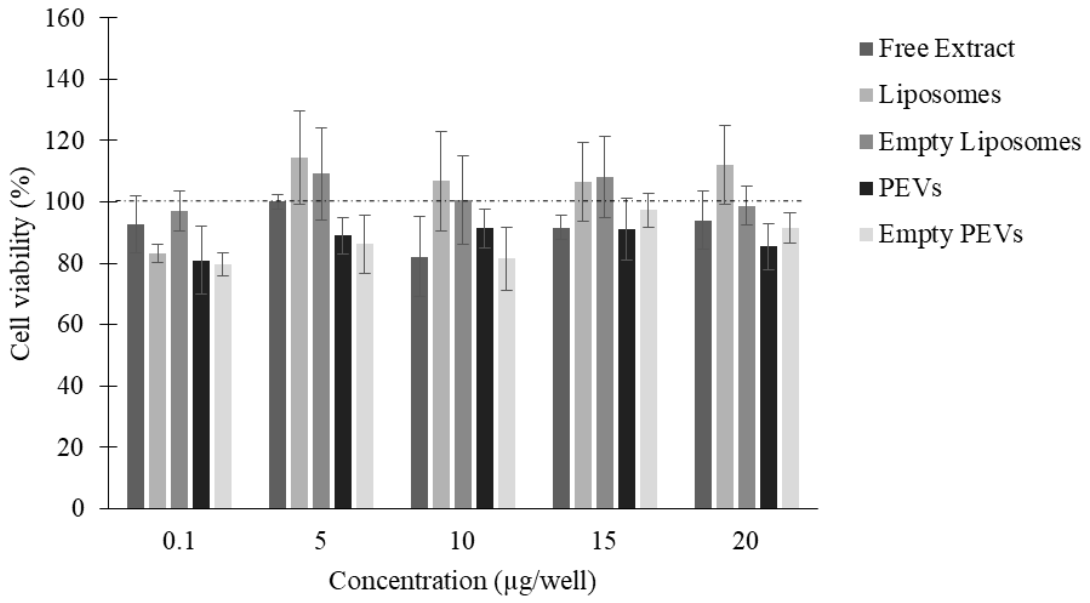

Figure 42. Viability of A431 upon exposure to A. rusticana samples for 24 h. Data are expressed as means ± standard error (SE); n=2 independent experiments; no differences statistically relevant among the different samples and among the control group (100% viability; not shown in the graph).

4.4.3.3. Antioxidant activity – DPPH, FRAP

The antioxidant activity of the horseradish formulations was estimated as a function of their radical scavenging and ferric reducing abilities (Table 25). The horseradish solution scavenged the DPPH radical moderately (43%, corresponding to ~90 µg/mL of Trolox equivalents). The level of antioxidant activity for the horseradish liposomes was 81% and for PEVs was 77%, both with a statistically significant difference from the horseradish solution (Table 25). This increase is due to the antioxidant contribution given by the phospholipids, in fact empty vesicles possessed a slight antioxidant activity as well.

The results of FRAP assay indicated that solution and the vesicles had a stronger power as ferric reducing abilities, with values around 733, 1090, and 1180 µg/mL of ferrous equivalents for solution, liposomes, and PEVs, respectively. The empty vesicles showed a reducing power similar to that of the free extract (Table 25).

	DPPH assay		FRAP assay
	AA (%)	***TE (µg Trolox equivalents/mL)***	***FE (µg Fe2+ equivalents/mL)***
Free extract solution	43.0 ± 9.6	90.0 ± 19.4	733.0 ± 6.8
Lip	*81.0 ± 10.9	*173.0 ± 23.1	*1090.0 ± 9.1
Empty lip	69.0 ± 16.6	147.0 ± 35.5	687.0 ± 32.4
PEVs	*77.0 ± 13.8	*164.0 ± 29.7	*,#1180.0 ± 37.5
Empty PEVs	62.0 ± 5.4	149.0 ± 30.5	637.0 ± 26.7

*Table 25. In vitro antioxidant activity of horseradish formulations. For the DPPH assay, results are expressed as AA (%) and TE (µg Trolox equivalents); for the FRAP assay, results are expressed as FE (µg Fe^{2+} equivalents/mL solution) and reported as the mean ± SD of at least three separate experiments, each performed in triplicate. * statistically different values (p<0.01) from the horseradish solution. # statistically different values (p<0.05) from the horseradish liposomes.*

4.4.3.4. Antioxidant activity - cells protection from chemically-induced oxidative stress

The antioxidant capacities of *A. rusticana* samples were investigated also as the ability to protect cells from hydrogen peroxide-induced oxidative stress. 10 µg in well were used for each cell pre-treatment. Figure 43 demonstrates that treatment with 2 mM H_2O_2 reduced 3T3 viability to 38% compared to the untreated cells and that there was some protection activity in cells pre-treated with horseradish samples, both the free extract and lipid vesicles formulation. For the other cell lines, there was a similar tendency (Fig. 44 and 45).

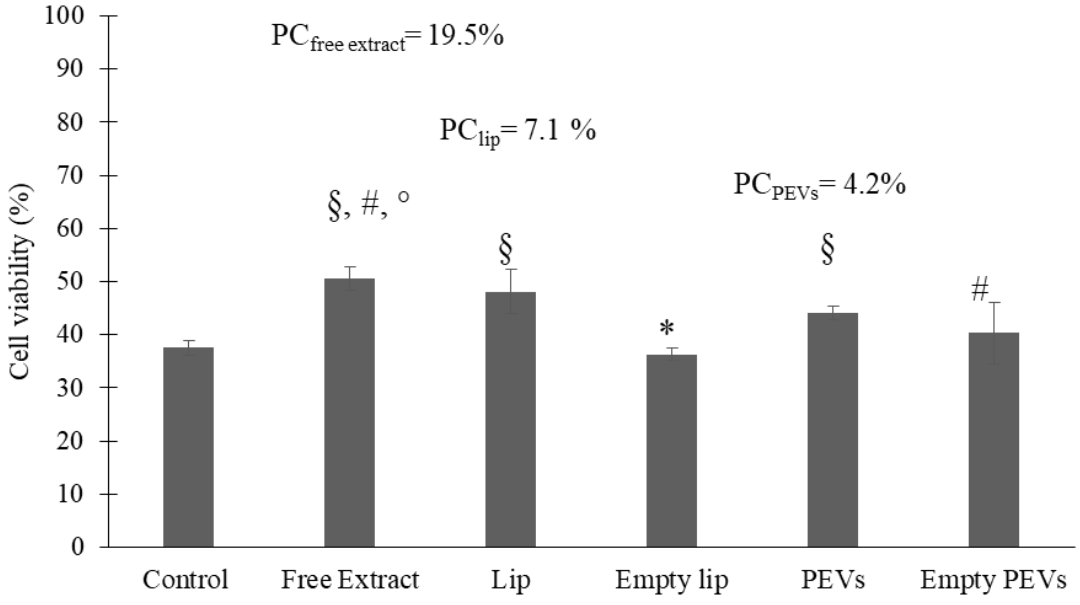

*Figure 43. Viability of 3T3 upon pre-treatment with A. rusticana samples and subsequent exposure to H_2O_2 2 mM. Data are expressed as means ± standard error (SE); n=2 independent experiments; § p<0.05 vs. control group (cells without pre-treatment); * p<0.01 vs lip; # p<0.01 vs. empty lip; ° p<0.01 vs. empty PEVs; φ p<0.05 vs PEVs. All samples were different from control cells without pre-treatment and H_2O_2 exposure (100% viability). When present, the PC% is also expressed.*

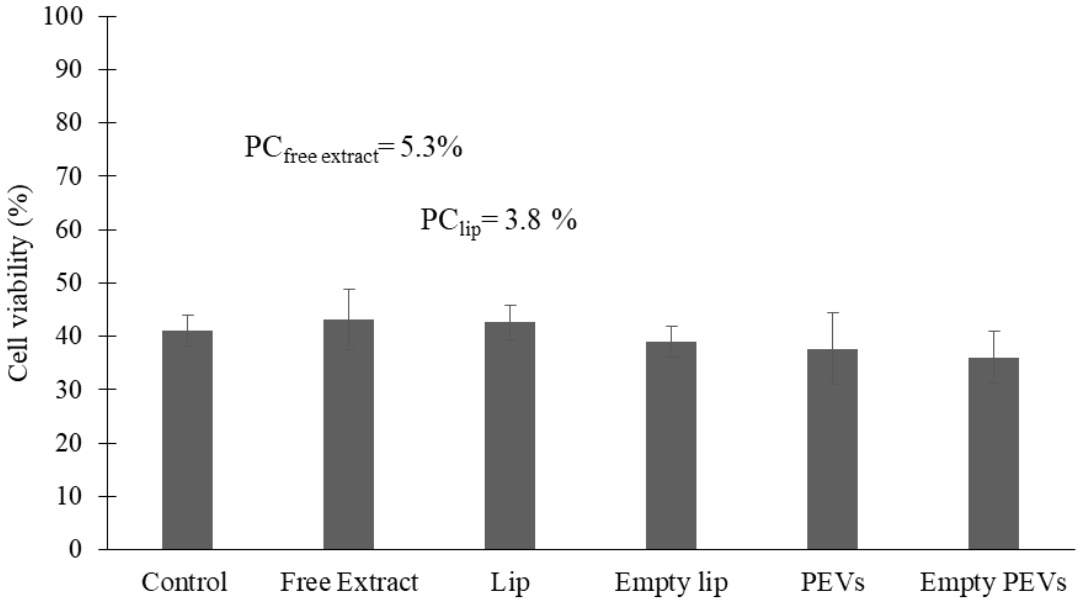

Figure 44. Viability of HaCaT upon pre-treatment with A. rusticana samples and subsequent exposure to H_2O_2 2 mM. Data are expressed as means ± standard error (SE); n=2 independent experiments; no statistically relevant differences among the samples, except for control cells without pre-treatment and H_2O_2 exposure (100% viability). When present, the PC% is also expressed.

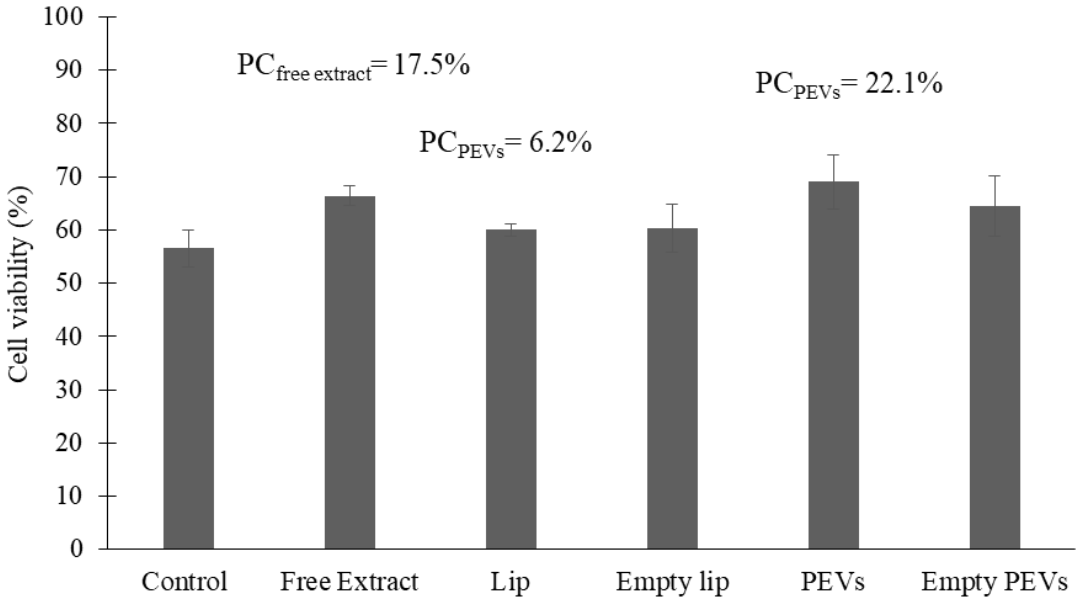

Figure 45. Viability of A431 upon pre-treatment with A. rusticana samples and subsequent exposure to H_2O_2 2 mM. Data are expressed as means ± standard error (SE); n=2 independent experiments; no statistically relevant differences among the samples, except for control cells without pre-treatment and H_2O_2 exposure (100% viability). When present, the PC% is also expressed.

4.4.3.5. Antibacterial activity

The *A. rusticana* extract showed antibacterial activity against *B. subtilis* and *S. aureus*. More precisely, MIC and MBC were 16 mg/mL for both strains (fig. 46). The antibacterial activity against

S. aureus was reported in previous studies for aqueous [127] and methanol [129] extracts from horseradish roots, although with a lower MBC values. No previous data are found for inhibitory activity against *B. subtilis*. It was not possible to assay the two vesicular formulations because MIC and MBC values were approximately the same concentration as that used for vesicle preparation (20 mg/mL). So, no more dilutions with bacteria medium could be performed (as required by the protocol described in the previous chapter, for appropriate bacteria growth). Our formulations had an extract concentration of 20 mg/mL of extract, which is above the MIC and MBC values, hence we expect them to possess antibacterial activity.

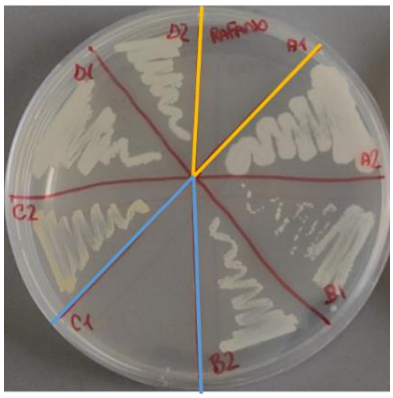

Figure 46. Antibacterial activity of A. rusticana extract (16 mg/mL) against Bacillus subtilis (A1, in orange) and Staphylococcus aureus (C1, in blue).

5. Discussions

5.1. *Myrtus communis* L.

The high antioxidant activity of the myrtle berry extract was proved in numerous studies documented in the literature in which it emerged that the antioxidant activity depends on the extracting solvents and processing conditions [170,171]. Moreover, the extracts are complex mixtures that could also contribute to diverse results. Based on our research, only one study on myrtle extract in vesicle formulation was reported. Despite this, the extract was obtained from myrtle leaves [172]. In our study, the myrtle liposomes were characterized by their smaller size (approximately 100 nm) and higher entrapment efficiency for the main compounds present in the ethanolic extract (more than 70%), improving the formulation's potential. These formulations resulted biocompatible at the concentration values tested on fibroblasts 3T3-L1 and able to prevent the small extent inner toxicity of the myrtle extract. Particularly, the MTT results showed that the slight cytotoxicity (~10-20% mortality) induced from myrtle solution (10 µg) is not found for liposomes; moreover, the endogenous ROS production slightly triggered by myrtle solution was mitigated by its incorporation in liposomes. As shown by the DPPH assay, the myrtle extract showed prominent antioxidant activity (96%) retained after the nanoformulation and confirmed by the FRAP assay. The results obtained in fibroblasts demonstrated not only that the liposome formulation did not stress the cells but also protected those from chemically induced oxidative stress more efficiently than the free myrtle extract.

5.2. *Prunus spinosa* L.

The chemical characterization of *P. spinosa* extract through LC-MS allowed us to identify different compounds commonly known for their biological importance. Two different kinds of phospholipid vesicles were formulated for this product, with the aim to potentiate biological activity. Both formulations had a size below 100 nm, with PG leading to the formation of vesicles smaller than liposomes (86 *vs* 94 nm). Both vesicles had similar PDI and ZP values, a unilamellar structure, and a similar ability to maintain their structure (size, PDI, and ZP) over time. However, PG-PEVs showed a lower EE% than liposomes for targeted compounds, with a decrease in efficiency between 7 and 20%. The biocompatibility of samples was confirmed by the absence of cytotoxicity in the different cell

models used (fibroblasts 3T3, keratinocytes HaCaT, and tumour keratinocytes A431), also at high concentrations. The biocompatibility was preliminarily tested as hemolytic activity in erythrocytes, one of the most widely used cell membrane systems. It is an easy method to gain some information about the samples' safety, faster than assays with cells.

Regarding the antioxidant power, the blackthorn's ability to scavenge DPPH radical significantly decreased in the two encapsulated forms. This could not necessarily be related to the sonication techniques used for vesicle preparation but rather to the low entrapment efficiency of hydroxycinnamic acids which are known to be potent antioxidants [173]. The antioxidant properties of these samples were assayed also as the ability to protect cells from the hydrogen peroxide-induced cytotoxic effect, but for the concentration values tested, no significant beneficial effects emerged, neither for the free solution nor for the nanoformulated forms. On the other hand, the antibacterial assay showed that the extract (16 mg/mL) had inhibitory activity against *S. aureus* and *S. epidermidis*.

5.3. *Ceratonia siliqua* L.

As reported in the literature, carob is rich in different compounds biologically active with antioxidant properties. The two most abundant compounds of the prepared extract were a gallic acid derivative and a quercetin derivative, both entrapped with a high efficiency (> 90%) in the produced liposomes.

The low hemolytic activity in erythrocytes demonstrated the safety of carob liposomes at the tested doses, which was confirmed by *in vitro* analyses in fibroblasts and keratinocytes. The MTT results showed that the free extract and liposomes were not toxic at all concentrations and in all the cell lines tested, although there was a small reduction in cell viability in some cases, values were always > 80%.

The DPPH and FRAP colourimetric tests showed that the antioxidant activity of carob extract was retained in the liposomal form. In 3T3 fibroblasts, liposomes had a better capacity than the solution to protect cells from chemically induced oxidative stress. In keratinocytes, there was an opposite behaviour, with greater antioxidant activity for the free extract.

5.4. *Armoracia rusticana* L.

The phospholipid vesicles prepared with this extract, conventional liposomes and Et-PEVs, displayed a small diameter (84 *vs.* 93 nm), with a PDI of 0.2, a negative surface charge, unilamellar structure, and

high entrapment efficiency of the two most copious compounds in the extract. The vesicles resulted to be biocompatible, both for hemolytic and MTT assays. Of note, the hemolytic activity of the free extract solution (16% at 2 mg/mL) was significantly reduced with the nanoformulated forms (1.5% for liposomes and 3% for Et-PEVs). Similarly, MTT results for 3T3 fibroblasts showed that conventional liposomes increased cell viability compared with the extract solution, mainly at high concentrations, differently from Et-PEVs. For HaCaT and A431 keratinocytes, there were no particular differences between the vesicle formulations and the extract solution. Related to the antioxidant property, DPPH and FRAP showed that the solution did not have a notable antioxidant activity, which however improved upon formulation in liposomes and PEVs, due to the contribution of the carriers' phospholipids. With *in vitro* tests in cells, there were different results: while for 3T3 fibroblasts the extract solution and liposomes had a slight ability to protect cells, this effect was not evident in HaCaT and A431 keratinocytes. Rather, the antibacterial assay showed that the free extract solution (16 mg/mL) had inhibitory activity against *S. aureus* and *B. subtilis*.

6. Conclusions

The nanoformulation of natural bioactive substances in phospholipid vesicles is one of the most promising strategies to overcome obstacles related to undesirable features of natural extracts.

In this research project, we focused on four plant extracts obtained with the conventional method of maceration in a green solvent. Although a few disadvantages, such as extraction time and solvent wastage, maceration in ethanol is one of the go-to methods for the extraction of phytochemical compounds, especially polyphenols, due to its simplicity, low cost, and environmentally friendly characteristics, compared to other methods [174]. The extracts were characterized to detect and quantify known biologically active compounds. We formulated the extracts in lipid-based nanocarriers by using a simple and fast method based on the sonication of phospholipid and extract in the dispersant medium. Therefore, both the extracts preparation and their subsequent nanoformulation were performed without the utilization of hazardous solvents.

Importantly, we obtained vesicles with a high entrapment efficiency of the main compounds characteristic of each extract, although some compounds showed lower values than others.

Moreover, all prepared vesicles were small in diameter (<100 nm) and this is an important matter because the particle size and shape determine the transport of the active ingredients through the skin layers, having an impact on the active ingredients' stability, release, and cellular uptake [12]. The electron scattering profile obtained with X-ray diffraction suggests that the extracts and PE molecules did not affect the bilayer structures, as highlighted by similar values for the parameters analyzed. Given the high encapsulation efficiencies for dosed compounds, the two possibilities are:

- the extract was mainly in the hydrophilic core of lipid vesicles;
- the extract does not affect the bilayer structure because of the low concentration or the low electron density contrast.

A weak point was the stability of the formulation for a long time, mainly related to the phospholipid nature and their tendency to oxidation and hydrolysis. Unfortunately, this is one of the most critical problems of vesicle formulations [50,51].

The biocompatibility of the nanoformulations was tested *in vitro* with different tests and cell models: all samples showed viability values of at least 80% in comparison with control cells. The nanoformulation

had the primary task of increasing extracts' bioavailability in cells and limiting potential toxicity without hindering their antioxidant action. As shown by the DPPH and FRAP assays, the antioxidant activity of each extract was retained after the nanoformulation, although some samples did not show powerful antioxidant activity in cells. However, it is true that the antioxidant action could be performed in different ways in cells, and in our case, only one type of test was performed, suggesting that further studies are needed.

List of figures

List of tables

Abbreviations

3T3 murine swiss albino fibroblasts

A431 human epidermoid carcinoma cell line

AA Antioxidant Activity

APD Avalanche Photodiode Detector

ATCC American Type Culture Collection

CM-H_2DCF-DA 5-(and-6)-chloromethyl-20,70-dichlorodihydrofluorescein diacetate, acetyl ester

Cryo-TEM Cryogenic Transmission Electron Microscopy

DLS Dynamic Light Scattering

DMEM Dulbecco's Modified Eagle's Medium

DMSO dymethylsufoxide

DPPH 2,2-diphenylpicrylhydrazyl

EDTA ethylenediaminetetraacetate

EE Entrapment Efficiency

ELS Electrophoretic Light Scattering

ESI Electrospray Ionization

Et ethanol

FBS Fetal Bovine Serum

FRAP Ferric ion reducing antioxidant power

GC-MS Gas Chromatography Mass Spectrometry

GUVs Giant Unilamellar Vesicles

HaCaT cultured human keratinocyte

HPLC High Performance Liquid Chromatography

LC-MS Liquid Chromatography-Mass Spectrometry

Lip Liposomes

LUVs Large Unilamellar Vesicles

MBC Minimum Bactericidal Concentration

MeOH methanol

MIC Minimum Inhibitory Concentration

MLVs Multilamellar Vesicles

MS/MS tandem mass spectrometry

MTT 3-[4,5-dimethylthiazol-2-yl]-2,5 diphenyl tetrazolium bromide

MVVs Multivesicular Vesicles

NIBS Non-Invasive Back-Scatter

P90G Phospholipon90G

PALS Phase Analysis Light Scattering

PBS Phosphate Buffered Saline

PC Protective Capacity

PCS Photon Correlation Spectroscopy

PDA Photodiode Array Detector

PDI Polydispersity Index

PE Penetration Enhancer

PEG Polyethylene Glycol

PEVs Penetration Enhancer containing Vesicles

PG Propylene Glycol

QTOF MS Quadrupole Time Of Flight Mass Spectrometry

ROS Reactive Oxygen Species

S75 fat-free soybean phospholipids with 70% phosphatidylcholine

SAXS Small-Angle X ray Scattering

SUVs Small Unilamellar Vesicles

TCC Total Compound Chromatogram

TPTZ 2,4,6-Tri(2-pyridyl)-1,3,5-triazine

ULVs Unilamellar Vesicles

UV–Vis Ultraviolet-Visible Spectroscopy

References

1. Su, S.; Kang, P.M. Recent advances in nanocarrier-assisted therapeutics delivery systems. *Pharmaceutics* 2020, *12*, 1–27.

2. Bangham, A.D.; Standish, M.M.; Watkins, J.C. Diffusion of univalent ions across the lamellae of swollen phospholipids. *J. Mol. Biol.* **1965**, *13*, 238–252, doi:10.1016/S0022-2836(65)80093-6.

3. Barenholz, Y. Doxil® - The first FDA-approved nano-drug: Lessons learned. *J. Control. Release* 2012, *160*, 117–134.

4. Levchenko, T.S.; Hartner, W.C.; Torchilin, V.P. Liposomes for cardiovascular targeting. *Ther. Deliv.* 2012, *3*, 501–514.

5. Bruch, G.E.; Fernandes, L.F.; Bassi, B.L.T.; Alves, M.T.R.; Pereira, I.O.; Frézard, F.; Massensini, A.R. Liposomes for drug delivery in stroke. *Brain Res. Bull.* 2019, *152*, 246–256.

6. Ross, C.; Taylor, M.; Fullwood, N.; Allsop, D. Liposome delivery systems for the treatment of Alzheimer's disease. *Int. J. Nanomedicine* 2018, *13*, 8507–8522.

7. Villalba, A.; Rodriguez-Fernandez, S.; Ampudia, R.M.; Cano-Sarabia, M.; Perna-Barrull, D.; Bertran-Cobo, C.; Ehrenberg, C.; Maspoch, D.; Vives-Pi, M. Preclinical evaluation of antigen-specific nanotherapy based on phosphatidylserine-liposomes for type 1 diabetes. *Artif. Cells, Nanomedicine Biotechnol.* **2020**, *48*, 77–83, doi:10.1080/21691401.2019.1699812.

8. Mehta, S.; Kulkarni, S.; Nikam, A.N.; Padya, B.S.; Pandey, A.; Mutalik, S. Liposomes as Versatile Platform for Cancer Theranostics: Therapy, Bio-imaging, and Toxicological Aspects. *Curr. Pharm. Des.* **2021**, *27*, 1977–1991, doi:10.2174/1381612827666210311142100.

9. Castañeda-Reyes, E.D.; Perea-Flores, M. de J.; Davila-Ortiz, G.; Lee, Y.; de Mejia, E.G. Development, characterization and use of liposomes as amphipathic transporters of bioactive compounds for melanoma treatment and reduction of skin inflammation: A review. *Int. J. Nanomedicine* 2020, *15*, 7627–7650.

10. Cheng, C.Y.; Barro, L.; Tsai, S.T.; Feng, T.W.; Wu, X.Y.; Chao, C.W.; Yu, R.S.; Chin, T.Y.; Hsieh, M.F. Epigallocatechin-3-gallate-loaded liposomes favor anti-inflammation of microglia cells and promote neuroprotection. *Int. J. Mol. Sci.* **2021**, *22*, 1–15, doi:10.3390/ijms22063037.

11. Laouini, A.; Jaafar-Maalej, C.; Limayem-Blouza, I.; Sfar, S.; Charcosset, C.; Fessi, H. Preparation, Characterization and Applications of Liposomes: State of the Art. *J. Colloid Sci. Biotechnol.* **2012**, *1*, 147–168, doi:10.1166/jcsb.2012.1020.

12. Santos, A.C.; Rodrigues, D.; Sequeira, J.A.D.; Pereira, I.; Simões, A.; Costa, D.; Peixoto, D.; Costa, G.; Veiga, F. Nanotechnological breakthroughs in the development of topical phytocompounds-based formulations. *Int. J. Pharm.* **2019**, *572*, doi:10.1016/j.ijpharm.2019.118787.

13. Singh, M.; Devi, S.; Rana, V.S.; Mishra, B.B.; Kumar, J.; Ahluwalia, V. Delivery of phytochemicals by liposome cargos: recent progress, challenges and opportunities. *J. Microencapsul.* **2019**, *36*, 215–235, doi:10.1080/02652048.2019.1617361.

14. Shah, S.; Dhawan, V.; Holm, R.; Nagarsenker, M.S.; Perrie, Y. Liposomes: Advancements and innovation in the manufacturing process. *Adv. Drug Deliv. Rev.* **2020**, *154–155*, 102–122, doi:10.1016/j.addr.2020.07.002.

15. Guimarães, D.; Cavaco-Paulo, A.; Nogueira, E. Design of liposomes as drug delivery system for therapeutic applications. *Int. J. Pharm.* 2021, *601*.

16. Patil, Y.P.; Jadhav, S. Novel methods for liposome preparation. *Chem. Phys. Lipids* 2014, *177*, 8–18.

17. Has, C.; Sunthar, P. A comprehensive review on recent preparation techniques of liposomes. *J. Liposome Res.* **2020**, *30*, 336–365, doi:10.1080/08982104.2019.1668010.

18. Lapinski, M.M.; Castro-Forero, A.; Greiner, A.J.; Ofoli, R.Y.; Blanchard, G.J. Comparison of liposomes formed by sonication and extrusion: Rotational and translational diffusion of an embedded chromophore. *Langmuir* **2007**, *23*, 11677–11683, doi:10.1021/la7020963.

19. Rieth, M.D.; Lozano, A. Preparation of DPPC liposomes using probe-tip sonication: Investigating intrinsic factors affecting temperature phase transitions. *Biochem. Biophys. Reports* **2020**, *22*, doi:10.1016/j.bbrep.2020.100764.

20. Mozafari, M.R.; Omri, A. Importance of divalent cations in nanolipoplex gene delivery. *J. Pharm. Sci.* **2007**, *96*, 1955–1966, doi:10.1002/jps.20902.

21. Skalko-Basnet, N.; Pavelic, Z.; Becirevic-Lacan, M. Liposomes containing drug and cyclodextrin prepared by the one-step spray-drying method. *Drug Dev. Ind. Pharm.* **2000**, *26*, 1279–1284, doi:10.1081/DDC-100102309.

22. Cui, J.; Li, C.; Deng, Y.; Wang, Y.; Wang, W. Freeze-drying of liposomes using tertiary butyl alcohol/water cosolvent systems. *Int. J. Pharm.* **2006**, *312*, 131–136, doi:10.1016/j.ijpharm.2006.01.004.

23. Li, C.; Deng, Y. A novel method for the preparation of liposomes: Freeze drying of monophase solutions. *J. Pharm. Sci.* **2004**, *93*, 1403–1414, doi:10.1002/jps.20055.

24. Sugawara, E.; Nikaido, H. Properties of AdeABC and AdeIJK efflux systems of Acinetobacter baumannii compared with those of the AcrAB-TolC system of Escherichia coli. *Antimicrob. Agents Chemother.* **2014**, *58*, 7250–7257, doi:10.1128/AAC.03728-14.

25. Otake, K.; Shimomura, T.; Goto, T.; Imura, T.; Furuya, T.; Yoda, S.; Takebayashi, Y.; Sakai, H.; Abe, M. Preparation of liposomes using an improved supercritical reverse phase evaporation method. *Langmuir* **2006**, *22*, 2543–2550, doi:10.1021/la051654u.

26. Jahn, A.; Vreeland, W.N.; Devoe, D.L.; Locascio, L.E.; Gaitan, M. Microfluidic directed formation of liposomes of controlled size. *Langmuir* **2007**, *23*, 6289–6293, doi:10.1021/la070051a.

27. Jahn, A.; Vreeland, W.N.; Gaitan, M.; Locascio, L.E. Controlled Vesicle Self-Assembly in Microfluidic Channels with Hydrodynamic Focusing. *J. Am. Chem. Soc.* **2004**, *126*, 2674–2675, doi:10.1021/ja0318030.

28. Wagner, A.; Vorauer-Uhl, K.; Kreismayr, G.; Katinger, H. The crossflow injection technique: An improvement of the ethanol injection method. *J. Liposome Res.* **2002**, *12*, 259–270, doi:10.1081/LPR-120014761.

29. Wagner, A.; Platzgummer, M.; Kreismayr, G.; Quendler, H.; Stiegler, G.; Ferko, B.; Vecera, G.; Vorauer-Uhl, K.; Prof, H.K. GMP production of liposomes - A new industrial approach. In Proceedings of the Journal of Liposome Research; Taylor & Francis, 2006; Vol. 16, pp. 311–319.

30. Laouini, A.; Jaafar-Maalej, C.; Gandoura-Sfar, S.; Charcosset, C.; Fessi, H. Spironolactone-loaded liposomes produced using a membrane contactor method: An improvement of the ethanol injection technique. *Prog. Colloid Polym. Sci.* **2011**, *139*, 23–28, doi:10.1007/978-3-642-28974-3_5.

31. Elsana, H.; Olusanya, T.O.B.; Carr-wilkinson, J.; Darby, S.; Faheem, A.; Elkordy, A.A. Evaluation of novel cationic gene based liposomes with cyclodextrin prepared by thin film hydration and microfluidic systems. *Sci. Rep.* **2019**, *9*, 1–17, doi:10.1038/s41598-019-51065-4.

32. Sercombe, L.; Veerati, T.; Moheimani, F.; Wu, S.Y.; Sood, A.K.; Hua, S. Advances and challenges of liposome assisted drug delivery. *Front. Pharmacol.* 2015, *6*, 286.

33. William, B.; Noémie, P.; Brigitte, E.; Géraldine, P. Supercritical fluid methods: An alternative to conventional methods to prepare liposomes. *Chem. Eng. J.* 2020, *383*, 123106.

34. Koppel, D.E. Analysis of macromolecular polydispersity in intensity correlation spectroscopy: The method of cumulants. *J. Chem. Phys.* **1972**, *57*, 4814–4820, doi:10.1063/1.1678153.

35. Danaei, M.; Dehghankhold, M.; Ataei, S.; Hasanzadeh Davarani, F.; Javanmard, R.; Dokhani, A.; Khorasani, S.; Mozafari, M.R. Impact of particle size and polydispersity index on the clinical applications of lipidic nanocarrier systems. *Pharmaceutics* 2018, *10*, 57.

36. Manconi, M.; Aparicio, J.; Vila, A.O.; Pendás, J.; Figueruelo, J.; Molina, F. Viscoelastic properties of concentrated dispersions in water of soy lecithin. In Proceedings of the Colloids and Surfaces A: Physicochemical and Engineering Aspects; Elsevier, 2003; Vol. 222, pp. 141–145.

37. Prabhu, S.; Murugan, K. Zeta potential measurements in colloidal suspensions. *Int. Conf. Syst. Sci. Control. Commun. Eng. Technol.* **2015**, 221–224.

38. Elizondo, E.; Moreno, E.; Cabrera, I.; Córdoba, A.; Sala, S.; Veciana, J.; Ventosa, N. Liposomes and other vesicular systems: Structural characteristics, methods of preparation, and use in nanomedicine. In *Progress in Molecular Biology and Translational Science*; Academic Press, 2011; Vol. 104, pp. 1–52.

39. Isalomboto Nkanga, C.; Murhimalika Bapolisi, A.; Ikemefuna Okafor, N.; Werner Maçedo Krause, R. General Perception of Liposomes: Formation, Manufacturing and Applications. In *Liposomes - Advances and Perspectives*; IntechOpen, 2019 ISBN 978-1-78984-495-5.

40. Maherani, B.; Arab-Tehrany, E.; R. Mozafari, M.; Gaiani, C.; Linder, M. Liposomes: A Review of Manufacturing Techniques and Targeting Strategies. *Curr. Nanosci.* **2011**, *7*, 436–452, doi:10.2174/157341311795542453.

41. Pattni, B.S.; Chupin, V. V.; Torchilin, V.P. New Developments in Liposomal Drug Delivery. *Chem. Rev.* 2015, *115*, 10938–10966.

42. Di Cola, E.; Grillo, I.; Ristori, S. Small angle X-ray and neutron scattering: Powerful tools for studying the structure of drug-loaded liposomes. *Pharmaceutics* **2016**, *8*, 1–16, doi:10.3390/pharmaceutics8020010.

43. El Maghraby, G.M.; Barry, B.W.; Williams, A.C. Liposomes and skin: From drug delivery to model membranes. *Eur. J. Pharm. Sci.* 2008, *34*, 203–222.

44. Carita, A.C.; Eloy, J.O.; Chorilli, M.; Lee, R.J.; Leonardi, G.R. Recent Advances and Perspectives in Liposomes for Cutaneous Drug Delivery. *Curr. Med. Chem.* **2017**, *25*, 606–635, doi:10.2174/0929867324666171009120154.

45. Schnablegger, H.; Singh, Y. The SAXS Guide. *Ant. Paar* **2011**, 1–99.

46. Bakonyi, M.; Berkó, S.; Budai-Szűcs, M.; Kovács, A.; Csányi, E. DSC for evaluating the encapsulation efficiency of lidocaine-loaded liposomes compared to the ultracentrifugation method. *J. Therm. Anal. Calorim.* **2017**, *130*, 1619–1625, doi:10.1007/s10973-017-6394-1.

47. Agarwal, S.; Krishnamurthy, K. *Histology, Skin - StatPearls - NCBI Bookshelf*; 2021;

48. Benson, H.A.E.; Grice, J.E.; Mohammed, Y.; Namjoshi, S.; Roberts, M.S. Topical and Transdermal Drug Delivery: From Simple Potions to Smart Technologies. *Curr. Drug Deliv.* **2019**, *16*, 444–460, doi:10.2174/1567201816666190201143457.

49. Souto, E.B.; Macedo, A.S.; Dias-Ferreira, J.; Cano, A.; Zielińska, A.; Matos, C.M. Elastic and ultradeformable liposomes for transdermal delivery of active pharmaceutical ingredients (Apis). *Int. J. Mol. Sci.* 2021, *22*.

50. Sguizzato, M.; Esposito, E.; Cortesi, R. Lipid-based nanosystems as a tool to overcome skin barrier. *Int. J. Mol. Sci.* 2021, *22*.

51. Sinico, C.; Fadda, A.M. Vesicular carriers for dermal drug delivery. *Expert Opin. Drug Deliv.* **2009**, *6*, 813–825, doi:10.1517/17425240903071029.

52. HANDJANI-VILA, R.M.; RIBIER, A.; RONDOT, B.; VANLERBERGHIE, G. Dispersions of lamellar phases of non-ionic lipids in cosmetic products. *Int. J. Cosmet. Sci.* **1979**, *1*, 303–314,

doi:10.1111/j.1467-2494.1979.tb00224.x.

53. Cevc, G.; Blume, G. Lipid vesicles penetrate into intact skin owing to the transdermal osmotic gradients and hydration force. *BBA - Biomembr.* **1992**, *1104*, 226–232, doi:10.1016/0005-2736(92)90154-E.

54. Touitou, E.; Dayan, N.; Bergelson, L.; Godin, B.; Eliaz, M. Ethosomes - Novel vesicular carriers for enhanced delivery: Characterization and skin penetration properties. *J. Control. Release* **2000**, *65*, 403–418, doi:10.1016/S0168-3659(99)00222-9.

55. El Maghraby, G.M.M.; Williams, A.C.; Barry, B.W. Skin delivery of oestradiol from lipid vesicles: Importance of liposome structure. *Int. J. Pharm.* **2000**, *204*, 159–169, doi:10.1016/S0378-5173(00)00493-2.

56. Dragicevic-Curic, N.; Scheglmann, D.; Albrecht, V.; Fahr, A. Temoporfin-loaded invasomes: Development, characterization and in vitro skin penetration studies. *J. Control. Release* **2008**, *127*, 59–69, doi:10.1016/j.jconrel.2007.12.013.

57. Dubey, V.; Mishra, D.; Dutta, T.; Nahar, M.; Saraf, D.K.; Jain, N.K. Dermal and transdermal delivery of an anti-psoriatic agent via ethanolic liposomes. *J. Control. Release* **2007**, *123*, 148–154, doi:10.1016/j.jconrel.2007.08.005.

58. Elsayed, M.M.A.; Abdallah, O.Y.; Naggar, V.F.; Khalafallah, N.M. PG-liposomes: novel lipid vesicles for skin delivery of drugs. *J. Pharm. Pharmacol.* **2010**, *59*, 1447–1450, doi:10.1211/jpp.59.10.0017.

59. Mura, S.; Manconi, M.; Fadda, A.M.; Sala, M.C.; Perricci, J.; Pini, E.; Sinico, C. Penetration enhancer-containing vesicles (PEVs) as carriers for cutaneous delivery of minoxidil: in vitro evaluation of drug permeation by infrared spectroscopy. *http://dx.doi.org/10.3109/10837450.2012.685661* **2013**, *18*, 1339–1345, doi:10.3109/10837450.2012.685661.

60. Mura, S.; Manconi, M.; Sinico, C.; Valenti, D.; Fadda, A.M. Penetration enhancer-containing vesicles (PEVs) as carriers for cutaneous delivery of minoxidil. *Int. J. Pharm.* **2009**, *380*, 72–79, doi:10.1016/j.ijpharm.2009.06.040.

61. Mura, S.; Manconi, M.; Valenti, D.; Sinico, C.; Vila, A.O.; Fadda, A.M. Transcutol containing vesicles for topical delivery of minoxidil. *J. Drug Target.* **2011**, *19*, 189–196, doi:10.3109/1061186X.2010.483516.

62. Hua, S. Lipid-based nano-delivery systems for skin delivery of drugs and bioactives. *Front. Pharmacol.* 2015, *6*, 219.

63. Sala, M.; Diab, R.; Elaissari, A.; Fessi, H. Lipid nanocarriers as skin drug delivery systems: Properties, mechanisms of skin interactions and medical applications. *Int. J. Pharm.* 2018, *535*, 1–17.

64. Dini, I.; Laneri, S. The new challenge of green cosmetics: Natural food ingredients for cosmetic formulations. *Molecules* 2021, *26*.

65. Erb, M.; Kliebenstein, D.J. Plant Secondary Metabolites as Defenses, Regulators, and Primary Metabolites: The Blurred Functional Trichotomy1[OPEN]. *Plant Physiol.* 2020, *184*, 39–52.

66. Amin, T.; Bhat, S.; Vikas Bhat, S. A Review on Phytosome Technology as a Novel Approach to Improve The Bioavailability of Nutraceuticals. *Int. J. Adv. Res. Technol.* **2012**, *1*.

67. Manach, C.; Scalbert, A.; Morand, C.; Rémésy, C.; Jiménez, L. Polyphenols: Food sources and bioavailability. *Am. J. Clin. Nutr.* 2004, *79*, 727–747.

68. Yang, B.; Dong, Y.; Wang, F.; Zhang, Y. Nanoformulations to enhance the bioavailability and physiological functions of polyphenols. *Molecules* 2020, *25*.

69. Gugleva, V.; Ivanova, N.; Sotirova, Y.; Andonova, V. Dermal drug delivery of phytochemicals with phenolic structure via lipid-based nanotechnologies. *Pharmaceuticals* 2021, *14*, 837.

70. Patra, J.K.; Das, G.; Fraceto, L.F.; Campos, E.V.R.; Rodriguez-Torres, M.D.P.; Acosta-Torres, L.S.;

Diaz-Torres, L.A.; Grillo, R.; Swamy, M.K.; Sharma, S.; et al. Nano based drug delivery systems: Recent developments and future prospects 10 Technology 1007 Nanotechnology 03 Chemical Sciences 0306 Physical Chemistry (incl. Structural) 03 Chemical Sciences 0303 Macromolecular and Materials Chemistry 11 Medical and He. *J. Nanobiotechnology* 2018, *16*, 1–33.

71. Spanidi, E.; Karapetsas, A.; Voulgaridou, G.P.; Letsiou, S.; Aligiannis, N.; Tsochantaridis, I.; Kynigopoulos, S.; Lambropoulou, M.; Mourtzinos, I.; Pappa, A.; et al. A new controlled release system for propolis polyphenols and its biochemical activity for skin applications. *Plants* **2021**, *10*, 1–27, doi:10.3390/plants10020420.

72. Serreli, G.; Jerković, I.; Gil, K.A.; Marijanović, Z.; Pacini, V.; Tuberoso, C.I.G. Phenolic Compounds, Volatiles and Antioxidant Capacity of White Myrtle Berry Liqueurs. *Plant Foods Hum. Nutr.* **2017**, *72*, 205–210, doi:10.1007/s11130-017-0611-8.

73. Hennia, A.; Miguel, M.; Nemmiche, S. Antioxidant Activity of Myrtus communis L. and Myrtus nivellei Batt. & Trab. Extracts: A Brief Review. *Medicines* **2018**, *5*, 89, doi:10.3390/medicines5030089.

74. Kordali, S.; Usanmaz, A.; Cakir, A.; Komaki, A.; Ercisli, S. Antifungal and Herbicidal Effects of Fruit Essential Oils of Four Myrtus communis Genotypes. *Chem. Biodivers.* **2016**, *13*, 77–84, doi:10.1002/cbdv.201500018.

75. Jabri, M.A.; Hajaji, S.; Rtibi, K.; Sebai, H. Role of Anti-Inflammatory, Reactive Oxygen Species Scavenging Activity and Nematicidal Properties of Myrtle Berry Seeds on Helminthiasis Treatment. *J. Med. Food* **2021**, *24*, 377–384, doi:10.1089/jmf.2020.0089.

76. Jabri, M.A.; Marzouki, L.; Sebai, H. Myrtle berries seeds aqueous extract abrogates chronic alcohol consumption-induced erythrocytes osmotic stability disturbance, haematological and biochemical toxicity. *Lipids Health Dis.* **2018**, *17*, doi:10.1186/s12944-018-0746-0.

77. Jabri, M.A.; Rtibi, K.; Ben-Said, A.; Aouadhi, C.; Hosni, K.; Sakly, M.; Sebai, H. Antidiarrhoeal, antimicrobial and antioxidant effects of myrtle berries (Myrtus communis L.) seeds extract. *J. Pharm. Pharmacol.* **2016**, *68*, 264–274, doi:10.1111/jphp.12505.

78. Jabri, M.A.; Tounsi, H.; Rtibi, K.; Marzouki, L.; Sakly, M.; Sebai, H. Ameliorative and antioxidant effects of myrtle berry seed (Myrtus communis) extract during reflux-induced esophagitis in rats. *Pharm. Biol.* **2016**, *54*, 1575–1585, doi:10.3109/13880209.2015.1107748.

79. Wannes, W.A.; Marzouk, B. Characterization of myrtle seed (Myrtus communis var. baetica) as a source of lipids, phenolics, and antioxidant activities. *J. Food Drug Anal.* **2016**, *24*, 316–323, doi:10.1016/j.jfda.2015.11.001.

80. Petretto, G.L.; Maldini, M.; Addis, R.; Chessa, M.; Foddai, M.; Rourke, J.P.; Pintore, G. Variability of chemical composition and antioxidant activity of essential oils between Myrtus communis var. Leucocarpa DC and var. Melanocarpa DC. *Food Chem.* **2016**, *197*, 124–131, doi:10.1016/j.foodchem.2015.10.056.

81. González-de-Peredo, A. V.; Vázquez-Espinosa, M.; Espada-Bellido, E.; Ferreiro-González, M.; Amores-Arrocha, A.; Palma, M.; Barbero, G.F.; Jiménez-Cantizano, A. Discrimination of myrtle ecotypes from different geographic areas according to their morphological characteristics and anthocyanins composition. *Plants* **2019**, *8*, doi:10.3390/plants8090328.

82. González de Peredo, A. V.; Vázquez-Espinosa, M.; Espada-Bellido, E.; Jiménez-Cantizano, A.; Ferreiro-González, M.; Amores-Arrocha, A.; Palma, M.; Barroso, C.G.; Barbero, G.F. Development of new analytical microwave-assisted extraction methods for bioactive compounds from myrtle (myrtus communis L.). *Molecules* **2018**, *23*, doi:10.3390/molecules23112992.

83. Bouaoudia-Madi, N.; Boulekbache-Makhlouf, L.; Kadri, N.; Dahmoune, F.; Remini, H.; Dairi, S.; Oukhmanou-Bensidhoum, S.; Madani, K. Phytochemical analysis of Myrtus communis plant: Conventional versus microwave assisted-extraction procedures. *J. Complement. Integr. Med.* **2017**, *14*,

20160098, doi:10.1515/jcim-2016-0098.

84. Franco, A.M.; Tocci, N.; Guella, G.; Dell'Agli, M.; Sangiovanni, E.; Perenzoni, D.; Vrhovsek, U.; Mattivi, F.; Manca, G. Myrtle Seeds (Myrtus communis L.) as a Rich Source of the Bioactive Ellagitannins Oenothein B and Eugeniflorin D2. *ACS Omega* **2019**, *4*, 15966–15974, doi:10.1021/acsomega.9b02010.

85. Usai, M.; Marchetti, M.; Culeddu, N.; Mulas, M. Chemical composition of myrtle (myrtus communis l.) berries essential oils as observed in a collection of genotypes. *Molecules* **2018**, *23*, doi:10.3390/molecules23102502.

86. Pereira, P.; Cebola, M.J.; Oliveira, M.C.; Bernardo Gil, M.G. Antioxidant capacity and identification of bioactive compounds of Myrtus communis L. extract obtained by ultrasound-assisted extraction. *J. Food Sci. Technol.* **2017**, *54*, 4362–4369, doi:10.1007/s13197-017-2907-y.

87. Tumen, I.; Senol, F.S.; Orhan, I.E. Inhibitory potential of the leaves and berries of Myrtus communis L. (myrtle) against enzymes linked to neurodegenerative diseases and their antioxidant actions. *Int. J. Food Sci. Nutr.* **2012**, *63*, 387–392, doi:10.3109/09637486.2011.629178.

88. Jabri, M.A.; Rtibi, K.; Sakly, M.; Marzouki, L.; Sebai, H. Role of gastrointestinal motility inhibition and antioxidant properties of myrtle berries (Myrtus communis L.) juice in diarrhea treatment. *Biomed. Pharmacother.* **2016**, *84*, 1937–1944, doi:10.1016/j.biopha.2016.11.008.

89. Paknejad, M.S.; Eftekhari, K.; Rahimi, R.; Vigeh, M.; Naghizadeh, A.; Karimi, M. Myrtle (Myrtus communis L.) fruit syrup for gastroesophageal reflux disease in children: A double-blind randomized clinical trial. *Phyther. Res.* **2021**, *35*, 6369–6376, doi:10.1002/ptr.7288.

90. Zohalinezhad, M.E.; Hosseini-Asl, M.K.; Akrami, R.; Nimrouzi, M.; Salehi, A.; Zarshenas, M.M. Myrtus communis L. Freeze-Dried Aqueous Extract Versus Omeprazol in Gastrointestinal Reflux Disease: A Double-Blind Randomized Controlled Clinical Trial. *J. Evidence-Based Complement. Altern. Med.* **2016**, *21*, 23–29, doi:10.1177/2156587215589403.

91. Aggul, A.G.; Demir, G.M.; Gulaboglu, M. Ethanol Extract of Myrtle (Myrtus communis L.) Berries as a Remedy for Streptozotocin-Induced Oxidative Stress in Rats. *Appl. Biochem. Biotechnol.* **2021**, doi:10.1007/s12010-021-03753-z.

92. Khodaie, S.-A.; Emadi, F.; Naseri, M.; Kamalinejad, M.; Riahi, S.M.; Alijaniha, F.; Roghani, M. The Effect of Myrtus communis Aqueous Extract-Containing Gel on Wound Healing in Streptozotocin-Induced Diabetic Rats. *Curr. Drug Discov. Technol.* **2020**, *17*, doi:10.2174/1570163817666200712163956.

93. Magiera, A.; Czerwińska, M.E.; Owczarek, A.; Marchelak, A.; Granica, S.; Olszewska, M.A. Polyphenol-Enriched Extracts of Prunus spinosa Fruits: Anti-Inflammatory and Antioxidant Effects in Human Immune Cells Ex Vivo in Relation to Phytochemical Profile. *Molecules* **2022**, *27*, doi:10.3390/molecules27051691.

94. Popović, B.M.; Blagojević, B.; Žďero Pavlović, R.; Mićić, N.; Bijelić, S.; Bogdanović, B.; Mišan, A.; Duarte, C.M.M.; Serra, A.T. Comparison between polyphenol profile and bioactive response in blackthorn (Prunus spinosa L.) genotypes from north Serbia-from raw data to PCA analysis. *Food Chem.* **2020**, *302*, doi:10.1016/j.foodchem.2019.125373.

95. Capek, P.; Košťálová, Z. Isolation, chemical characterization and antioxidant activity of Prunus spinosa L. fruit phenolic polysaccharide-proteins. *Carbohydr. Res.* **2022**, *515*, doi:10.1016/j.carres.2022.108547.

96. Pozzo, L.; Russo, R.; Frassinetti, S.; Vizzarri, F.; Árvay, J.; Vornoli, A.; Casamassima, D.; Palazzo, M.; Della Croce, C.M.; Longo, V. Wild Italian Prunus spinosa L. Fruit exerts in vitro antimicrobial activity and protects against in vitro and in vivo oxidative stress. *Foods* **2020**, *9*, doi:10.3390/foods9010005.

97. Backes, E.; Leichtweis, M.G.; Pereira, C.; Carocho, M.; Barreira, J.C.M.; Kamal Genena, A.; José

Baraldi, I.; Filomena Barreiro, M.; Barros, L.; C.F.R. Ferreira, I. Ficus carica L. and Prunus spinosa L. extracts as new anthocyanin-based food colorants: A thorough study in confectionery products. *Food Chem.* **2020**, *333*, doi:10.1016/j.foodchem.2020.127457.

98. Murati, T.; Miletić, M.; Kolarić, J.; Lovrić, V.; Kovačević, D.B.; Putnik, P.; Jurčević, I.L.; Đikić, D.; Dragović-Uzelac, V.; Kmetič, I. Toxic activity of Prunus spinosa L. Flower extract in hepatocarcinoma cells. *Arh. Hig. Rada Toksikol.* **2019**, *70*, 303–309, doi:10.2478/aiht-2019-70-3322.

99. Marchelak, A.; Owczarek, A.; Matczak, M.; Pawlak, A.; Kolodziejczyk-Czepas, J.; Nowak, P.; Olszewska, M.A. Bioactivity potential of Prunus spinosa L. flower extracts: Phytochemical profiling, cellular safety, pro-inflammatory enzymes inhibition and protective effects against oxidative stress in vitro. *Front. Pharmacol.* **2017**, *8*, doi:10.3389/fphar.2017.00680.

100. Meschini, S.; Pellegrini, E.; Condello, M.; Occhionero, G.; Delfine, S.; Condello, G.; Mastrodonato, F. Cytotoxic and apoptotic activities of Prunus spinosa trigno ecotype extract on human cancer cells. *Molecules* **2017**, *22*, doi:10.3390/molecules22091578.

101. Magiera, A.; Czerwińska, M.E.; Owczarek, A.; Marchelak, A.; Granica, S.; Olszewska, M.A. Polyphenols and Maillard Reaction Products in Dried Prunus spinosa Fruits: Quality Aspects and Contribution to Anti-Inflammatory and Antioxidant Activity in Human Immune Cells Ex Vivo. *Molecules* **2022**, *27*, doi:10.3390/molecules27103302.

102. Coppari, S.; Colomba, M.; Fraternale, D.; Brinkmann, V.; Romeo, M.; Rocchi, M.B.L.; Di Giacomo, B.; Mari, M.; Guidi, L.; Ramakrishna, S.; et al. Antioxidant and anti-inflammaging ability of prune (Prunus spinosa l.) extract result in improved wound healing efficacy. *Antioxidants* **2021**, *10*, 1–21, doi:10.3390/antiox10030374.

103. Tiboni, M.; Coppari, S.; Casettari, L.; Guescini, M.; Colomba, M.; Fraternale, D.; Gorassini, A.; Verardo, G.; Ramakrishna, S.; Guidi, L.; et al. Prunus spinosa extract loaded in biomimetic nanoparticles evokes in vitro anti-inflammatory and wound healing activities. *Nanomaterials* **2021**, *11*, 1–14, doi:10.3390/nano11010036.

104. Karakas, N.; Okur, M.E.; Ozturk, I.; Ayla, S.; Karadag, A.E.; Polat, D.Ç. Antioxidant activity of blackthorn (Prunus spinosa L.) fruit extract and cytotoxic effects on various cancer cell lines. *Medeni. Med. J.* **2019**, *34*, 297–304, doi:10.5222/MMJ.2019.87864.

105. Condello, M.; Pellegrini, E.; Spugnini, E.P.; Baldi, A.; Amadio, B.; Vincenzi, B.; Occhionero, G.; Delfine, S.; Mastrodonato, F.; Meschini, S. Anticancer activity of "Trigno M", extract of Prunus spinosa drupes, against in vitro 3D and in vivo colon cancer models. *Biomed. Pharmacother.* **2019**, *118*, doi:10.1016/j.biopha.2019.109281.

106. Balta, I.; Sevastre, B.; Mireşan, V.; Taulescu, M.; Raducu, C.; Longodor, A.L.; Marchiş, Z.; Mariş, C.S.; Coroian, A. Protective effect of blackthorn fruits (Prunus spinosa) against tartrazine toxicity development in albino Wistar rats. *BMC Chem.* **2019**, *13*, doi:10.1186/s13065-019-0610-y.

107. Farag, M.A.; El-Kersh, D.M. Volatiles profiling in Ceratonia siliqua (Carob bean) from Egypt and in response to roasting as analyzed via solid-phase microextraction coupled to chemometrics. *J. Adv. Res.* **2017**, *8*, 379–385, doi:10.1016/j.jare.2017.05.002.

108. Gioxari, A.; Amerikanou, C.; Nestoridi, I.; Gourgari, E.; Pratsinis, H.; Kalogeropoulos, N.; Andrikopoulos, N.K.; Kaliora, A.C. Carob: A Sustainable Opportunity for Metabolic Health. *Foods* 2022, *11*.

109. Stavrou, I.J.; Christou, A.; Kapnissi-Christodoulou, C.P. Polyphenols in carobs: A review on their composition, antioxidant capacity and cytotoxic effects, and health impact. *Food Chem.* 2018, *269*, 355–374.

110. Darwish, W.S.; Khadr, A.E.S.; Kamel, M.A.E.N.; Abd Eldaim, M.A.; El Sayed, I.E.T.; Abdel-Bary, H.M.; Ullah, S.; Ghareeb, D.A. Phytochemical characterization and evaluation of biological activities of egyptian carob pods (Ceratonia siliqua l.) aqueous extract: In vitro study. *Plants* **2021**, *10*,

doi:10.3390/plants10122626.

111. Farag, M.A.; El-Kersh, D.M.; Ehrlich, A.; Choucry, M.A.; El-Seedi, H.; Frolov, A.; Wessjohann, L.A. Variation in Ceratonia siliqua pod metabolome in context of its different geographical origin, ripening stage and roasting process. *Food Chem.* **2019**, *283*, 675–687, doi:10.1016/j.foodchem.2018.12.118.

112. Çavuşoğlu, K.; Kurt, D.; Yalçın, E. A versatile model for investigating the protective effects of Ceratonia siliqua pod extract against 1,4-dioxane toxicity. *Environ. Sci. Pollut. Res.* **2020**, *27*, 27885–27892, doi:10.1007/s11356-020-08545-2.

113. Peng, Z.T.; Xia, Y.J.; Yashiro, T.; Gao, X.; Dong, T.T.X.; Tsim, K.W.K.; Wang, H.Y. Novel phenylpropanoids and isoflavone glycoside are isolated and identified from the carob pods (Ceratonia siliqua L.). *Nat. Prod. Res.* **2022**, doi:10.1080/14786419.2022.2076230.

114. Ayache, S. Ben; Saafi, E.B.; Emhemmed, F.; Flamini, G.; Achour, L.; Muller, C.D. Biological activities of aqueous extracts from carob plant (Ceratonia siliqua L.) by antioxidant, analgesic and proapoptotic properties evaluation. *Molecules* **2020**, *25*, doi:10.3390/molecules25143120.

115. Saratsi, K.; Hoste, H.; Voutzourakis, N.; Tzanidakis, N.; Stefanakis, A.; Thamsborg, S.M.; Mueller-Harvey, I.; Hadjigeorgiou, I.; Sotiraki, S. Feeding of carob (Ceratonia siliqua) to sheep infected with gastrointestinal nematodes reduces faecal egg counts and worm fecundity. *Vet. Parasitol.* **2020**, *284*, doi:10.1016/j.vetpar.2020.109200.

116. Alzoubi, K.H.; Alibbini, S.; Khabour, O.F.; El-Elimat, T.; Al-zubi, M.; Alali, F.Q. Carob (Ceratonia siliqua L.) Prevents Short-Term Memory Deficit Induced by Chronic Stress in Rats. *J. Mol. Neurosci.* **2018**, *66*, 314–321, doi:10.1007/s12031-018-1161-8.

117. Rico, D.; Martín-Diana, A.B.; Martínez-Villaluenga, C.; Aguirre, L.; Silván, J.M.; Dueñas, M.; De Luis, D.A.; Lasa, A. In vitro approach for evaluation of carob by-products as source bioactive ingredients with potential to attenuate metabolic syndrome (MetS). *Heliyon* **2019**, *5*, doi:10.1016/j.heliyon.2019.e01175.

118. Valero-Muñoz, M.; Ballesteros, S.; Ruiz-Roso, B.; Pérez-Olleros, L.; Martín-Fernández, B.; Lahera, V.; de las Heras, N. Supplementation with an insoluble fiber obtained from carob pod (Ceratonia siliqua L.) rich in polyphenols prevents dyslipidemia in rabbits through SIRT1/PGC-1α pathway. *Eur. J. Nutr.* **2019**, *58*, 357–366, doi:10.1007/s00394-017-1599-4.

119. Rtibi, K.; Selmi, S.; Grami, D.; Saidani, K.; Sebai, H.; Amri, M.; Eto, B.; Marzouki, L. Ceratonia siliqua L. (immature carob bean) inhibits intestinal glucose absorption, improves glucose tolerance and protects against alloxan-induced diabetes in rat. *J. Sci. Food Agric.* **2017**, *97*, 2664–2670, doi:10.1002/jsfa.8091.

120. Qasem, M.A.; Noordin, M.I.; Arya, A.; Alsalahi, A.; Jayash, S.N. Evaluation of the glycemic effect of Ceratonia siliqua pods (Carob) on a streptozotocin-nicotinamide induced diabetic rat model. *PeerJ* **2018**, *2018*, doi:10.7717/peerj.4788.

121. Lunz, K.; Stappen, I. Back to the roots-an overview of the chemical composition and bioactivity of selected root-essential oils. *Molecules* **2021**, *26*, doi:10.3390/molecules26113155.

122. Kroener, E.M.; Buettner, A. Unravelling important odorants in horseradish (Armoracia rusticana). *Food Chem.* **2017**, *232*, 455–465, doi:10.1016/j.foodchem.2017.04.042.

123. Marzocco, S.; Calabrone, L.; Adesso, S.; Larocca, M.; Franceschelli, S.; Autore, G.; Martelli, G.; Rossano, R. Anti-inflammatory activity of horseradish (Armoracia rusticana) root extracts in LPS-stimulated macrophages. *Food Funct.* **2015**, *6*, 3778–3788, doi:10.1039/c5fo00475f.

124. Gafrikova, M.; Galova, E.; Sevcovicova, A.; Imreova, P.; Mucaji, P.; Miadokova, E. Extract from armoracia rusticana and its flavonoid components protect human lymphocytes against oxidative damage induced by hydrogen peroxide. *Molecules* **2014**, *19*, 3160–3172, doi:10.3390/molecules19033160.

125. Kroener, E.M.; Buettner, A. Sensory-analytical comparison of the aroma of different horseradish varieties (Armoracia rusticana). *Front. Chem.* **2018**, *6*, doi:10.3389/fchem.2018.00149.

126. Negro, E.J.; Sendker, J.; Stark, T.; Lipowicz, B.; Hensel, A. Phytochemical and functional analysis of horseradish (Armoracia rusticana) fermented and non-fermented root extracts. *Fitoterapia* **2022**, *162*, doi:10.1016/j.fitote.2022.105282.

127. Park, H.W.; Choi, K.D.; Shin, I.S. Antimicrobial activity of isothiocyanates(itcs) extracted from horseradish(armoracia rusticana) root against oral microorganisms. *Biocontrol Sci.* **2013**, *18*, 163–168, doi:10.4265/bio.18.163.

128. Eichel, V.; Schüller, A.; Biehler, K.; Al-Ahmad, A.; Frank, U. Antimicrobial effects of mustard oil-containing plants against oral pathogens: An in vitro study. *BMC Complement. Med. Ther.* **2020**, *20*, doi:10.1186/s12906-020-02953-0.

129. Mickymaray, S.; Al Aboody, M.S. In vitro antioxidant and bactericidal efficacy of 15 common spices: Novel therapeutics for urinary tract infections? *Med.* **2019**, *55*, doi:10.3390/medicina55060289.

130. Popović, M.; Maravić, A.; Čulić, V.Č.; Đulović, A.; Burčul, F.; Blažević, I. Biological effects of glucosinolate degradation products from horseradish: A horse that wins the race. *Biomolecules* **2020**, *10*, doi:10.3390/biom10020343.

131. Herz, C.; Tran, H.T.T.; Márton, M.R.; Maul, R.; Baldermann, S.; Schreiner, M.; Lamy, E. Evaluation of an Aqueous Extract from Horseradish Root (Armoracia rusticana Radix) against Lipopolysaccharide-Induced Cellular Inflammation Reaction. *Evidence-based Complement. Altern. Med.* **2017**, *2017*, doi:10.1155/2017/1950692.

132. Manuguerra, S.; Caccamo, L.; Mancuso, M.; Arena, R.; Rappazzo, A.C.; Genovese, L.; Santulli, A.; Messina, C.M.; Maricchiolo, G. The antioxidant power of horseradish, Armoracia rusticana, underlies antimicrobial and antiradical effects, exerted in vitro. *Nat. Prod. Res.* **2020**, *34*, 1567–1570, doi:10.1080/14786419.2018.1517121.

133. Kofroňová, M.; Hrdinová, A.; Mašková, P.; Soudek, P.; Tremlová, J.; Pinkas, D.; Lipavská, H. Strong antioxidant capacity of horseradish hairy root cultures under arsenic stress indicates the possible use of Armoracia rusticana plants for phytoremediation. *Ecotoxicol. Environ. Saf.* **2019**, *174*, 295–304, doi:10.1016/j.ecoenv.2019.02.028.

134. Lunz, K.; Stappen, I. Back to the roots-an overview of the chemical composition and bioactivity of selected root-essential oils. *Molecules* **2021**, *26*, 3020–3024, doi:10.3390/molecules26113155.

135. Chowański, S.; Chudzińska, E.; Lelario, F.; Ventrella, E.; Marciniak, P.; Miądowicz-Kobielska, M.; Spochacz, M.; Szymczak, M.; Scrano, L.; Bufo, S.A.; et al. Insecticidal properties of Solanum nigrum and Armoracia rusticana extracts on reproduction and development of Drosophila melanogaster. *Ecotoxicol. Environ. Saf.* **2018**, *162*, 454–463, doi:10.1016/j.ecoenv.2018.07.030.

136. Kim, H.J.; Jeong, A.H.; Lee, J.H.; Park, J.H. Persistence enhancement of a promising tick repellent, benzyl isothiocyanate, by yeast microcarriers. *Molecules* **2021**, *26*, doi:10.3390/molecules26226817.

137. Aissani, N.; Tedeschi, P.; Maietti, A.; Brandolini, V.; Garau, V.L.; Caboni, P. Nematicidal activity of allylisothiocyanate from horseradish (Armoracia rusticana) roots against Meloidogyne incognita. *J. Agric. Food Chem.* **2013**, *61*, 4723–4727, doi:10.1021/jf4008949.

138. Choi, K.D.; Kim, H.Y.; Shin, I.S. Antifungal activity of isothiocyanates extracted from horseradish (Armoracia rusticana) root against pathogenic dermal fungi. *Food Sci. Biotechnol.* **2017**, *26*, 847–852, doi:10.1007/s10068-017-0104-4.

139. Ren, J.J.; Zhang, D.; Hou, P.X.; Wu, H. Effects of horseradish oil and eight isothiocyanates vapour treatment on postharvest disease control and their efficacy as preservatives of mature green tomato. *Plant Dis.* **2020**, *104*, 2688–2695, doi:10.1094/PDIS-03-20-0498-RE.

140. Indice Albums Galleria della flora Available online:

https://www.actaplantarum.org/galleria_flora/albums_new.php?p1=2&p2=0&p4=-1&p5=0&sf=1&p6=2&p3=P (accessed on Dec 13, 2022).

141. Montoro, P.; Serreli, G.; Gil, K.A.; D'Urso, G.; Kowalczyk, A.; Tuberoso, C.I.G. Evaluation of bioactive compounds and antioxidant capacity of edible feijoa (Acca sellowiana (O. Berg) Burret) flower extracts. *J. Food Sci. Technol.* **2020**, *57*, 2051–2060, doi:10.1007/s13197-020-04239-2.

142. Dührkop, K.; Fleischauer, M.; Ludwig, M.; Aksenov, A.A.; Melnik, A. V; Meusel, M.; Dorrestein, P.C.; Rousu, J.; Böcker, S. SIRIUS 4: a rapid tool for turning tandem mass spectra into metabolite structure information. *Nat. Methods* **2019**, *16*, 299–302, doi:10.1038/s41592-019-0344-8.

143. Hoffmann, M.A.; Nothias, L.F.; Ludwig, M.; Fleischauer, M.; Gentry, E.C.; Witting, M.; Dorrestein, P.C.; Dührkop, K.; Böcker, S. High-confidence structural annotation of metabolites absent from spectral libraries. *Nat. Biotechnol.* **2022**, *40*, 411–421, doi:10.1038/s41587-021-01045-9.

144. Maritim, S.; Boulas, P.; Lin, Y. Comprehensive analysis of liposome formulation parameters and their influence on encapsulation, stability and drug release in glibenclamide liposomes. *Int. J. Pharm.* **2021**, *592*, 120051, doi:10.1016/j.ijpharm.2020.120051.

145. Tziveleka, L.A.; Pippa, N.; Ioannou, E.; Demetzos, C.; Roussis, V. Development of Ulvan-Containing Liposomes as Antibacterial Drug Delivery Platforms. *J. Funct. Biomater.* **2022**, *13*, doi:10.3390/jfb13040186.

146. Heftberger, P.; Kollmitzer, B.; Heberle, F.A.; Pan, J.; Rappolt, M.; Amenitsch, H.; Kučerka, N.; Katsaras, J.; Pabst, G. Global small-angle X-ray scattering data analysis for multilamellar vesicles: the evolution of the scattering density profile model. *J. Appl. Crystallogr.* **2014**, *47*, 173–180, doi:10.1107/S1600576713029798.

147. Pabst, G.; Rappolt, M.; Amenitsch, H.; Laggner, P. Structural information from multilamellar liposomes at full hydration: Full q-range fitting with high quality X-ray data. *Phys. Rev. E - Stat. Physics, Plasmas, Fluids, Relat. Interdiscip. Top.* **2000**, *62*, 4000–4009, doi:10.1103/PhysRevE.62.4000.

148. Pedersen, J.S. Analysis of small-angle scattering data from colloids and polymer solutions: Modeling and least-squares fitting. *Adv. Colloid Interface Sci.* **1997**, *70*, 171–210, doi:10.1016/S0001-8686(97)00312-6.

149. Caddeo, C.; Pucci, L.; Gabriele, M.; Carbone, C.; Fernàndez-Busquets, X.; Valenti, D.; Pons, R.; Vassallo, A.; Fadda, A.M.; Manconi, M. Stability, biocompatibility and antioxidant activity of PEG-modified liposomes containing resveratrol. *Int. J. Pharm.* **2018**, *538*, 40–47, doi:10.1016/j.ijpharm.2017.12.047.

150. Caddeo, C.; Díez-Sales, O.; Pons, R.; Fernàndez-Busquets, X.; Fadda, A.M.; Manconi, M. Topical anti-inflammatory potential of quercetin in lipid-based nanosystems: In vivo and in vitro evaluation. *Pharm. Res.* **2014**, *31*, 959–968, doi:10.1007/s11095-013-1215-0.

151. Luna-Vázquez-gómez, R.; Arellano-García, M.E.; Toledano-Magaña, Y.; García-Ramos, J.C.; Radilla-Chávez, P.; Salas-Vargas, D.S.; Casillas-Figueroa, F.; Ruiz-Ruiz, B.; Pestryakov, A.; Bogdanchikova, N. Bell Shape Curves of Hemolysis Induced by Silver Nanoparticles: Review and Experimental Assay. *Nanomaterials* 2022, *12*.

152. Pérez, L.; Pinazo, A.; Morán, M.C.; Pons, R. Aggregation behavior, antibacterial activity and biocompatibility of catanionic assemblies based on amino acid-derived surfactants. *Int. J. Mol. Sci.* **2020**, *21*, 1–23, doi:10.3390/ijms21238912.

153. Garcia, M.T.; Ribosa, I.; González, J.J.; Comelles, F. Surface activity, self-aggregation and antimicrobial activity of catanionic mixtures of surface active imidazolium- or pyridinium-based ionic liquids and sodium bis(2-ethylhexyl) sulfosuccionate. *J. Mol. Liq.* **2020**, *303*, doi:10.1016/j.molliq.2020.112637.

154. Lennette, E.H.; Spaulding, E.H.; Truant, J.P. Manual of Clinical Microbiology.

AM.SOC.MICROBIOL.,WASHINGTON,D.C. **1974**, *(970p.) $U*, doi:10.4269/ajtmh.1971.20.3.tm0200030508a.

155. Präbst, K.; Engelhardt, H.; Ringgeler, S.; Hübner, H. Basic colorimetric proliferation assays: MTT, WST, and resazurin. In *Methods in Molecular Biology*; 2017; Vol. 1601, pp. 1–17.

156. Tuberoso, C.I.G.; Boban, M.; Bifulco, E.; Budimir, D.; Pirisi, F.M. Antioxidant capacity and vasodilatory properties of Mediterranean food: The case of Cannonau wine, myrtle berries liqueur and strawberry-tree honey. In Proceedings of the Food Chemistry; Food Chem, 2013; Vol. 140, pp. 686–691.

157. KNApSAcK Core System Available online: http://www.knapsackfamily.com/knapsack_core/top.php (accessed on Dec 11, 2022).

158. Blaženović, I.; Kind, T.; Ji, J.; Fiehn, O. Software tools and approaches for compound identification of LC-MS/MS data in metabolomics. *Metabolites* **2018**, *8*, 31, doi:10.3390/metabo8020031.

159. Mikulic-Petkovsek, M.; Stampar, F.; Veberic, R.; Sircelj, H. Wild Prunus Fruit Species as a Rich Source of Bioactive Compounds. *J. Food Sci.* **2016**, *81*, C1928–C1937, doi:10.1111/1750-3841.13398.

160. Guimarães, R.; Barros, L.; Dueñas, M.; Carvalho, A.M.; Queiroz, M.J.R.P.; Santos-Buelga, C.; Ferreira, I.C.F.R. Characterisation of phenolic compounds in wild fruits from Northeastern Portugal. *Food Chem.* **2013**, *141*, 3721–3730, doi:10.1016/j.foodchem.2013.06.071.

161. Jaiswal, R.; Matei, M.F.; Ullrich, F.; Kuhnert, N. How to distinguish between cinnamoylshikimate esters and chlorogenic acid lactones by liquid chromatography-tandem mass spectrometry. *J. Mass Spectrom.* **2011**, *46*, 933–942, doi:10.1002/jms.1972.

162. Zhou, R.R.; Liu, X.H.; Chen, L.; Huang, J.H.; Liang, X.J.; Wan, D.; Zhang, S.H.; Huang, L.Q. Comparison of the Antioxidant Activities and Phenolic Content of Five Lonicera Flowers by HPLC-DAD/MS-DPPH and Chemometrics. *Int. J. Anal. Chem.* **2020**, *2020*, doi:10.1155/2020/2348903.

163. Sun, H.; Liu, M.; Lin, Z.; Jiang, H.; Niu, Y.; Wang, H.; Chen, S. Comprehensive identification of 125 multifarious constituents in Shuang-huang-lian powder injection by HPLC-DAD-ESI-IT-TOF-MS. *J. Pharm. Biomed. Anal.* **2015**, *115*, 86–106, doi:10.1016/j.jpba.2015.06.013.

164. Wang, Y.; Vorsa, N.; Harrington, P.D.B.; Chen, P. Nontargeted Metabolomic Study on Variation of Phenolics in Different Cranberry Cultivars Using UPLC-IM - HRMS. *J. Agric. Food Chem.* **2018**, *66*, 12206–12216, doi:10.1021/acs.jafc.8b05029.

165. Chen, P.; Lin, X.; Yang, C.H.; Tang, X.; Chang, Y.W.; Zheng, W.; Luo, L.; Xu, C.; Chen, Y.H. Study on Chemical Profile and Neuroprotective Activity of Myrica rubra Leaf Extract. *Molecules* **2017**, *22*, doi:10.3390/molecules22071226.

166. Bottone, A.; Montoro, P.; Masullo, M.; Pizza, C.; Piacente, S. Metabolomics and antioxidant activity of the leaves of Prunus dulcis Mill. (Italian cvs. Toritto and Avola). *J. Pharm. Biomed. Anal.* **2018**, *158*, 54–65, doi:10.1016/j.jpba.2018.05.018.

167. Sabatini, L.; Fraternale, D.; Di Giacomo, B.; Mari, M.; Albertini, M.C.; Gordillo, B.; Rocchi, M.B.L.; Sisti, D.; Coppari, S.; Semprucci, F.; et al. Chemical composition, antioxidant, antimicrobial and anti-inflammatory activity of Prunus spinosa L. fruit ethanol extract. *J. Funct. Foods* **2020**, *67*, 103885, doi:10.1016/j.jff.2020.103885.

168. Hsouna, A. Ben; Trigui, M.; Mansour, R. Ben; Jarraya, R.M.; Damak, M.; Jaoua, S. Chemical composition, cytotoxicity effect and antimicrobial activity of Ceratonia siliqua essential oil with preservative effects against Listeria inoculated in minced beef meat. *Int. J. Food Microbiol.* **2011**, *148*, 66–72, doi:10.1016/j.ijfoodmicro.2011.04.028.

169. Aissani, N.; Coroneo, V.; Fattouch, S.; Caboni, P. Inhibitory effect of carob (Ceratonia siliqua) leaves methanolic extract on Listeria monocytogenes. *J. Agric. Food Chem.* **2012**, *60*, 9954–9958, doi:10.1021/jf3029623.

170. Snoussi, A.; Hayet, B.H.K.; Essaidi, I.; Zgoulli, S.; Moncef, C.M.; Thonart, P.; Bouzouita, N. Improvement of the composition of Tunisian myrtle berries (Myrtus communis L.) alcohol extracts. *J. Agric. Food Chem.* **2012**, *60*, 608–614, doi:10.1021/jf202883s.

171. Polat, B.; Oba, S.; Karaman, K.; Arici, M.; Sagdic, O. Comparison of different solvent types for determination biological activities of myrtle berries collected from Turkey. *Qual. Assur. Saf. Crop. Foods* **2014**, *6*, 221–227, doi:10.3920/QAS2013.0241.

172. Gorjian, H.; Raftani Amiri, Z.; Mohammadzadeh Milani, J.; Ghaffari Khaligh, N. Preparation and characterization of the encapsulated myrtle extract nanoliposome and nanoniosome without using cholesterol and toxic organic solvents: A comparative study. *Food Chem.* **2021**, *342*, 128342, doi:10.1016/j.foodchem.2020.128342.

173. Teixeira, J.; Gaspar, A.; Garrido, E.M.; Garrido, J.; Borges, F. Hydroxycinnamic acid antioxidants: An electrochemical overview. *Biomed Res. Int.* 2013, *2013*.

174. Sridhar, A.; Ponnuchamy, M.; Kumar, P.S.; Kapoor, A.; Vo, D.V.N.; Prabhakar, S. Techniques and modeling of polyphenol extraction from food: a review. *Environ. Chem. Lett.* 2021, *19*, 3409–3443.

Annex

List of publications produced during the PhD program.

De Luca, M.; Lucchesi, D.; Tuberoso, C.I.G.; Fernàndez-Busquets, X.; Vassallo, A.; Martelli, G.; Fadda, A.M.; Pucci, L.; Caddeo, C. Liposomal Formulations to Improve Antioxidant Power of Myrtle Berry Extract for Potential Skin Application. *Pharmaceutics* **2022**, *14*, 910. https://doi.org/10.3390/pharmaceutics14050910

Pappalardo, I.; Santarsiero, A.; De Luca, M.; Acquavia, M.A.; Todisco, S.; Caddeo, C.; Bianco, G.; Infantino, V.; Martelli, G.; Vassallo, A. Exploiting the Anti-Inflammatory Potential of White Capsicum Extract by the Nanoformulation in Phospholipid Vesicles. *Antioxidants* **2021**, *10*, 1683. https://doi.org/10.3390/antiox10111683

Vassallo, A.; Santoro, V.; Pappalardo, I.; Santarsiero, A.; Convertini, P.; De Luca, M.; Martelli, G.; Infantino, V.; Caddeo, C. Liposome-Mediated Inhibition of Inflammation by Hydroxycitrate. *Nanomaterials* **2020**, *10*, 2080. https://doi.org/10.3390/nano10102080

De Luca, M.; Pappalardo, I.; Limongi, A.R.; Viviano, E.; Radice, R.P.; Todisco, S.; Martelli, G.; Infantino, V.; Vassallo, A. Lipids from Microalgae for Cosmetic Applications. *Cosmetics* **2021**, *8*, 52. https://doi.org/10.3390/cosmetics8020052

Acknowledgments

I would like to thank everyone who contributed to this project.

Firstly, I would like to thank my supervisor, Prof. Antonio Vassallo, and also Prof. Giuseppe Martelli for involving me in this experience and for their support during my PhD study.

I am extremely grateful to Prof. Carla Caddeo for the constant support, all the advice and teachings received, and for having encouraged me all the time. I would also like to thank her collaborators at the University of Cagliari, particularly Prof. Carlo Tuberoso and the CeSAR team for their technical support in my study.

I would like to thank Prof. Ramon Ponce for welcoming me into his research team, for all the explanations he patiently gave me, and for all the help received. I would also like to thank Prof. Teresa Garcia and Carmen Moran for the enthusiasm with which they contributed to my experiments, which was not at all obvious. My gratitude extends to the entire IQAC research team, for the warm welcome and the nice time spent in Barcelona.

Finally, I would like to thank my family, friends, and colleagues for their encouragement and support.

Maria